SEISMIC BEHAVIOR OF MICROPILES

By

JOO CHAI WONG

A thesis submitted in partial fulfillment of
the requirements for the degree of

MASTER OF SCIENCE IN CIVIL ENGINEERING

WASHINGTON STATE UNIVERSITY
Department of Civil and Environmental Engineering

May 2004

To the Faculty of Washington State University:

The members of the Committee appointed to examine the thesis of JOO CHAI WONG find it satisfactory and recommend that it be accepted.

Chair

ACKNOWLEDGEMENTS

First and foremost, the author would like to express his heartfelt gratitude and sincere appreciation to his advisor, Dr. Adrian Rodriguez-Marek. His invaluable knowledge, tireless guidance, boundless patience and continuous support rendered throughout every phase of the project are immensely gratified.

Special thanks are extended to Washington State Department of Transportation under the Grant Number T2696-02 for granting the fund. Without the fund, the author would not be able to support himself to study abroad in this prestigious university.

The author also deeply indebted to Prof. Balasingam Muhunthan and Prof. Rafik Itani for being the Master's Committees.

Of equal importance to the entire completion of this project is Dr. Thomas Weaver from the University of Idaho. His genuine interest, doubtless unselfishness and sincere involvement in my project, especially his taught on the derivation of p-y curves are greatly appreciated.

The author also acknowledge gratefully to Tom Weber for providing him with computer resources and Vicki Ruddick for assisting him in the secretarial staff.

The author would also like to thank all the individuals below who have painted unfading colors of my life in the United States. They are Angela Taylor, Tobias, Serge Aizen, Brian Bayne, Clint Wilson, Adel Acortez, Eddy, Tao, Miyuki, Jong, Hau, Yoke, Julynn, Vicky, Luke (computer genius), Brent (workout partner), Masaki, Dr. Cole, Sasi, Sathish, Surendra, Jeff, Zhao Jun, Brenda Ang, Michael Bracher, April Hammer, Curtis, Ryuici, Matt (soccer guy), T J, Ikue, Siva, Lindy, Steve, Mindy, Zain, So, Christine, Aaron Fong, Saiful, Jit Chung Tan, Tonny Fong, and Clarence Chua.

Last but not least, special thanks to my parents, brother, and sister who have been accompanying me (via phone calls) through my ups and downs in the United States even though they are at a distance from me. The sweet voices from my nieces (Wei Ting Wong and Shui Shin Tan) and nephew (Khee Choon Wong) via the phone calls have soothed the wound of loneliness here occasionally.

SEISMIC BEHAVIOR OF MICROPILES

Abstract

By Joo Chai Wong, M.S.
Washington State University
May 2004

Chair: Adrian Rodriguez-Marek

Micropiles are grouted and small diameter piles that are traditionally used in foundation retrofit. Experimental evidence has indicated that micropiles behave well under seismic loading due to their high flexibility. Moreover, observations in the 1995 Kobe Earthquake indicate a good performance of friction piles under seismic loading. However, the seismic behavior of micropiles is not fully understood due to the limited number of full- and model-scale tests, as well as the limited amount of numerical modeling studies for micropiles.

This project focuses on Finite Element modeling (FEM) of single micropile and micropile groups under both static and dynamic loading. Initially, dynamic FE soil models were developed to conduct site response analyses. The lateral vertical boundaries of the soil were set up in such a way that the reflection of the arrival waves at the boundaries was avoided. The results of the site response analyses were verified against the well-validated code, SHAKE.

Subsequently, FE models for micropiles were developed with two constitutive soil models, i.e. a linear elastic and a bounding surface plasticity model. The micropile/soil interface was modeled either with perfect bonding or with frictional interface elements. For dynamic loading cases, a SDOF (single degree-of-freedom)

superstructure was placed on top of the micropiles. Parametric studies were performed for various independent variables including load intensity, non-linearity of soil, and soil stiffness for the static case; and soil non-linearity, input motion intensity, frequency contents of input motion, and the natural period of the superstructure for the dynamic case. The static and dynamic behavior of micropiles were studied via the effects of aforementioned independent variables on the deflections and bending moments along the micropile length.

TABLE OF CONTENTS

LIST OF TABLES

LIST OF FIGURES

CHAPTER 1
INTRODUCTION

1.1 INTRODUCTION AND PROBLEM STATEMENT

Micropiles are drilled and grouted small diameter replacement piles that are commonly used in foundation retrofit. Micropiles are reinforced and typically have diameters less than 300 mm. The advantages of using micropile systems include (a) their high flexibility during seismic conditions, (b) micropiles can be installed in low overhead clearance (less than 3.5 m), in all types of soils and ground conditions, (c) minimal disturbance is caused during construction, (d) inclined micropiles can be easily constructed, (e) they are able to resist axial and lateral loads, (f) only small volumes of earth to be excavated due to small diameter, (g) little disturbance is caused during drilling through an existing structure due to their small diameters, and (h) they can be drilled with boring machines that do not cause much noise.

Experimental evidence indicates that micropiles behave well under seismic loading due to their high flexibility. Moreover, observations in the 1995 Kobe Earthquake indicated a good performance of friction piles under seismic loading. However, the seismic behavior of a single micropile and a micropile group (micropiles) is not fully understood due to the limited number of full- and model-scale tests, as well as the limited amount of numerical modeling studies of micropiles.

The Finite Element (FE) method provides a tool to understand the seismic behavior of micropiles. FE analyses can be used to systematically alter the parameters that affect the seismic response of micropiles. However, the dynamic analysis of soil-micropile-structure interaction is a very complex problem. The problem includes soil non-linearity (e.g. variation of soil shear modulus and damping with strains), gapping and slippage between the micropile and the soil, complex boundary conditions (especially at the vertical lateral boundaries), and possible pile non-linearity.

1.2 OBJECTIVE

The scope of the research project focuses on the FE modeling of micropiles. The objectives of the project are to study:

(a) the construction of a dynamic FE model for site response analyses where the lateral boundaries and soil behavior are modeled appropriately,

(b) the static behavior of a single micropile,

(c) the seismic behavior of a single micropile,

(d) the seismic behavior of a micropile group which includes vertical and inclined micropiles, and

(e) the behavior of *p-y* curves back-calculated from the FE models.

1.3 ORGANIZATION OF THE THESIS

The thesis consists of six chapters. A brief description of each of the chapters in the thesis is presented herein.

Chapter 1 presents the problem statement, the objectives of the study conducted, and the organization of the entire thesis.

An extensive literature review is presented in Chapter 2. Topics include post earthquake observations, analysis methods used in site response and soil-structure-interaction problems, behavior of micropiles, and design guidelines implemented for micropiles in the United States.

Chapter 3 discusses about the numerical modeling for the seismic site response and the soil-pile-structure interaction. The validation of the FE models is also presented.

Chapter 4 presents the parametric study of the behavior of a single micropile under static and dynamic loading. The parametric study for a micropile group under dynamic loading is also included.

Chapter 5 presents the back-calculation, validation and behavior of *p-y* curves. The *p-y* curves were back-calculated from the FE models used for a single micropile under static loading.

Finally, Chapter 6 lists the conclusions drawn from the study and the recommendations for future research.

CHAPTER 2
LITERATURE REVIEW

2.1 INTRODUCTION

The response of a structure subjected to seismic or dynamic loading primarily depends on the characteristic of the site response, the external loading, the mechanical properties of the surrounding soils, and the structure itself. An extensive literature review was conducted on site response and soil-structure interaction problems. Before dwelling on these problems, post earthquake observations were reviewed. Past earthquakes have indicated contradictory observations of the influence of battered piles on the response of a structure.

2.2 POST EARTHQUAKE OBSERVATIONS

Post earthquake observations provide an excellent indication of pile performance under earthquake loading. Different degrees of structural damage have been observed relating to different types and inclinations of piles supporting the structure. The following paragraphs present several post earthquake observations.

The October 17, 1989 Loma Prieta earthquake (moment magnitude, M_w, of 7.1) yielded important observations on pile performance. SEAOC (1991) reports that the 7th Street Terminal Complex suffered extensive damage as the 16 in. square pre-stressed concrete battered piles supporting the Public Container Wharf failed in tension at their connection to the deck. Similar damage was observed at the Matson Terminal Wharf on 7 Street with additional damage to the back row of the vertical piles. Failure of the 16 in. square pre-stressed concrete battered piles at or near the pile cap connection was noticed at the Oakland Outer Harbor Pier 7. In San Francisco, the Ferry Plaza Pier suffered tensile failure at the connection of the deck to the pre-stressed concrete battered piles. These structural damages have become some of the post earthquake observations that have caused several codes, such as the seismic Eurocode EC8 (1994) and the French Seismic Code (AFPS 1990), to discourage or avoid the use of battered piles in a seismic region.

However, Gazetas and Mylonakis (1998) give a “green light” to battered piles as they presented theoretical and field evidence demonstrating that battered piles are of benefit rather than detrimental to structures supported on piles and also to the piles themselves. It is worth noting that in the abovementioned Loma Prieta earthquake observations, many failures occurred at the connection between the structure and the battered piles. These failures most probably were due to inadequate detailing at the connection and also improper connection of piles to pile caps (Mitchell et al. 1991). This implies that the bridge failures were not resulted from the poor performance of battered piles, but from poor connection design.

The Kobe earthquake occurred (M_w = 6.9) on January 17, 1995. Field evidence reveals that one of the few quay-walls that survived in a harbor of Kobe was a composite wall supported by battered piles. However, the nearby wall relying on vertical piles suffered very severe damage.

Berrill et al. (1997) investigated the near-failure response of the foundation of the Loading Road Bridge after the Edgecumbe earthquake (1997) in New Zealand. The foundation was embedded in liquefied sands. The authors state that “the motion towards the river was impeded by the buried raked-pile foundations which resisted the lateral spreading of the upper 6 m of soil toward the river channel."

These post earthquake observations indicate that the seismic role of battered piles should receive much greater attention.

2.3 ANALYSIS METHODS

In this section, the analysis methods used in the past in site response and FE analyses for laterally loaded piles and micropiles are discussed in the followings.

2.3.1 Site Response

Understanding the response of a site to seismic waves is a prerequisite for studying the dynamic soil-pile-structure interaction analysis of a pile-supported structure on a site. The problem of site response analysis is simple in nature. With a given geological profile and an input ground motion at a prescribed location, the objective of site response analysis is to determine the soil response at other locations. Since soil is a nonlinear material, the properties used to describe the soil must also reflect these "nonlinear" characteristics. The two most common methods used to describe nonlinear soil response are i.e. (a) the equivalent linear method, and (b) the nonlinear method.

2.3.1.1 Equivalent linear method

Idriss and Seed (1968) were the first to develop the equivalent linear method for modeling the nonlinear hysteretic behavior of soil. Due to its simplicity, it still remains the most popular method for site response analysis today. In this method, the maximum shear strain is multiplied by an "equivalent" constant strain ratio to obtain an "effective" strain that is assumed constant throughout the time history of excitation. Subsequently, the shear modulus and the damping associated with this constant strain are used for the entire history of shaking. This method is incorporated in the computer program, SHAKE (Schnabel et al. 1972), the latest version of which is SHAKE91 (Idriss and Sun 1992). Note that the method implies an approximation because constant values of shear modulus and damping are not representative since the shear modulus and damping change with varying strains throughout the duration of excitation.

2.3.1.2 Nonlinear method

Seed et al. (1993) showed that there was a significant difference between the results from an equivalent linear method and a nonlinear method at high levels of shaking. Moreover, high frequency response tends to be damped out by the use of linear viscous damping in the equivalent linear method (Martin and Seed 1982). Consequently, various researchers have fully studied nonlinear methods for site response analyses. Lok (1999) classifies the nonlinear models into three different classes, i.e. (a) mechanical models, (b) empirical models, and (c) plasticity models.

Mechanical models are the models in which the soil behavior is represented by a combination of simple mechanical elements, such as springs, dashpots, and sliders, placed in series or in parallel. Numerous researchers such as Iwan (1967), Joyner and Chen (1975), Taylor and Larkin (1978) have developed and incorporated these models to represent the soil hysteretic non-linearity.

Empirical models are models where empirically derived functions are used to describe the nonlinear stress-strain behavior of soils subject to cyclic loading. The commonly used empirical models include the Ramberg-Osgood (Ramberg and Osgood 1943), the Davidenkov, and the hyperbolic models (Kondner 1963). Researchers that have used empirical models to solve site response problems include Streeter et al. (1974), Lee and Finn (1978), Martin and Seed (1982), Lee and Finn (1991), and Pyke (1992).

Plasticity models are models based on the framework of plasticity theory to characterize the nonlinear hysteretic soil behavior during unload-reload cycles. Rodriguez-Marek (2000) cites that plasticity models provide the most flexibility in representing details of soil behavior, including yielding, pore pressure generation, and soil response to multi-directional loading paths. The use of plasticity theory in site response was motivated by the need for an improved constitutive law which would better represent stress-strain behavior near failure (Lok 1999). Plasticity based models have been incorporated into site response procedures by numerous investigators (e.g. Scott 1985, Finn 1988, Borja and Amies 1994, Li et al. 1998, Borja et al. 1999 and Rodriguez-Marek 2000).

2.3.1.3 Radiation boundary conditions

Usually, a soil site is assumed to consist of horizontal soil layers overlying a uniform half space (bedrock). The soil site often extends to great depths and it becomes necessary to introduce an artificial boundary at a certain depth. This boundary should account for the correct distribution of the reflected and transmitted energy at the bedrock-soil boundary. To account for these conditions, this boundary is represented by a viscous boundary (represented by viscous dashpots) in a FE model (Lysmer and Kuhlemeyer 1969). They defined the viscous boundary with these two equations:

$$\sigma = \rho V_p \dot{w} \tag{2.1}$$

$$\tau = \rho V_s \dot{u} \tag{2.2}$$

where σ and τ are the normal and shear stresses, respectively, at the boundary; ρ, V_s, and V_p are the mass density, P-wave velocity, and S-wave velocity, respectively; and $\dot{w}$ and $\dot{u}$ are the relative normal and tangential velocities across the boundary, respectively. They named this boundary as the standard viscous boundary. They have shown that this boundary can result in appropriate energy transmitting properties since the boundary can absorb both harmonic and non-harmonic waves due to its frequency independent absorption characteristic.

2.3.2 Soil-Structure Interaction

The response of pile-supported structures during dynamic loadings can be significantly influenced by the behavior of the interface between the structure and the foundation-soil or so called soil-structure interaction (SSI). At these interfaces, the bonding is not perfect. In reality, relative motions, such as sliding and gapping, occur at the interfaces between the pile and the soil when the pile-supported structure system is subject to static and dynamic loadings. These relative motions plus the resulting mechanisms of load transfer from the structure to the soil and vice versa result in strong nonlinear SSI. Consequently, analytical closed-form solutions become very difficult and numerical techniques, such as the boundary element method, the finite difference method, the finite element method (FEM), and the Beam-on-Nonlinear-Winkler approach are used. Since this research project focuses on the FE modeling of micropiles, the literature review concentrates on the FE modeling for laterally loaded piles and micropiles.

2.3.2.1 Finite element method

FEM provides a rigorous and flexible approach for modeling SSI problems. It can model almost any geometry configurations, soil and pile materials, load application, boundary conditions and etc. In addition, the soil continuity and the soil nonlinearity can be taken into account using FEM. However, the accuracy of the FEM results primarily depends on both the accuracy of the constitutive models and the use of appropriate input soil property values that are used in the FE models. Another drawback is the long computation time, especially for a three-dimensional (3-D) model. In the followings, the FE modeling of laterally loaded piles and micropiles conducted in the past will be described. The behavior drawn from the FE analyses of micropiles will be described in Section 2.4.3.

2.3.2.1.1 FEM of laterally loaded piles

Blaney et al. (1976) studied the dynamic response of a single pile embedded in a horizontally stratified soil deposit using FEM as an extension of the original work done by Kausel (1974) and Kausel et al. (1975). The soil around the pile was represented by the finite elements, the far field was represented by a “consistent boundary matrix”, and the pile was represented by a series of beam segments. The soils were assumed to be linear elastic resting on a rigid base.

Kuhlemeyer (1979) used a formulation for a good approximation to a bending FE to obtain an efficient FE solution to a 3-D problem of static and dynamic laterally loaded piles. Two layered systems were investigated for the static case, and a homogeneous, isotropic, and elastic half space soil profile was modeled for the case of dynamic loading.

Ostadan (1983) developed special inter-pile elements to model the piles and the soils together within the same element in two or three dimensions, as shown in Figure 2.1. In general, each element has 4 global nodes and 12 degrees of freedom (DOF) in two

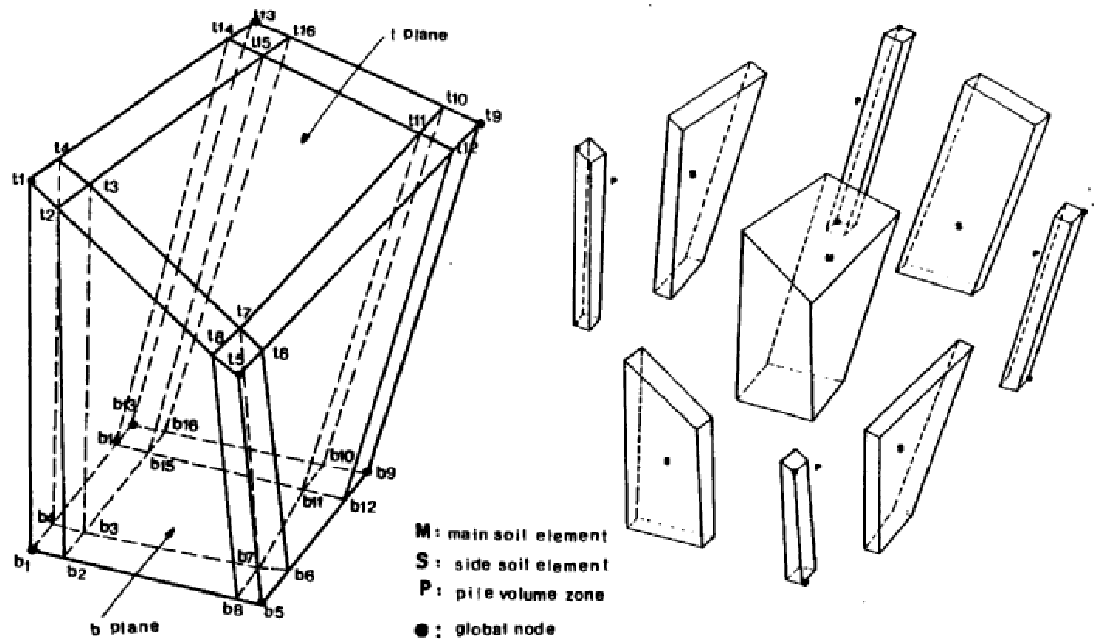

Figure 2.1 Inter-pile elements (after Ostadan 1983)

dimensions, and 8 global nodes and 48 DOF in three dimensions. Two methods, the full and the simplified methods, were developed based on the flexible volume method. Both methods were formulated in frequency domain. The non-linearity of the soil was taken into account using the equivalent linear method.

Trochanis et al. (1988) developed a 3-D finite element model to examine the effect of the nonlinear behavior of soils on the axial and lateral response of one pile and two piles due to monotonic and low frequency cyclic loading. The FE analysis was carried out using the computer code, ABAQUS. Figures 2.2 and 2.3 show the FE meshes for a single pile and two piles, respectively. Slippage and gapping were incorporated at the pile-soil interface using the pile-soil interface elements with Coulomb's friction theory. The pile and soils were modeled as 27-node quadratic isoparametric 3-D brick solid elements. In addition, the thin-layer interface elements were represented by two

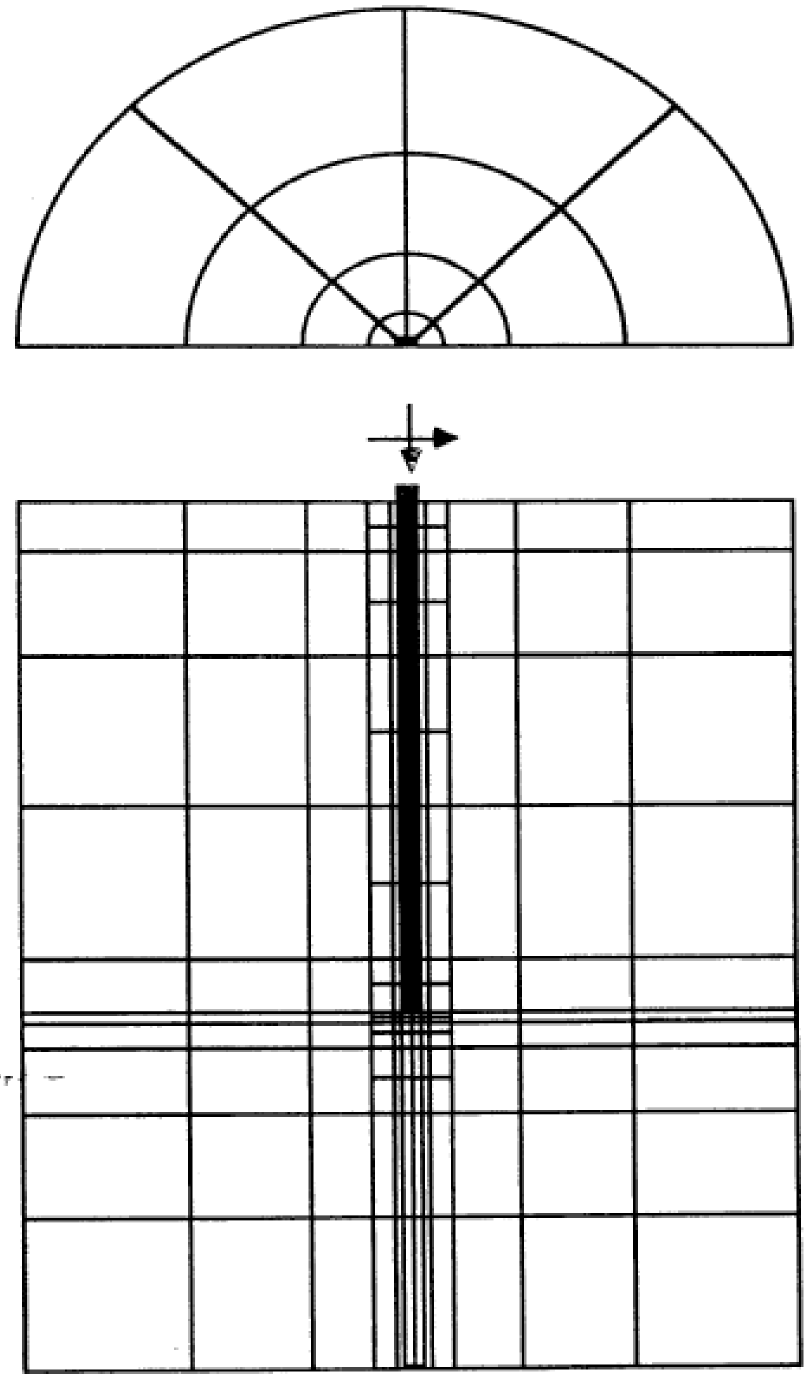

Figure 2.2 Finite element mesh for single pile analysis (after Trochanis et al. 1988)

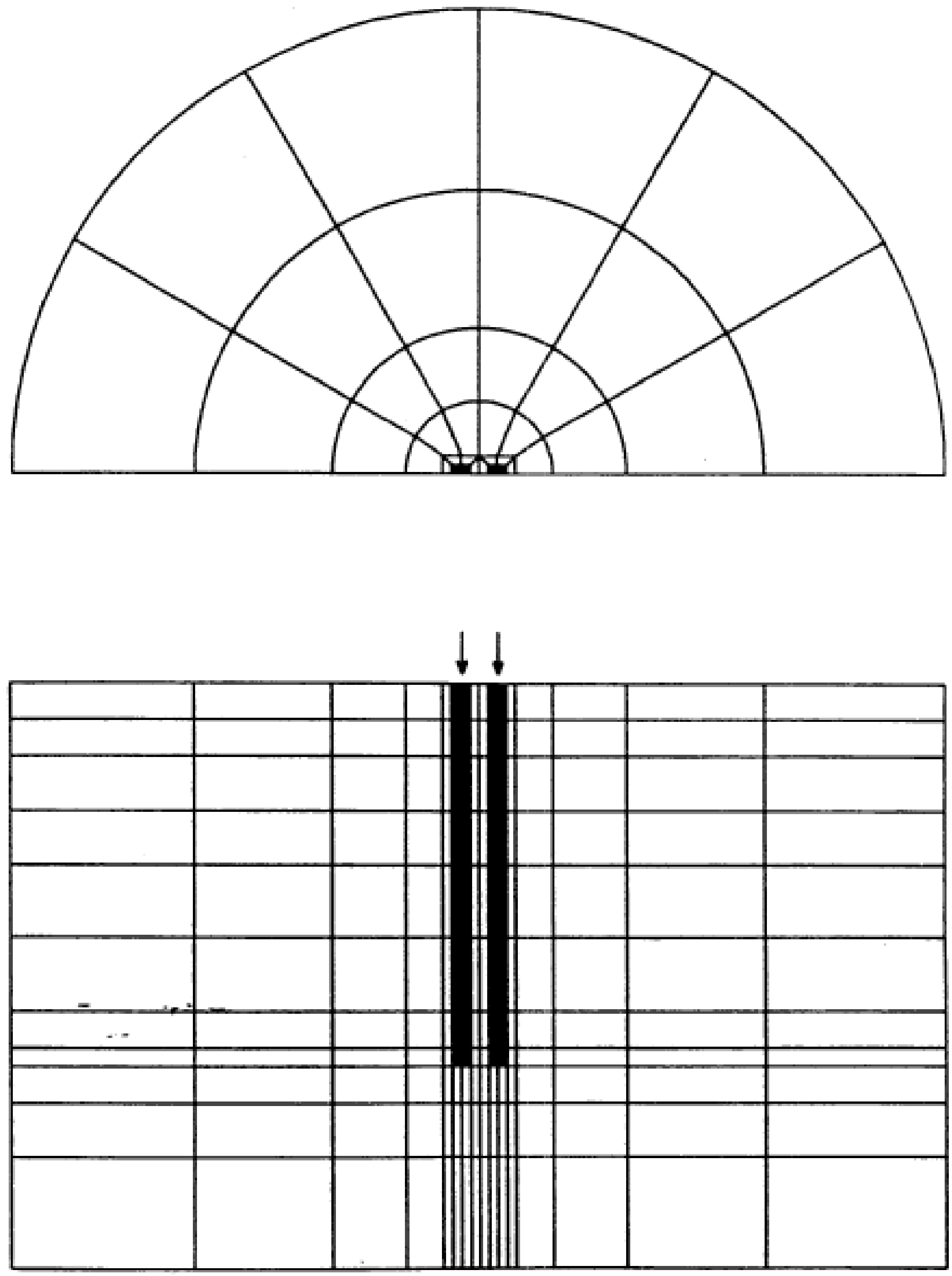

Figure 2.3 Finite element mesh for two piles analysis (after Trochanis et al. 1988)

9-node surfaces so that they are compatible with the 9-node sides of the 27-node bricks. These interface elements were assumed to have zero initial thickness unless otherwise specified. The piles were modeled with a linear elastic material and the soils were represented with both a classical linear elastic model and a nonlinear model. The nonlinear constitutive model used for the soils was an extension of the Drucker-Prager plasticity model. A simplified model was developed and it was capable to capture the main phenomenological features of the 3-D model.

Brown et al. (1989) derived p-y curves from the bending moments in a pile from a 3-D FE model. A simple elasto-plastic material model was used for the soil to characterize undrained static loading in clayey soils. The soil elements were linear elastic and perfectly plastic with a yield surface defined by the Von Mises criterion. The pile elements were linear elastic. At the pile-soil interface, thin elements which had a very low yield strength (uniaxial yield strength of 0.1 psi or 0.7 kPa) and a tension cutoff were used. In other words, slippage at the pile-soil interface with a relatively small friction, and gap formation behind the pile were allowed.

Brown and Shie (1990) developed a 3-D FE model of a laterally loaded single pile embedded in clay to perform parametric studies of several factors affecting the lateral response of piles. Figure 2.4 shows the 3-D mesh with the pile displaced laterally into the soil. The model developed was similar to the one by Brown et al. (1989) except that different soil models were used. Apart from the linear elastic soil elements, two different plasticity models were implemented for the soil. The first one was a simple elasto-plastic model with a constant yield strength Von Mises envelope. The model parameters used were 8 psi (55 kPa) uniaxial yield strength, 1600 psi (11,000 kPa) Young's modulus, and

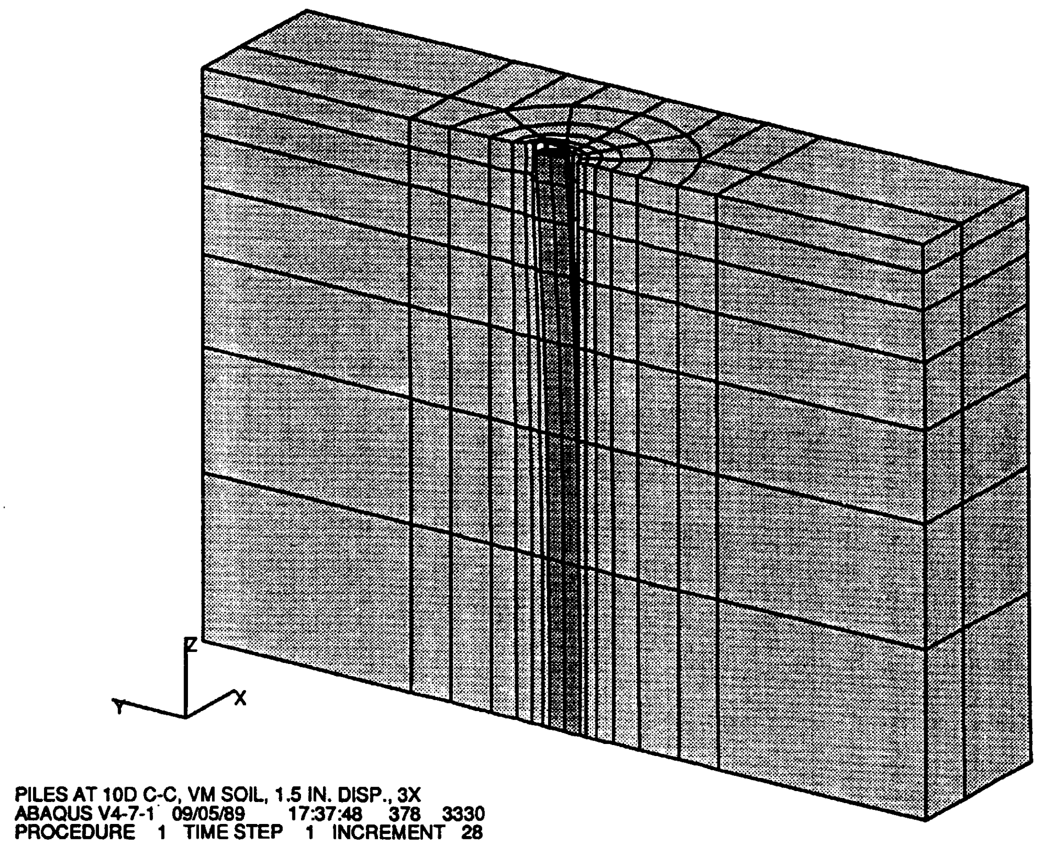

Figure 2.4 Three-dimensional finite element meshes for a laterally displaced single pile (after Brown and Shie 1990)

0.45 Poisson's ratio. The second one was an extended Drucker-Prager model with non-associated flow. An angle ψ of 0° was used which resulted in a constant volume plastic deformation. Besides the constitutive models for soils, in order to model the pile-soil interface more realistically, an elastic stiffness was included to allow for a small shear deformation before slippage took place.

A quasi 3-D model was developed for analyzing the dynamic soil-pile-structure interaction using a quasi 3-D FE program as shown in Figure 2.5 (Wu 1994, Finn et al. 1997, and Wu and Finn 1997). In this model, the dynamic response was assumed to be governed by the shear waves in the XOY and YOZ planes, and the compression waves in the direction of shaking, Y (refer to Figure 2.5). The deformations in the vertical direction and in the direction normal to shaking were neglected. Models with a single pile and a 2 x 2 pile group were developed for analyzing the centrifuge tests performed by Gohl (1991) at the California Institute of Technology (Caltech). In both models (single pile and pile groups), each pile was modeled as a 2-node beam elements and the soils were represented by 8-node brick elements. Dynamic soil-pile interaction was maintained by enforcing displacement compatibility between the piles and soils. Tension cutoff and shearing failure were incorporated in the program to simulate the gapping behind the pile and the yielding in the near field, respectively. Compatibility between the shear strains,

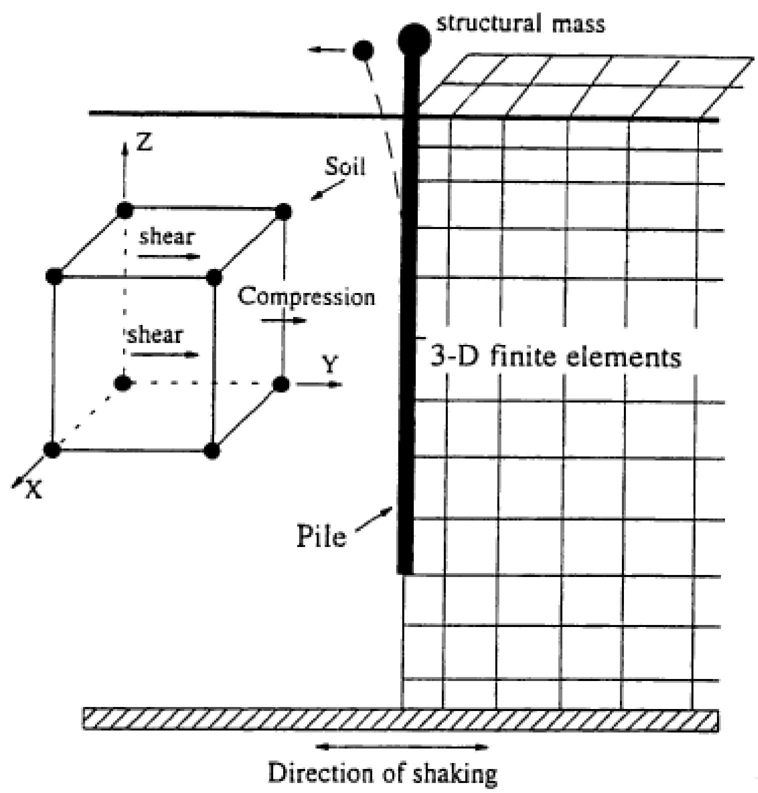

Figure 2.5 Quasi 3-D model of pile-soil response (after Wu 1994)

and the shear modulus and damping ratio was enforced at selected times during shaking, rather than at the end of shaking. This was done to ensure the time histories of shear modulus and damping ratios in each soil element were followed during the analysis, in contrast to the use of a single effective value for the entire time history that results from using the equivalent linear approach. In the single pile model, the superstructure mass was a rigid body and its motion was represented by a concentrated mass at its center of gravity. A very stiff beam element was connected between the superstructure mass and the pile head with its flexural rigidity 1000 times that of the pile. In the model of pile group, the rigid pile cap was modeled as a concentrated mass at the center of gravity of the pile cap and the mass was rigidly connected to the pile heads with a very stiff massless beam element.

Bransby (1999) carried out 2-D and 3-D analyses for a single pile subject to lateral head loading. The soil was modeled for two different cases, linear elastic soil and undrained power-law soil. Triangular elements were used for the meshes in the analyses. A linear distribution of pore pressure and a cubic distribution of strain were assumed to exist across the element (cubic strain triangles). The 2-D FE analysis was used to find the load-transfer relationships for a laterally loaded pile and suggested that these curves could be implemented as p-y curves in the analysis of a laterally loaded pile.

Teerawut (2002) studied the effect of the diameter of the piles on the p-y curves using full-scale tests and a 3-D FEM approach. The diameters that were evaluated in the full-scale tests range from 0.4 m to 1.2 m. The full-scale tests involved both vibration tests and lateral load tests. The type of the piles used was Cast-In-Drilled-Hole (CIDH) piles, which were installed in dense weakly cemented sand. Meanwhile, the 3-D FE models were developed using linear and nonlinear material models. The nonlinear model used was an elasto-plastic material with hardening using a 3-D J2 plasticity model with the Von-Mises yield criterion and a linear hardening law. The meshes for the model developed are shown in Figure 2.6. The soil was modeled using 8-node hexahedron (brick) solid elements and the pile was represented with a series of beam elements. The pile and soil elements were connected with a rigid link element. In order to reach the goal of the study, the EI of the pile, the pile length, and the Young's modulus of the soil were kept constant throughout the analysis. In the FE analysis, the pile diameter modeled ranged from 0.15 m to 1.07 m. Pinned supports were used at the bottom of the mesh and roller supports were implemented at four vertical planes as boundary conditions.

2.3.2.1.2 FEM of micropiles

Kishishita et al. (2000) performed a 2-D FEM analysis of micropiles subject to earthquake input motions. Figure 2.7 shows a typical grid used in the analysis. The soil was modeled with linear and nonlinear analyses. In the linear analysis, three soil models with different shear wave velocities were used in the upper layer (as Ground 2 in Figure 2.7). Four different types of piles were used in each of these linear soil models, such as precast piles, cast-in-situ piles, high-capacity micropiles, and high-capacity raking micropiles. Two earthquake input motions were used in the analyses, the 1940 El Centro Earthquake and the 1995 Kobe Earthquake. In the nonlinear analysis, only the soil model with the lowest shear wave velocity (the softest soil) was used. But, the nonlinear analysis was still conducted with the aforementioned four types of piles used in the linear case. A modified Ramberg-Osgood model was used for the soil, a tri-linear model for the cast-in-situ piles, a modified Takeda model for the pre-cast piles, and a bilinear model for high-capacity micropiles.

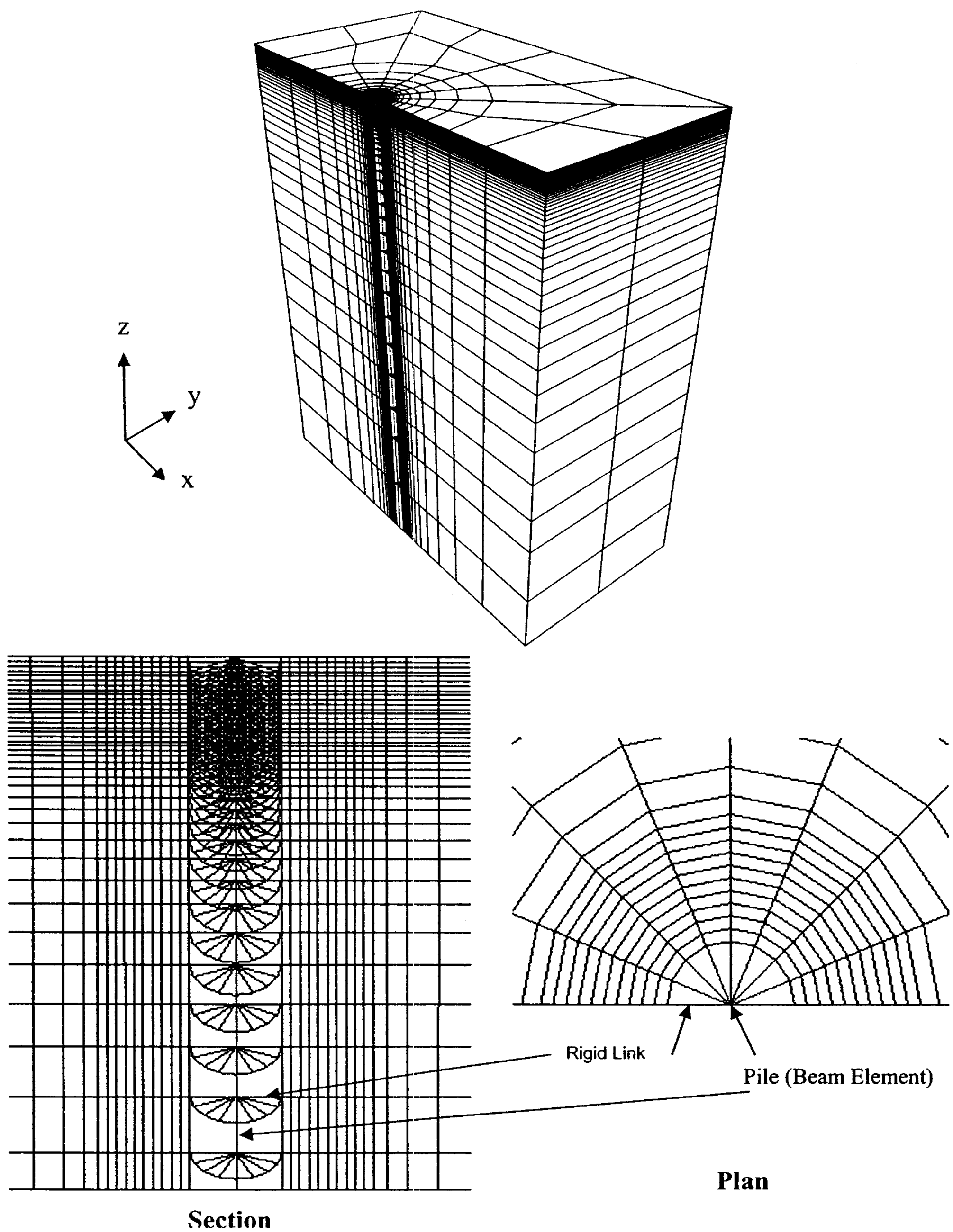

Figure 2.6 Finite element meshes for a single pile (after Teerawut 2002)

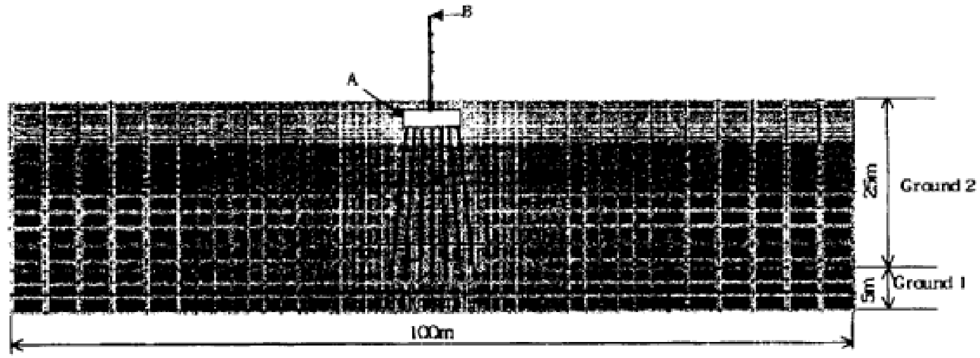

Figure 2.7 Typical 2-D finite element meshes used in the analysis (after Kishishita et al. 2000)

Shahrour et al. (2001) conducted a 3-D FEM analysis of micropiles using a finite element program, PECPLAS. Figure 2.8 illustrates the finite element meshes used in the numerical simulation. A single micropile and a micropile group supporting a superstructure were simulated in the analyses. The micropile group includes 1 x 3 micropiles, 3 x 3 micropiles, and 3 x 5 micropiles. These micropiles were modeled as embedded in a homogeneous soil layer overlaying a rigid bedrock. The soil-micropile-structure system was assumed to be elastic with Rayleigh material damping. The cross-section of the micropile was assumed to be square. The superstructure was modeled as a single degree-of-freedom composing of a concentrated mass and a column. The base of the soil mass was assumed to be rigid. Periodic conditions were imposed at lateral boundaries for the displacement field. The seismic loading was applied at the base of the soil mass as a harmonic acceleration with its frequency equal to the fundamental frequency of the soil.

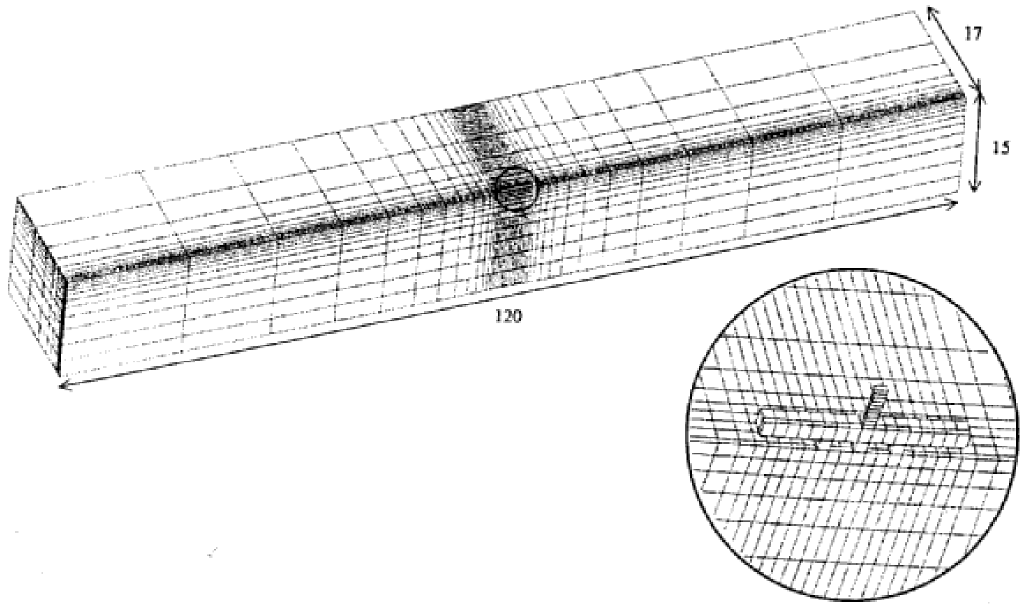

Figure 2.8 Finite element meshes for a single pile (after Shahrour et al. 2001)

Ousta and Shahrour (2001) studied the seismic behavior of micropiles in saturated soils by performing 3-D FEM analyses using PECPLAS. Figure 2.9 shows the finite element meshes used for a single micropile in the numerical simulation. The analyses were carried out using the (u-p) approximation for the fluid-soil coupling (Zienkiewicz et al. 1980) and a cyclic elastoplastic constitutive relation that was developed within the framework of the bounding surface concept for representing nonlinear soil behavior. Single micropile, 2 x 2 micropile group, and 3 x 3 micropile group were modeled in the analyses. The micropiles were assumed to be linear elastic. The base of the soil layer was assumed to be rigid and impervious. Water table was assumed to exist at the ground surface. Periodic conditions were applied at the lateral boundaries for both pore-pressure and displacements. Seismic loading was applied at the base of the soil layer with a harmonic acceleration.

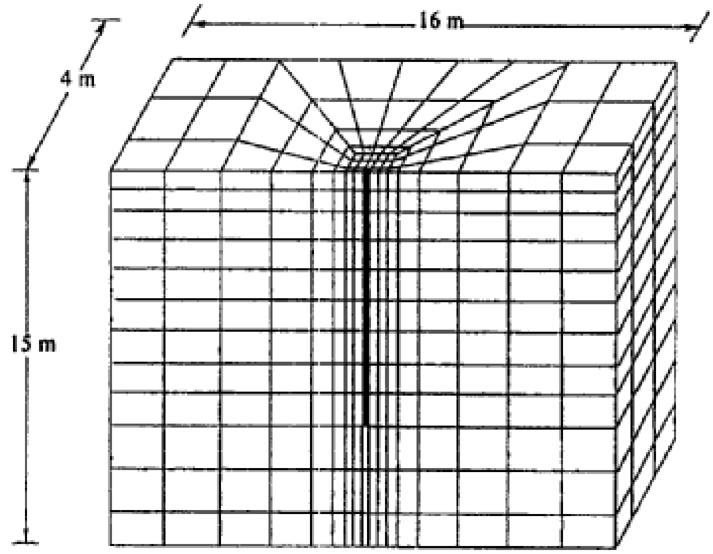

Figure 2.9 Finite element meshes for a single pile (after Ousta and Shahrour 2001)

Sadek and Shahrour (2003) investigated the influence of pile inclination on the seismic behavior of a micropile group. A 2 x 2 vertical micropile group and a 2 x 2 inclined micropile group with a 20° inclination to the vertical axis were used. Figure 2.10 shows the 3-D FE model and also the configuration of the inclined micropiles. As modeled in Shahrour et al. (2001) and Ousta and Shahrour (2001), the micropiles were embedded in a homogeneous soil layer underlain by a rigid bedrock. The soil-micropile-structure system was assumed to be elastic with Rayleigh material damping. The superstructure was a single degree-of-freedom system with a concentrated mass and column. A harmonic acceleration with the soil's fundamental frequency was applied at the base of the soil mass. However, the micropiles were modeled as 3-D elastic beam elements. The pile cap was modeled with a separation from the ground surface. The

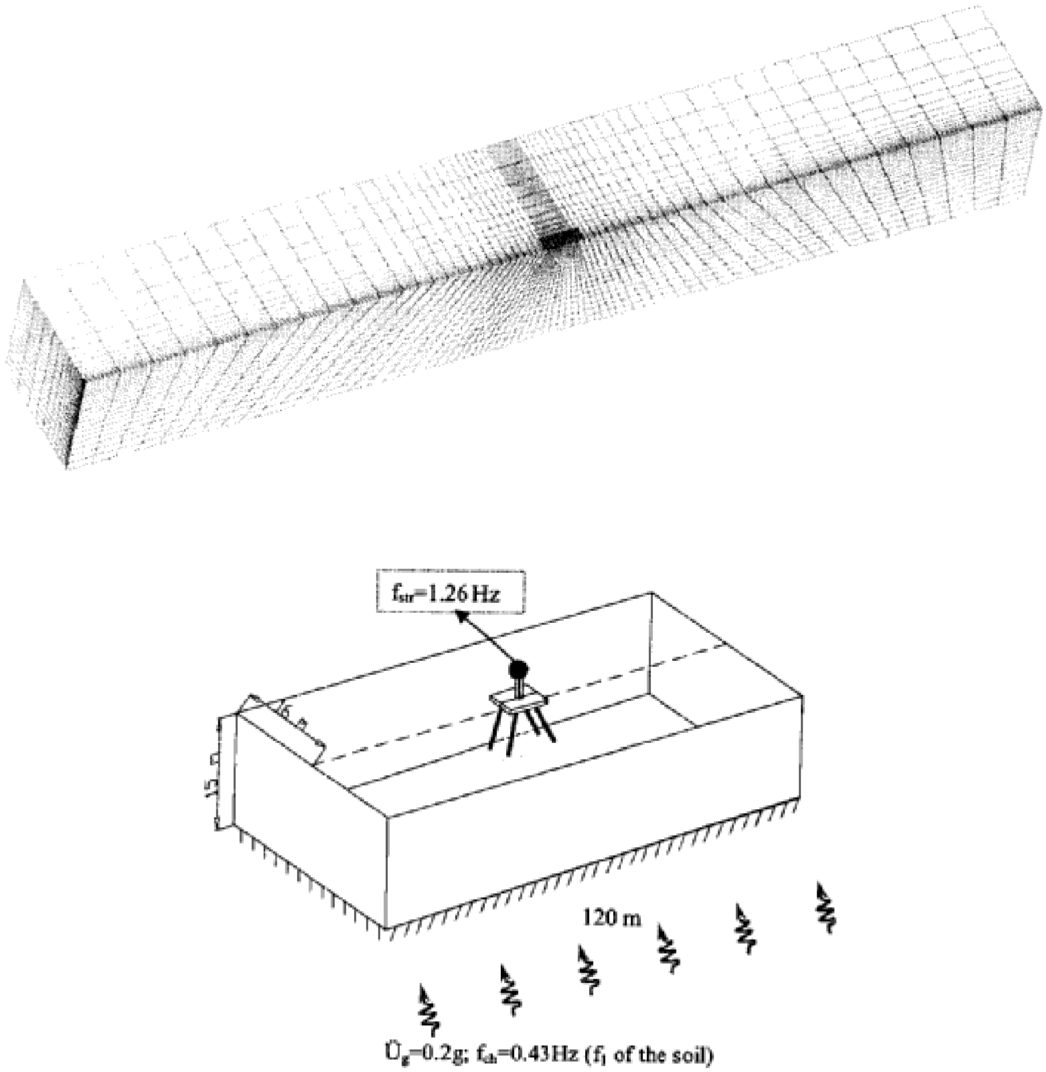

Figure 2.10 Three-dimensional finite element meshes and configuration for 2 x 2 inclined piles (after Sadek and Shahrour 2003)

Young's modulus of the soil, $E_s(z)$, was assumed to increase with depth, z, based on the equations below:

$$E_s(z) = E_{so}\left[\frac{p(z)}{p_a}\right]^{0.5} \tag{2.3}$$

$$p(z) = \left[\frac{(1+2K_o)}{3}\right]\rho_s z \qquad \text{if } z = z_o, p(z) = p(z_o) \tag{2.4}$$

where $p(z) =$ the mean stress due to the self-weight of the soil at the depth z

p_a = a reference pressure of 100 kPa

E_{so} = the Young's modulus of soil when $p = p_a$

K_o = the coefficient of lateral earth pressure at rest

z_o = the thickness of the soil layer that is closest to the surface with constant Young's modulus

2.4 BEHAVIOR OF MICROPILES

This section reviews the experiments that have been conducted on micropiles in recent years. In addition, parametric studies and observations based on the experimental and numerical results are also reviewed.

2.4.1 Introduction

Usually the design of a conventional pile is controlled by the external (i.e. ground-related) carrying capacity. Meanwhile, the design of a micropile is normally governed by the internal design, i.e. the selection of pile components (Bruce and Juran 1997). Due to sophisticated micropile installation methods, high grout/ground bond capacities with relatively small cross-section can be achieved. This highlights the fact that micropiles are designed to transfer the load to the ground through skin friction only.

2.4.2 Experiments on Micropiles

Yamane et al. (2000) conducted lateral and vertical load tests on micropiles. The study was focused on the vertical behavior of micropiles. However, they performed lateral load tests on seven single micropiles to study the bending capacity. Five of micropiles were composite micropiles, consisting of steel pipes, grout, and thread-lugged bars; another micropile is identical to the previous five but with coupling joints for the steel pipes. Another micropile is a plain steel pipe only.

Yang et al. (2000) carried out a series of shaking table tests to study the behavior of a single micropile under seismic loading. A hollow aluminium model micropile was inserted in a level dry sand deposit that was prepared in the laminar container bolted to the shake table. Sinusoidal vibrations were applied in the horizontal direction. Three SSI models were used to compute the pile response, i.e. a) the standard dynamic beam-on-Winkler-foundation model, b) the simplified beam-on-Winkler-foundation, and c) the 'Pilate' model.

Juran et al. (2001) performed a series of centrifuge tests on single micropile, micropile groups, and micropile network. Various micropile configurations, inclinations, number of micropiles, and loading levels were conducted. Finite difference programs, LPILE and GROUP, were used to simulate the representative centrifuge model tests. These tests were used to study the structure-soil-micropile behavior and also to investigate the response of the micropile systems subject to earthquake loading.

Geosystems, L.P. (2002) carried out lateral load tests on micropile groups and micropile networks at field to study their lateral performance. Different micropile numbers and configurations were installed and tested with different directions of lateral loading. Most of the micropiles installed were of the Ischebeck Titan type.

2.4.3 Parametric Study and Observations

The parametric study and observations made on micropile based on the past experimental and numerical results are presented as follows.

2.4.3.1 Relative rigidity E_p/E_s

The linear and nonlinear numerical analyses done by Kishishita (2000) show that the relative rigidity E_p/E_s influenced the horizontal displacements of the top structure and micropile cap; E_p and E_s are the Young's modulus of pile and soil, respectively. The displacement increased when the relative rigidity E_p/E_s increased (the soil becomes softer).

2.4.3.2 Pile inclination

The numerical results by Kishishita (2000), and the centrifuge tests by Juran et al. (2001) show that the horizontal displacement of the raked micropiles was smaller than that of the vertical micropiles.

The results by Juran et al. (2001) reveal that when the inclination of the micropiles increased, the fundamental frequency of the micropile system increased.

The results of the FE analyses by Sadek and Shahrour (2003) generally show that in a seismic analysis, when the inclination of the micropiles increased, the lateral stiffness, the bending moment, and the axial force increased, but, the shear force, and the lateral acceleration at the micropile cap and superstructure decreased.

2.4.3.3 Property of superstructure

Shahrour et al. (2001) state that the mass and the frequency of the superstructure affect the inertial interaction in SSI problems. Their results illustrate that in a single micropile analysis, as the mass of the superstructure increased, the lateral displacement, the bending moment, and the shearing force at the pile head increased. It was also observed that when the frequency of the superstructure became close to the loading frequency, the horizontal displacement of the superstructure, the bending moment and the shear force increased significantly. This observation shows the important role of the frequency of the superstructure in the design of micropile foundation systems.

2.4.3.4 Pile spacing

Shahrour et al. (2001) and Ousta and Shahrour (2001) show that the bending moment increased with increasing micropile spacing. This increase is attributed to frame action. However, Shahrour et al. (2001) show that the influence of the micropile spacing on the distribution of shearing forces is negligible.

2.4.3.5 Number of piles

Similar to the case of pile spacing, the results from the FE analyses by Shahrour et al. (2001), and Ousta and Shahrour (2001) show that when the number of piles increased, the bending moment increased. However, unlike the case in pile spacing, the shear force increased with the increase in the number of piles.

2.4.3.6 Shaking intensity

The shake table test results by Yang et al. (2000) show that with weak base shaking (< 0.25g), the micropile follows the motion of the soil and the maximum bending moments occur near the sand surface. This indicates that inertial effect plays an important role in micropile bending during shaking.

However, during strong base shaking (≥ 0.25g), the micropile did not follow the motion of the soil and the effects of the nonlinear soil behavior clearly affected the seismic micropile behavior. Moreover, under strong base shaking, the maximum bending moments occurred near the pile bottom, which indicated that the micropile bending was dominated by the deformation of surrounding soil and the inertial effect from the pile head could be ignored. Yang et al. (2000) also commented that the frequency domain method might not be suitable and a time history analysis is needed for strong shaking or high excitation frequencies.

2.4.3.7 Pile type

The numerical analyses by Kishishita (2000) reveal that the horizontal displacements of the top structure and micropile cap were not affected by the pile type. The horizontal response at these two places was almost the same even though four different pile types were used in his analyses, i.e. precast piles, cast-in-situ piles, high-capacity micropiles and raked high-capacity micropiles. He claims that this phenomenon occurs because the micropile cap follows the response of the soil.

2.4.3.8 Pile linearity and nonlinearity

A trilinear model was used for cast-in-situ pile, a modified Takeda model for pre-cast pile and a bilinear model for high-capacity micropile in the numerical analyses performed by Kishishita (2000). The numerical results show that during a real earthquake (e.g. the Kobe Earthquake input), the high-capacity micropiles maintained linearity while the precast and cast-in-situ piles yielded. Therefore, high-capacity micropiles provide high ductility and resistance against earthquakes.

2.4.3.9 Group effect

The numerical analyses by Shahrour et al. (2001) and the centrifuge test data by Juran et al. (2001) illustrate that a positive group effect was observed in micropile group. The numerical results by Shahrour et al. (2001) show that the positive group effect was observed for the kinematic interaction because the maximum bending moment at the central part (around mid-height of micropile) decreased when the number of micropiles increased from 9 (3 X 3) to 15 (3 X 5). Meanwhile, the experimental data (in cohesionless soil) by Juran et al. (2001) illustrate the positive group effect for selected frequency of excitation (a=0.3g) which caused a reduction in bending moments and displacements of micropile groups with s/D=3 as compared to the data from s/D=5.

2.4.3.10 Load distribution in micropile group

Internal forces are influenced by the position of the micropile in a micropile group. In other words, seismic loading is not distributed equally in the micropile group. The experimental data of Juran et al. (2001) and the numerical analyses of Shahrour et al. (2001) clearly show that the loads taken by the corner micropiles are higher than the one taken by the center micropile.

2.4.3.11 Coupling joints

The field test results by Yamane et al. (2000) reveals that the micropile (steel pipes, grout, and thread-lugged bars) with coupling joints provided higher strength and stiffness as compared to the ones of an identical micropile without coupling joints.

2.4.3.12 Pile diameter

The full-scale test results by (Teerawut 2002) illustrate that the effect of the pile diameter on the stiffness of p-y curves is affected by the relative density of the sand. In the case of dense weakly cemented sand, the effect of the pile diameter on the p-y curves was insignificant before the soil reaches its ultimate resistance. However, in the case of loose sand, the stiffness of the p-y curves increased with an increase in pile diameter. In other words, increasing the relative density will decrease the pile diameter effect on the p-y curves apparently.

It was also observed that as the pile diameter increased, the natural frequency of the soil-pile system increased due to an increase in soil-pile system stiffness.

Besides, as the pile diameter increased, the damping ratio increased due to the fact that the damping of the soil primarily comes from the radiation damping which is dependent on the contact area and the excitation frequency. The radiation damping increases with an increase in the contact area between the pile and soil, and also with an increase in the excitation frequency.

2.5 DESIGN GUIDELINES

Up to the date the author wrote this thesis, there are two complete design guideline documents on micropiles published in the United States. The first one was published by the U.S. Department of Commerce of National Technical Information Service in 1997. It has four volumes and the second volume (named "Drilled and Grouted Micropiles – State-of-Practice Review: Volume 2: Design") reviews the state-of-practice of micropile design. The second design guideline document (Micropile Design and Construction Guidelines: Implementation Manual) was published by the Federal Highway Administration (FHWA) in 2000. In this section, a very brief summary of the design guidelines of micropiles on the geotechnical aspects from these two documents will be presented below.

2.5.1 Drilled and Grouted Micropiles – State-of-Practice Review: Volume 2: Design

In this document, a new and rigorous classification criteria for micropiles was developed. The classification system is based on two criteria, (1) philosophy of behavior (design), and (2) method of grouting (construction). Using the first criteria, micropiles are classified into two types, i.e. CASE 1 and CASE 2 micropiles. CASE 1 micropiles refers to the micropile elements (single or group) that are loaded directly. The load is primarily resisted structurally by the steel reinforcement and geotechnically by the grout/ground bond zones of the individual piles. CASE 2 micropiles are the elements that circumscribe and internally reinforce the soil behaving like a reinforced soil composite (mass), as opposed to individual piles, to resist the applied loads. Thus, they are usually more lightly reinforced as compared to CASE 1 micropiles.

To evaluate the geotechnical capacity of micropile subject to axial, lateral, or combined loading, appropriate determination of grout/ground interface parameters and the initial stress state in the ground after micropile installation (mainly because of the grouting pressure) are required. The geotechnical design guidelines for single micropile subject to axial loading will base on the criteria of ultimate load capacity and vertical displacement control. Similarly, ultimate load capacity and horizontal displacement control will be used for the one subject to lateral loading. On the other hand, the design methods used can be consisted of (a) empirical methods for ultimate load prediction, (b) load-transfer interface models for vertical displacement estimation, and (c) site-specific loading tests.

For a single micropile design, there are no specific design codes for types A, B, C, and D micropiles in the United States (please refer to the document for the definition of these four types of micropiles). For type A micropiles, the design usually requires compliance with specifications that have been established for large-diameter drilled shafts (e.g. AASHTO 1992, Caltrans 1994). Meanwhile, the British Standard BS 8081 (1989), referring to the work of Littlejohn and Bruce (1977), and the French code (CCTG 1993), following the field correlations by Bustamante and Doix (1985), would apply to types B, C, and D micropiles.

Due to the absence of design codes relating to lateral performance of micropiles, the current design practice will usually require lateral load tests that follow the present codes for drilled shafts (e.g. UBC 1994, BCNYC 1991, AASHTO 1992). For preliminary design, the design codes, like API (1988), CCTG (1993), and Caltrans (1994), referring to research works by Matlock (1970) and Reese et al. (1994) will be followed.

Similarly, there are no design codes developed for micropile groups and networks in the United States. As in the case of single micropiles, the design criteria used for micropile groups and networks is the ultimate load capacity and the displacement control. The ultimate load capacity and displacement are influenced by the pile spacing, soils, site conditions, types of micropiles and pile cap. It is highlighted that the group efficiency factor is significantly dependent on the pile installation technique.

There is no good reference of design codes can be used for estimating the ultimate axial loading capacity of micropile groups and networks since the laboratory and full-scale test results from various investigators (Lizzi 1978, Plumelle 1984, Maleki 1995) exhibit contradictory group effects. However, one of the design codes "mentioned" in the report is AASHTO (1992), following Terzaghi and Peck (1948), and this method has been used for conventional piles. It estimates the axial group capacity as the lesser of (a) the sum of the ultimate capacities of the individual piles in the group, or (b) the axial load capacity for the block failure of the group (a rectangular block). The French CCTG (1993) recommendations can be adapted for a preliminary conservative calculation of the group efficiency factor as its suggested Converse-Labarre group efficiency equation gives conservative results.

To estimate micropile group vertical displacement, several approaches have been adopted:

a) empirical correlations relating the vertical displacement of pile groups to that of a single pile (e.g. Skempton 1953, Vesic 1969, Meyerhof 1976, Fleming et al. 1985),

b) continuum elastic methods using the Mindlin's equations (1936) (e.g. Butterfield and Banerjee 1971, Randolph and Wroth 1979, Poulos and Davis 1980, Yamashita et al. 1987),

c) load-transfer models and hybrid methods (e.g. O'Neill et al. 1977, Chow 1986, Lee 1993, Maleki and Frank 1994), and

d) a pure shear interface model assuming no radial movement developed by Randolph and Wroth (1979).

To estimate the ultimate lateral capacity of micropile groups, similar to the case of axial group capacity, one of the ways mentioned is the lesser of a) number of micropiles times the lateral load capacity of a single pile in the group, or b) lateral load capacity of an rectangular block containing the micropiles and the soils between them. To account for the group effect on the lateral load capacity and pile deflections, different design codes (e.g. AASHTO 1992, CCTG 1993, BOCA 1990) specify different minimum spacing between the piles. However, when the piles are close to each other, the interaction between them has to be considered. Group efficiency factors for side-by-side piles and line-by-line piles were mentioned in the report as well.

To estimate the lateral load-deflection of a pile group, one of the common approaches is the usage of p-y curves (e.g. Reese et al. 1994, Brown et al. 1987, Bogard and Matlock 1983). Reese et al. (1994) suggest that the most rational way of analyzing the lateral load-displacement response of pile groups is the use of p-y curves for a single pile modified with the use of "softening" factors to allow for group interaction effects.

It seems like there is no recommendation made from any design codes for the design guidelines for the micropile networks. The reticulated micropile network design concept developed by Lizzi (1982) is still new in foundation engineering and there is no sufficient field data to evaluate this concept.

2.5.2 Micropile Design and Construction Guidelines: Implementation Manual

In this manual, the Service Load Design Method (SLD) and the Load Factor Design Method (LFD) are used for micropiles in accordance with the 1996 AASHTO Standard Specifications for Highway Bridges, 16th edition. The micropiles are usually assumed to transfer their load to the ground through grout-to-ground skin friction without the contribution from the end bearing, except when the micropile is embedded on rock. The dependence on skin friction is geotechnically equivalent in tension and compression. There are no step-by-step design procedures for micropiles outlined in this manual. However, the manual presents several geotechnical micropile design guidelines and considerations.

The guidelines include the estimation of load transfer (grout-to-ground bond) parameters for different soil layers, the determination of the micropile bond length to support the loading, and the evaluation of the group effect for axially loaded micropiles. This manual emphasizes that the geotechnical load capacity of a micropile is highly sensitive to the processes used during pile construction, especially the techniques used for drilling the pile shafts, flushing the drill cuttings, and grouting the pile. Table 5-2 in this manual tabulates the estimated unit values for grout-to-ground bond nominal (ultimate) strengths for various installation methods and ground conditions. These values are estimated based on the experience of the local Contractors or Geotechnical Engineers. Based on the estimated grout-to-ground bond strength, the bond length is determined to support the structural loading. Usually, the group effects in micropiles are beneficial, especially in granular soils, due to the compaction of the soil from pressure grouting.

The geotechnical considerations include:

a) prediction of anticipated structural axial displacements,
b) long term ground creep displacement,
c) settlement of pile groups,
d) lateral load capacity,
e) lateral stability (buckling), and
f) downdrag and uplift considerations.

When the micropile designs require strict displacement criteria, it may be necessary to predict pile stiffness and deflection limits during design and confirm the predictions through field load tests. Large creep deformation can occur in fine-grained clayey soils. Therefore, extended load testing should be performed to verify performance within acceptable limits. Micropiles in a group can cause additional displacement due to the consolidation of the soil layer, especially the cohesive ones below the micropile group. This is because when a single pile transfers its load to the soil in the immediate vicinity of the pile, a pile group can distribute its load to the soil layer below the group. The behavior of a laterally loaded micropile depends on the properties of the micropile such as diameter, depth, bending stiffness, fixity conditions of the pile in the footing, and on the properties of the surrounding soils. Considerations must be made to the combined stresses due to the bending induced by the lateral displacement and axial loading. The lateral capacity can be increased by inclining the micropiles and installing an oversized upper casing. The buckling of micropiles is only of concern in soils with the poorest mechanical properties, like loose silts, peat, and soft unconsolidated clays. The micropiles that extends above the ground or those that are subject to scour should be checked for buckling reduction. The small surface area of a micropile reduces the ability of the settling or expansive soils to transfer loads to micropiles. However, the use of battered micropiles should be avoided in the settling or expansive soils because the settlement or expansion will induce excessive lateral loading on the micropiles.

CHAPTER 3
NUMERICAL MODELING

3.1 INTRODUCTION

In this chapter, the non-linear constitutive model used for the soil in the FE models will be discussed initially. Dynamic soil models for site response analyses were developed and validated against a well-validated software, SHAKE. Subsequently, the FE models for single micropile and micropile groups under static and dynamic loading will be presented.

3.2 SOIL MODEL

The response of soils subject to seismic loading can be highly nonlinear. Therefore, soil non-linearity should be taken into account in site response and SSI analyses. In the FE method, soil non-linearity is represented by mathematical relationships that describe the non-linear stress-strain behavior of the soil. Generally, soil models based on the plasticity theory are used. The model developed by Borja and Amies (1994) has been used in this study. This model has been presented to work well in cohesive soils under undrained cyclic loading (Borja and Amies 1994; Borja et al. 1999; and Rodriguez-Marek 2000).

The model was constructed through the reformulation of the Dafalias and Popov (1977) bounding surface plasticity model to accommodate multi-axial stress reversals and cyclic loading in clays within a total stress approach. The model is based on the concept of a vanishing elastic region undergoing pure translation inside a bounding surface, and a modulus hardening function which changes with stress distance of the elastic region from the unloading point (Borja and Amies 1994). The core of the model is the development of the general criteria for loading and unloading for three-dimensional (3-D) stress condition that assumes the hardening modulus decreases monotonically with deformation with continued loading. Therefore, the model can be implemented into 3-D non-linear finite element analysis codes.

3.2.1 General Description

Figure 3.1 shows a general framework of the model where two functions, F and B, exist in the model, with the condition that F is always inside B. F represents the yield function and B acts as the bounding surface. The vanishing of the elastic region corresponds to the limit when the size of F approaches zero. The location of the vanishing elastic region is represented by the stress deviation tensor σ'.

Inside the bounding surface, a point F_o is assumed to exist with coordinates σ_o' in a 3-D stress space. F_o represents the point where the soil experienced the most recent elastic unloading. Therefore, F_o is identified as the point where the hardening modulus H' is infinity. Similarly, B is identified as the surface where the hardening modulus H' reaches a limiting value, H_o. In other words, the soil is assumed to behave elastically at point F_o and to follow a linear kinematic hardening plasticity law at the bounding surface B. For any point that resides between point F_o and surface B, its hardening modulus is interpolated between the values of infinity at F_o and H_o on surface B. A yield surface F is defined inside the bounding surface passing through that point which is defined by the current stress tensor σ'. The interpolation of the hardening modulus H' is generated from well-accepted one-dimensional models for soils (Borja and Amies 1994).

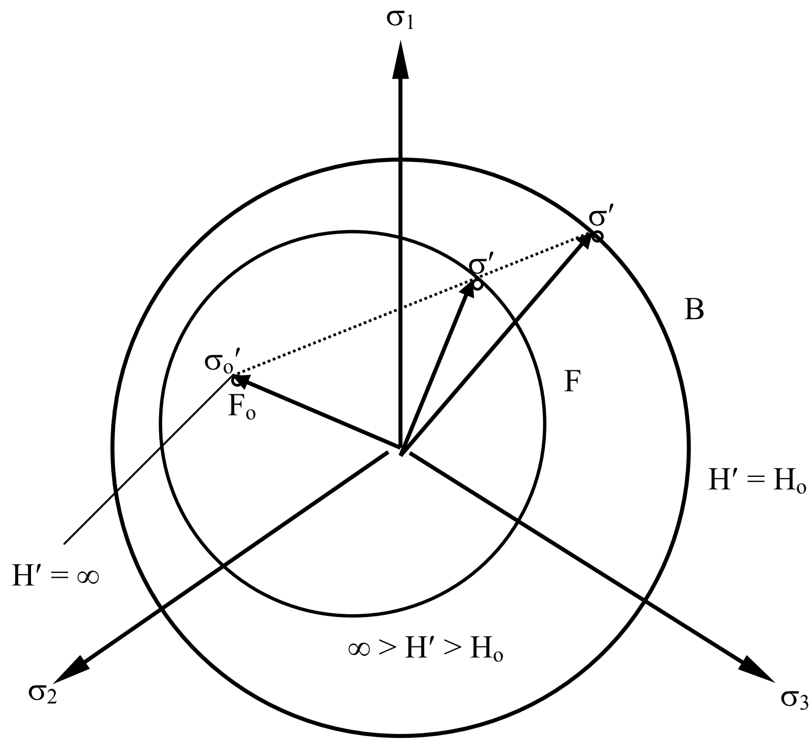

Figure 3.1 Schematic diagram of the bounding surface plasticity model showing unloading point F_o, yield surface F, and bounding surface B on π plane. Contours of constant H' are centered about F_o where H' is infinite, decreasing to H_o on B (Adapted from Borja and Amies 1994)

3.2.2 Mathematic Formulation

Only the key equations of the model will be presented and briefly discussed here. For the details of the mathematical development of the model, please refer Borja and Amies (1994), Borja et al. (1999), and Rodriguez-Marek (2000).

The tensorial strain rate consists of the elastic and plastic strain rates:

$$\dot{\varepsilon} = \dot{\varepsilon}^{e} + \dot{\varepsilon}^{p} \tag{3.1}$$

where ε is the total strain tensor and the dot indicates the differentiation with respect to time. From the generalized Hooke's law, the total stress tensorial stress rate can be obtained through its relationship with the elastic strain rate:

$$\dot{\sigma} = c^e : (\dot{\varepsilon} - \dot{\varepsilon}^p) \tag{3.2}$$

where σ is the total stress tensor and c^e is the rank four elasticity tensor.

Plastic strains are associated with the yield surface *F* and the bounding surface *B*. The yield function *F* has the form of a J_2 type plasticity model:

$$F = \xi' : \xi' - r^2 = 0 \tag{3.3}$$

where $\xi' = \sigma' - \alpha =$ translated stress deviation tensor; $r =$ radius of the yield function; $\sigma' =$ deviatoric part of σ; and $\alpha =$ deviatoric back stress tensor representing the center of *F*.

Similarly, the bounding surface *B* has the form:

$$B = \sigma' : \sigma' - R^2 = 0 \tag{3.4}$$

where *R* is the radius of the bounding surface *B*.

In soils, the radius *R* can be related to the undrained shear strength, s_u, which is determined from an unconfined compressive strength test on a normally consolidated clay:

$$R = \sqrt{\frac{8}{3}} \times s_u \tag{3.5}$$

Via a series of mathematical material mechanics derivations (see Borja and Amies 1994), a rate constitutive equation is obtained as:

$$\dot{\sigma} = K \quad tr(\dot{\varepsilon})\, \boldsymbol{1} + 2\ \mathrm{G} \left(1 + \frac{3G}{H'}\right)^{-1} \dot{\varepsilon}' \tag{3.6}$$

where K is the elastic bulk modulus, $\boldsymbol{1}$ is the rank two identity tensor, and tr is the trace operator.

3.2.3 Hardening Function

The hardening modulus H' is defined in such a way as to fit accepted one-dimensional cyclic stress-strain relationships. Moreover, the criteria for loading and unloading conditions is clearly defined since the plastic deformations are known to increase proportionally with the distance from the point of the recent unloading (Borja and Amies 1994). The hardening modulus is obtained via an interpolation from the elastic value at the recent unloading point (H' =infinity) to a limiting value of H_o at the bounding surface B.

An exponential hardening modulus has been chosen for this study. The interpolation for the hardening modulus has the form:

$$H' = h\kappa^{m} \tag{3.7}$$

where h is the modulus parameter that controls the rate of shear stiffness degradation; m is the dimensionless quantity that controls the shape of the secant modulus versus the strain amplitude curve; and κ is a dimensionless scalar quantity that satisfies the condition

$$\left\| \sigma' + \kappa\left(\sigma' - \sigma'_o\right) \right\| = R \tag{3.8}$$

3.2.4 Loading and Unloading Conditions

It is important to define whether a stress increment constitutes loading or unloading. The loading and unloading conditions for stresses on the bounding surface are given by the Kuhn-Tucker conditions (Simo and Hughes 1998). According to this condititION, the unloading condition on the bounding surface is postulated when

$$\lambda > 0 \text{ and } f < 0 \tag{3.9}$$

where λ is the consistency parameter, and f is the given yield surface. The numerical implementation of the loading and unloading conditions follows commonly used return mapping algorithms (Simo and Hughes 1998).

The definition for the loading and unloading conditions for a point inside the bounding surface is more complicated. Borja and Amies (1994) define the unloading as the condition when the direction of the load step results in the hardening modulus to increase. Consequently, the loading condition is postulated as

$$-\frac{(1+\kappa)\sigma' + \kappa(1+\kappa)(\sigma' - \sigma_o')}{\sigma' : (\sigma' - \sigma_o') + \kappa\|\sigma' - \sigma_o'\|^2} : \dot{\varepsilon}' > 0 \tag{3.10}$$

Upon unloading, the position of F_o will be shifted to the current position that is defined by the stress tensor σ'. For the numerical implementation of Equation 3.10, see Borja and Amies (1994).

3.2.5 Model Parameters

The parameters of this constitutive model and the other parameters used along with the numerical implementation of the model are briefly discussed in this section. There are eight inputs that are needed to completely define the model so that the model can be executed in the program. The first three inputs are shear wave velocity, v_s, Poisson's ratio, ν, and soil density, ρ. The fourth and fifth inputs are the exponential degradation parameters, h, and m. The parameter h controls the rate of shear stiffness degradation, and m controls the shape of the secant modulus versus strain amplitude curve. These two parameters are modified in order to match the curves of the shear modulus reduction and the soil damping increase versus shear strain of a soil. Generally, an increase in m results in an increase in the curvature of the shear modulus reduction curves, while an increase in h causes a shift to the right of shear modulus reduction and damping curves (Rodriguez-Marek, 2000). The sixth input is β, a trapezoidal integration parameter. The seventh input is R, the radius of the bounding surface. The value of R is defined as $R = \sqrt{8/3}s_u$, where s_u is the unconfined compressive strength of the soil. Finally, the eighth input is H_o, a model parameter that defines the plastic modulus after the soil has reached the bounding surface. H_o can be obtained from the slope of the stress-strain curve at large strains.

3.3 MODELING OF SEISMIC SITE RESPONSE

3.3.1 FE Models for Seismic Site Response

Four dynamic FE models were developed to perform the site response studies using the FEM software, ABAQUS. The progressive development of these four FE models were designed in such a way that the fourth model is appropriate to be used in SSI analyses (with a micropile installed in the soil) and the FE model has negligible boundary effects on the micropile response. The results from these models were verified against the well-validated equivalent linear code, SHAKE.

Initially, a 3-D FE mesh was built to represent a soil with a height of 10 m (Figure 3.2). The mesh has a constant unit area throughout the height and consists of ten 8-node tri-linear brick elements. Throughout the entire mesh, two directions of motion were restrained so that each node has only one degree-of-freedom. Horizontal displacement inputs were applied at the four bottom nodes using the Yerba Buena records from the 1989 Loma Prieta Earthquake. A linear elastic model was used for the soil and no material damping was added. The Young's modulus and Poisson's ratio used were 5.772 x 10^7 N/m^2 and 0.48, respectively and the density used was 1950 kg/m^3.

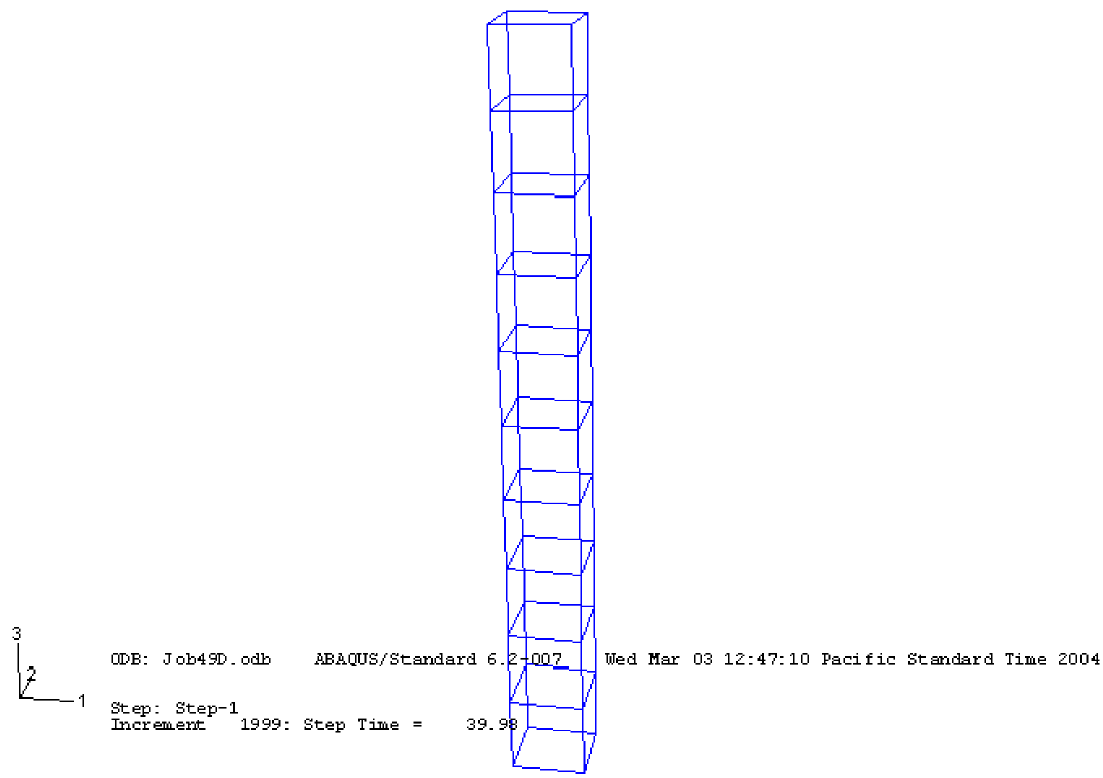

Figure 3.2 Dynamic FE soil column model

The second FE site response model used the same mesh as the first model but the constitutive model developed by Borja and Amies (1994) was used for the soil, and dashpots were installed at the four bottom nodes to simulate a viscous transmitting boundary (see Section 2.3.1.3). The model and numerical parameters are given in Table 3.1 The shear modulus reduction and damping curves associated with these parameters are presented in Figure 3.3.

Parameter	Value
v_s	100 m/s
ν	0.48
ρ	1950 kg/m^3
h	0.8
m	0.8
β	0.5
R	0.02
H_o	1×10^{-6}

Table 3.1 Model and numerical parameters used for the FE models in site response analyses

Note that the Borja and Amies (1994) model predicts only hysteretic damping. Soils, however, also exhibit viscous damping at small strains. Material damping was thus added to simulate the small strain damping of soils. In this study, Rayleigh's damping was used for this purpose. Figure 3.4 illustrates the dependency of Rayleigh damping on frequency. The Rayleigh's damping ratio coefficients, α_1 and α_2, are the stiffness and mass proportional damping ratios, respectively. To reduce the frequency dependency of damping around the frequencies of interest, α_1 and α_2 are defined as follows:

$$\alpha_1 = \frac{2\xi}{\omega_1 + \omega_2}$$

$$\alpha_2 = \frac{2\omega_1\omega_2\xi}{\omega_1 + \omega_2} = \omega_1\omega_2\alpha_1 \tag{3.11}$$

where ω_1 and ω_2 are two reference natural frequencies; and ξ is the desired damping ratio (with reference to critical damping). Usually, ω_1 is the fundamental natural frequency of the soil column and ω_2 is chosen in such a way that the resultant damping ratio matches the desired damping ratio ξ. Figure 3.4 implies that between ω_1 and ω_2, the resulting damping ratio is lower than the desired critical damping ratio and out of this range, the system is over-damped (Rodriguez-Marek 2000). In this site response analysis, α_1 = 0.00042441, α_2 = 0.52359878, and ξ = 2.0 % are used.

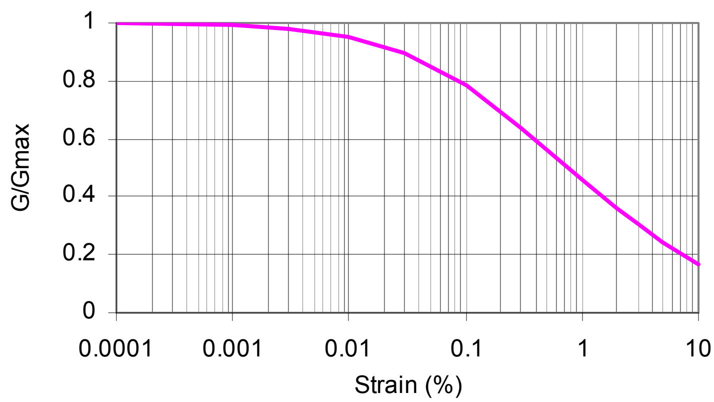

(a) Modulus reduction curve

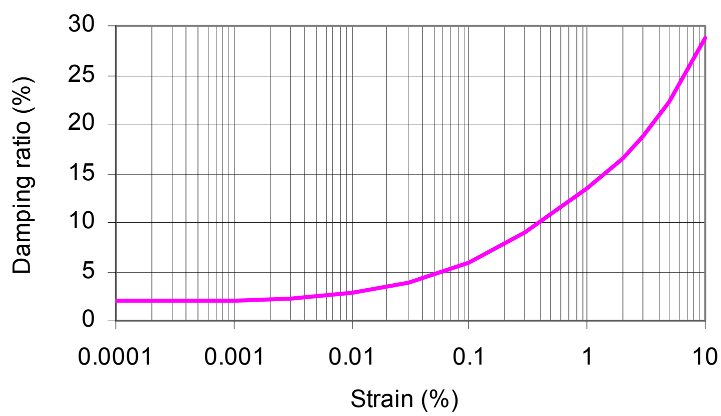

(b) Damping ratio increase curve

Figure 3.3 (a) Modulus reduction and (b) damping ratio increase curves used in the second FE site response model

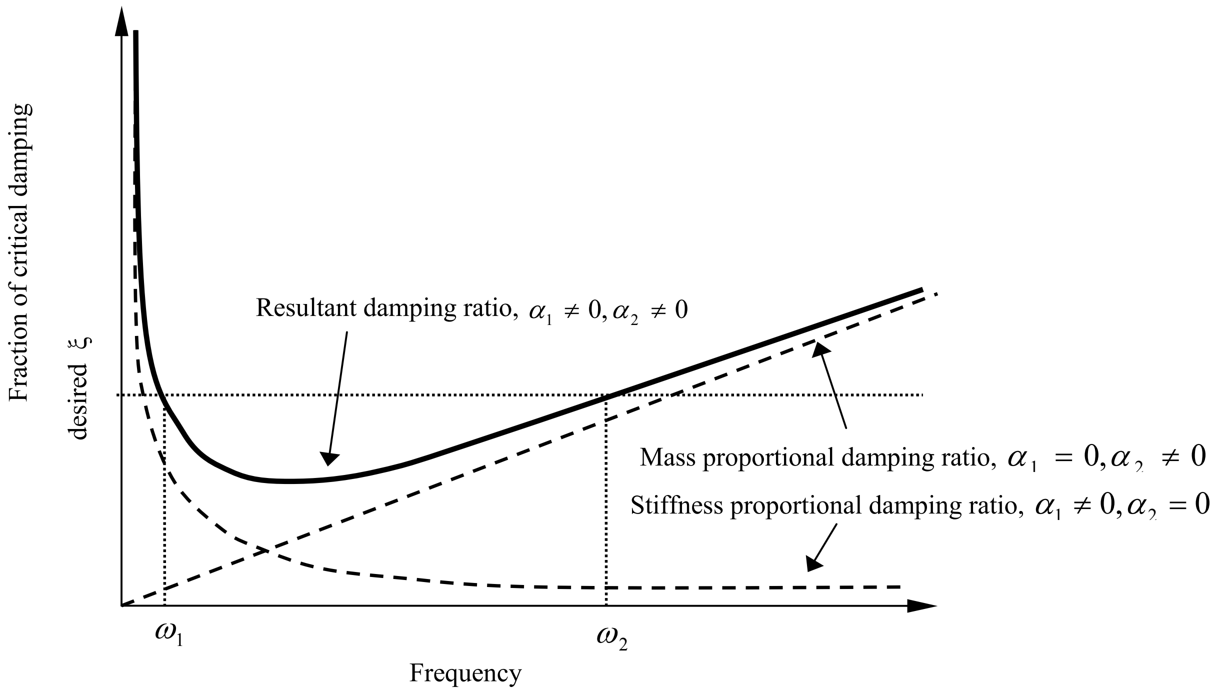

Figure 3.4 Relationship between the Rayleigh's damping and frequency

The SSI analyses that will be introduced later include inclined micropiles. This implies the need for 3-D FE analyses. A 3-D FE model was developed for performing the site response analyses, however it took a very long time to complete each site response analysis. Due to time constraints, a model with plain strain condition (2-D) was developed to save computation time. The third FE site response model was a 2-D mesh of 100 m in length and 10 m in height as illustrated in Figure 3.5. A length of 100 m in length was assumed to be long enough to simulate the free field condition. Dashpots were installed at the base of the model to simulate the viscous boundary (as shown by the large dots at the base in Figure 3.5. The constitutive model and numerical parameters remain the same as in the second model.

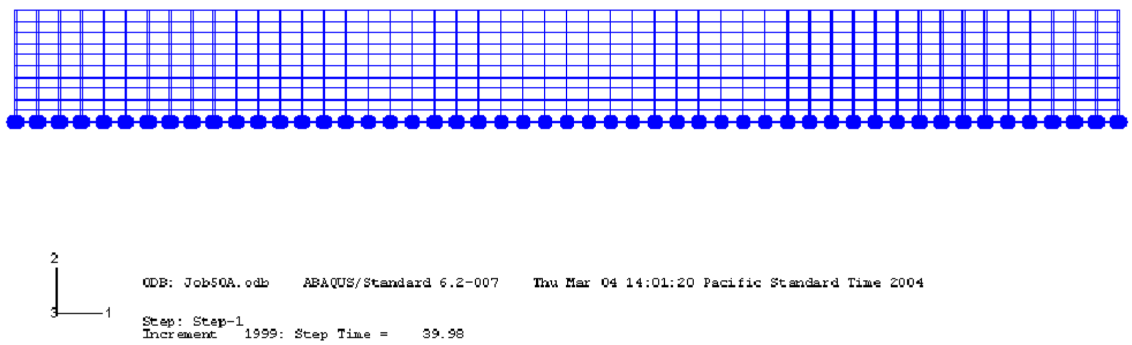

Figure 3.5 FE model for site response analysis with plain strain condition

If a pile is installed in the mesh as shown in Figure 3.5 (third model), horizontally traveling waves will be generated. When the shear waves travel to the edge of the soil layer, they will be partially reflected. This is not true in real conditions where these waves will not be reflected into the system. Therefore, it is very important to model the edges of the soil layer in such a way that the shear waves will not be reflected. This can be achieved by adding two soil columns with the same soil material properties at the two vertical edges of the soil layer and connect them to the soil layer with dashpots. The dashpot coefficients must be proportional to the shear wave velocity and the density of the soil layer. With the inclusion of the dashpots, the length of the soil layer can be shortened without including boundary effects. Therefore, the length of the soil layer used in this fourth model was 20 m long. The mesh generated from the software, ABAQUS, does not show the dashpots connecting between the soil layer and the soil columns. Thus, a schematic drawing is constructed to show the set up of the fourth FE model (Figure 3.6). Meanwhile, the properties of all the FE site response models are summarized in Table 3.2.

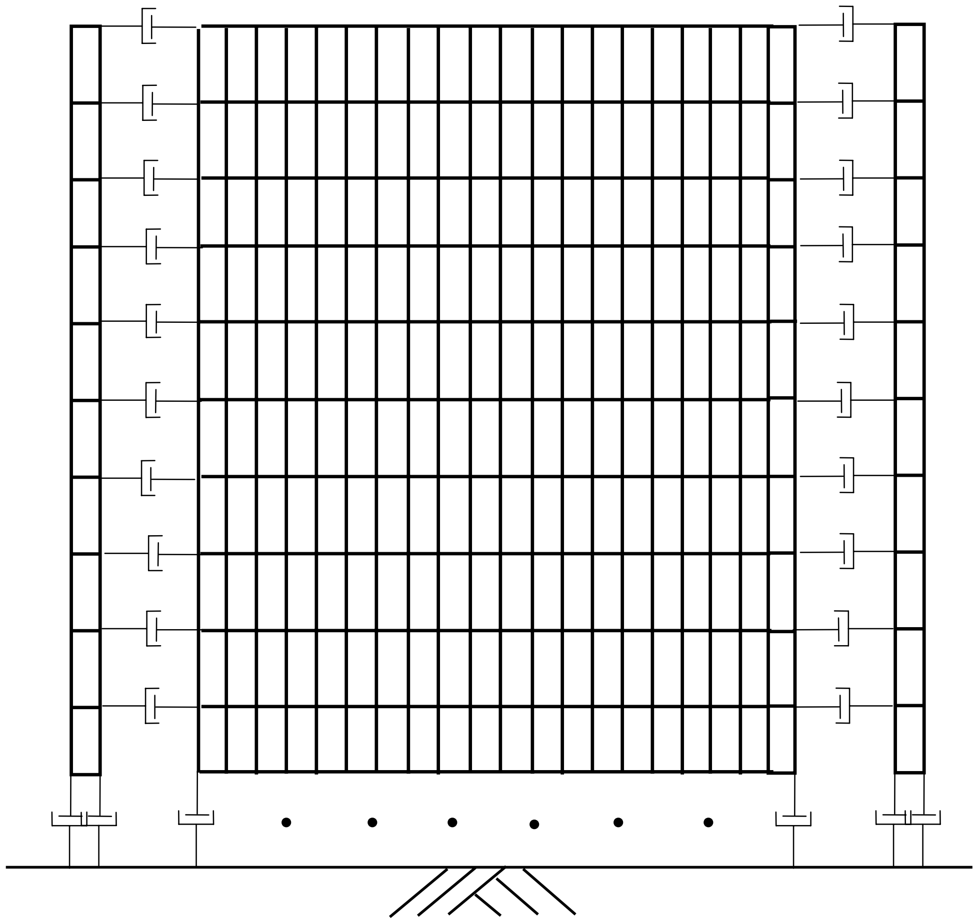

Not to scale

Figure 3.6 FE model of coupling vertical transmitting boundaries and free field

FE Model	Figure	FE mesh	Soil model	Dashpots	Soil columns
1	3.2	Column	Linear elastic	Not used	Not used
2	3.2	Column	Borja and Amies (1994)	Used at base	Not used
3	3.5	2-D, 100 m x 10 m	Borja and Amies (1994)	Used at base	Not used
4	3.6	2-D, 20 m x 10 m	Borja and Amies (1994)	Used at base and edges	Used

Table 3.2 Summary of all FE site response model properties

3.4 MODELING OF SOIL-PILE-SOIL INTERACTION

3.4.1 FE Models for Single Micropile under Static Loading

Figure 3.7 illustrates a general 3-D FE mesh for single micropile embedded in clay. The clay and the micropile were made out of solid elements and modeled with 8-node tri-linear brick elements. Only half of this symmetrical geometry was modeled to decrease the number of degrees-of-freedom (DOF) and thus to reduce the computational time. The clay layer was 12 m high and the micropile was 8 m in length and 0.2 m in diameter. The length of the micropile was chosen to be 8 m so that it would be long enough to act as a flexible long pile where the responses at the toe are zero and the toe has negligible effects on the responses of the micropile head. Meanwhile, the boundary of the clay was located at 50d (d = diameter) from the micropile center. This length has been determined to be approximately the shortest length of the boundary from micropile center such that the boundary position is away from the additional stress caused by the lateral load on the micropile. Figure 3.8 shows the effects of various boundary positions on the deflection of the micropile head; y_{200} is the deflection of the micropile head when the boundary is 200d from the micropile center, y is the deflection with its corresponding boundary position, L_b is the distance of the boundary from the micropile center, and d is the micropile diameter. From the graph, the 50d boundary has found to have negligible effects on the responses of the micropile head.

The lateral load was applied horizontally at the center of the top of micropile. The micropile head should be modeled with fixed head conditions since it is usually connected to micropile cap. Therefore, in this FE model, the micropile head was only allowed to move laterally and restrained against rotation. The edge and bottom of the clay

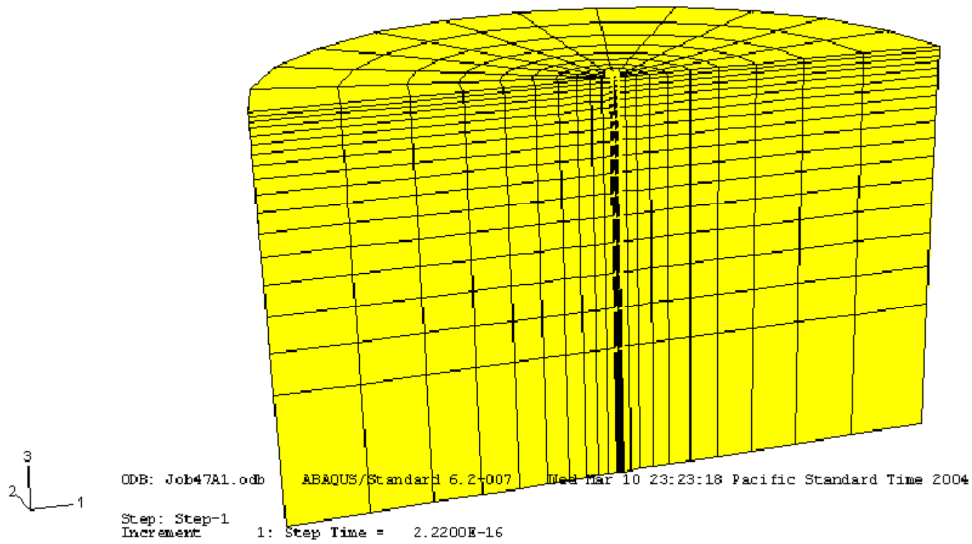

(a) Overall view

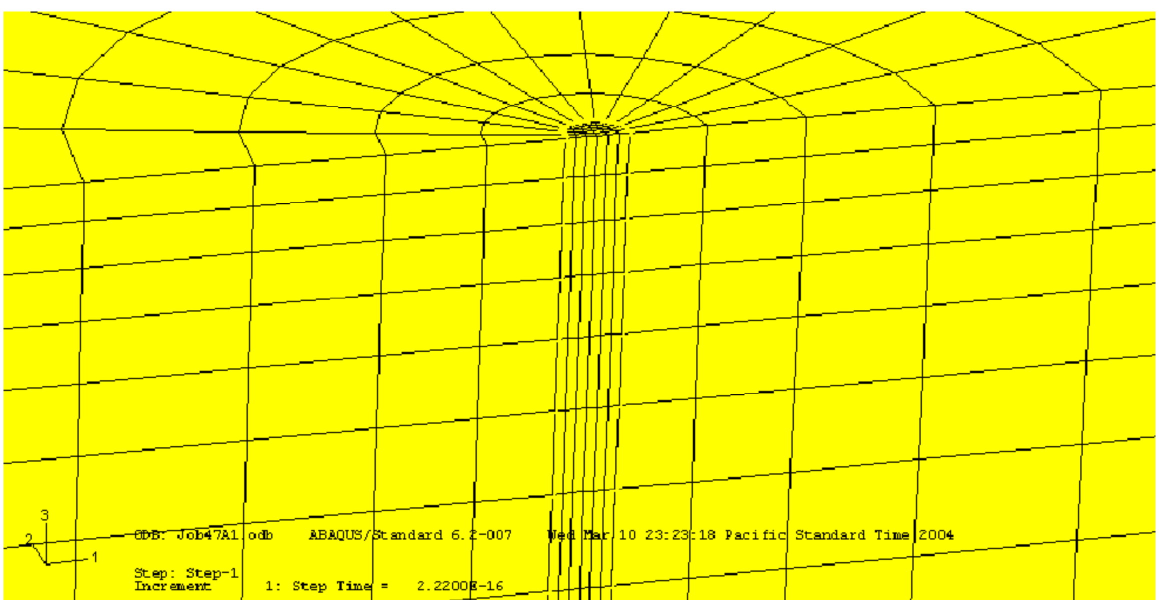

(b) Close-up view

Figure 3.7 FE mesh for laterally loaded single micropile

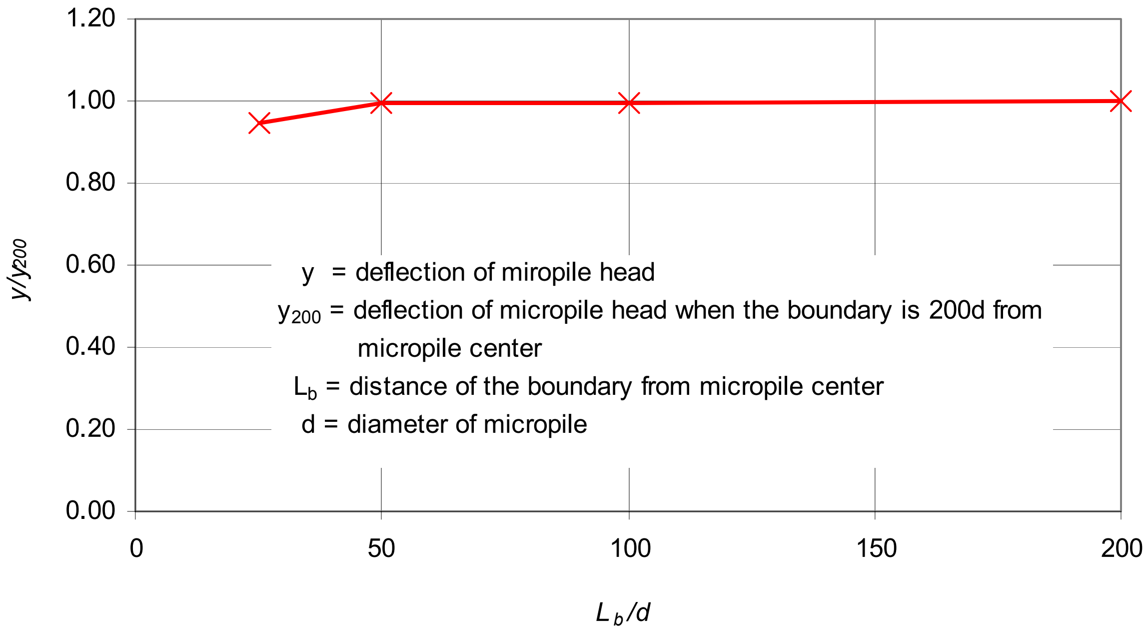

Figure 3.8 Effect of different boundary positions on the deflection of the micropile head

were restrained against translation and rotation. Besides, in both clay and micropile, the DOF into the symmetrical face of the geometry were restrained.

The mesh size used in the model has been determined to be small enough by verifying the deflection at the micropile head with the solution from the elastic continuum theory using the boundary element method (Davies and Budhu 1986). The following sections describe five FE models used to study the static response of a single micropile.

3.4.1.1 Model 1: Linear elastic and perfect bonding

The first FE model for a single micropile statically and laterally loaded was modeled using a linear elastic model for the micropile and the clay. The Young's moduli used for the clay and micropile were 4.69 x 10^8 N/m^2 and 2.30 x 10^{10} N/m^2, respectively. The Poisson's ratio used for the clay and micropile were 0.48 and 0.30, respectively. Five different loadings were applied at the micropile head, i.e. 10 kN, 50 kN, 100 kN, 150 kN, and 200 kN. Note that these loading values represent half of the actual load values since only half of the full geometry was modeled.

3.4.1.2 Model 2: Linear elastic and interface elements

The second FE model was similar to Model 1 except that gapping and sliding were incorporated at the interfaces between the micropile and the soil. This was done to examine the effect of the interface elements on the response of the micropile.

3.4.1.3 Model 3: Linear elastic, interface elements, with varying soil modulus

The third FE model was identical to Model 2 except that different Young's modulus values were used for the clay, i.e. 1.0×10^6, 1.0×10^7, 1.0×10^8, and 1.0×10^9 N/m^2. This was done to study how the Young's modulus affects the response of the micropile. A loading of 100 kN was applied at the micropile head in this FE model.

3.4.1.4 Model 4: Plasticity model (highly nonlinear) and interface elements

The fourth FE model was similar to Models 2 and 3 except that the plasticity model developed by Borja and Amies (1994) was used for the clay. The constitutive model's properties were chosen to fit the modulus reduction curve for a PI = 0 material (Vucetic and Dobry 1991, see Figure 3.9). The PI = 0 curve was selected because it exhibits the stronger non-linearity of the family of curves modeled by Vucetic and Dobry (1991). Stronger non-linearity implies a larger modulus reduction (G/G_{max}) and higher damping values for any given strain level. Figure 3.10 shows the damping ratio curve derived from the constitutive model where its properties fit the modulus reduction for a material with PI = 0 (Vucetic and Dobry 1991, see Figure 3.9). Note that the model overpredicts the damping ratio as compared to the one by Vucetic and Dobry (1991) (See Figure 3.10). However, the damping ratio derived from the model is considered reasonable at strains smaller than 0.1 %. Meanwhile, Figure 3.11 presents the stress-strain curve of the highly nonlinear soil and Table 3.3 shows the model and numerical parameters used in this FE model. Note that the failure strength of the soil is 110 kN/m^2. Only three static loadings were used, i.e. 10 kN, 50 kN, and 60 kN because the strains due to loadings larger than 60 kN were too high and divergence in the numerical solutions occurred.

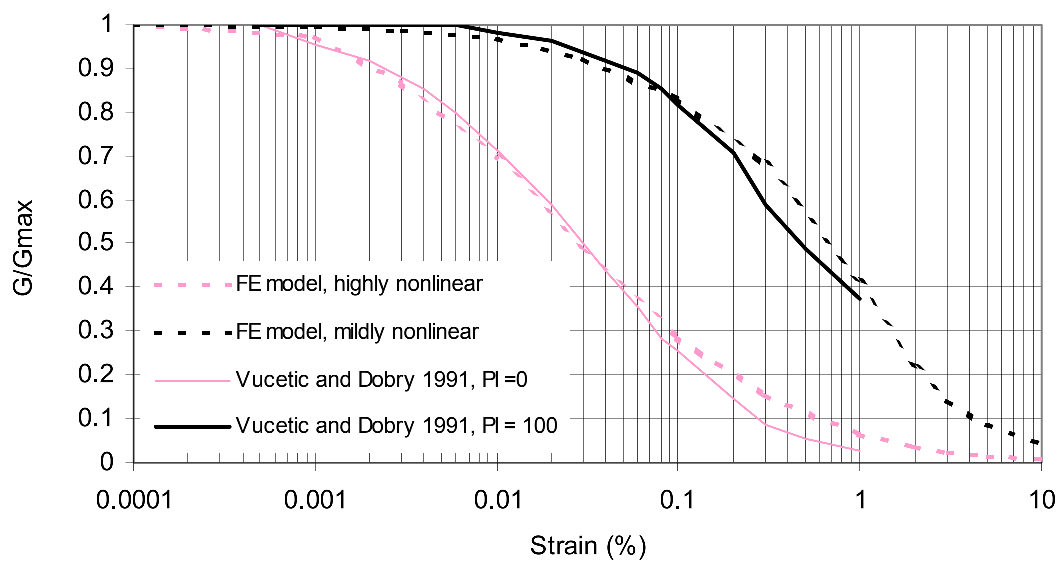

Figure 3.9 Modulus reduction curves for fine-grained soils with different plasticity indexes from Vucetic and Dobry (1991) and plasticity model

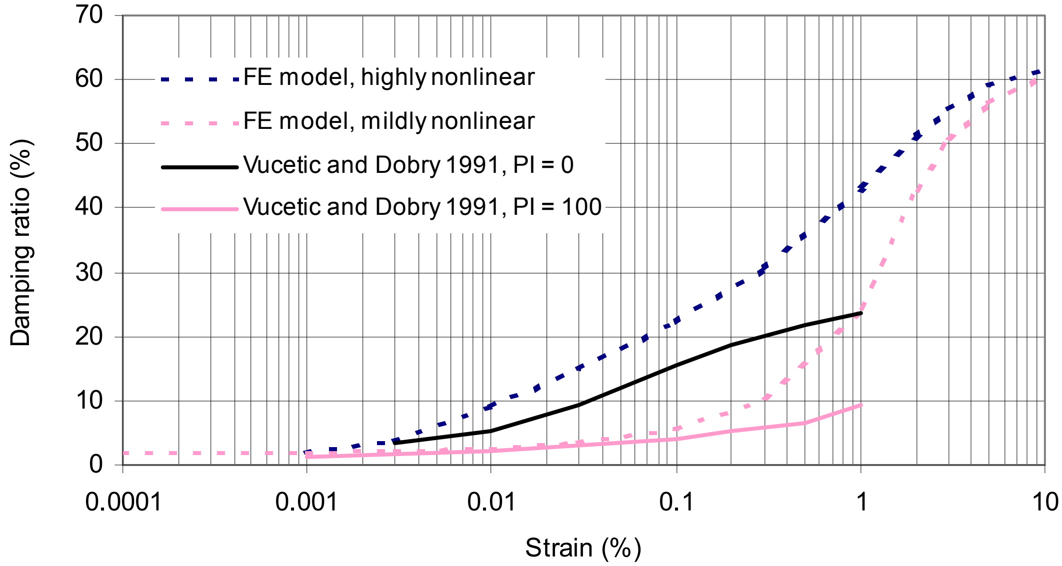

Figure 3.10 Damping ratio increase curves from plasticity model with its properties fit the modulus reduction curves (PI = 0 and 100) from Vucetic and Dobry (1991)

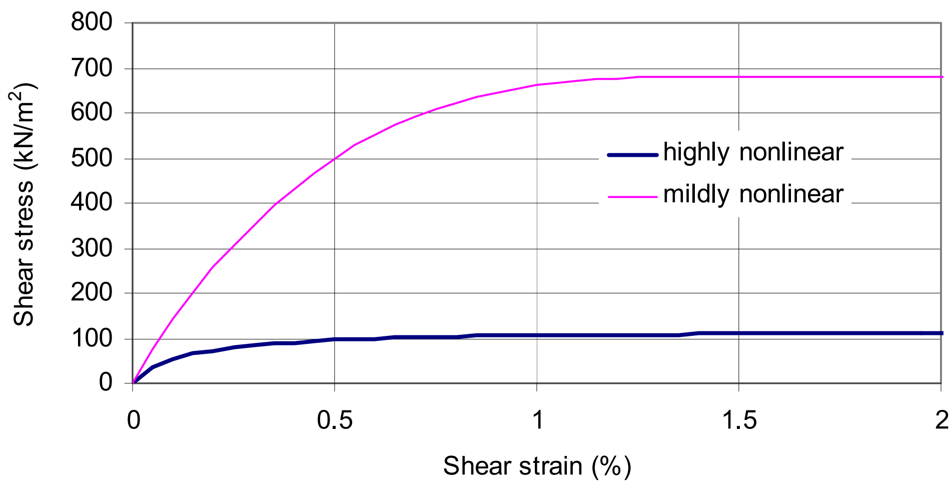

Figure 3.11 Stress-strain curves for highly and mildly nonlinear soils used in Models 4 and 5, respectively

Parameter	Value
v_s	300 m/s
ν	0.48
ρ	1762 kg/m^3
h	0.585
m	1.082
β	0.5
R	0.0007
H_o	1×10^{-4}

Table 3.3 Model and numerical parameters used in Model 4

3.4.1.5 Model 5: Plasticity model (mildly nonlinear) and interface elements

The fifth model was a replica of Model 4 except that the plasticity model parameters were chosen to fit the curve shown for PI = 100 (Vucetic and Dobry 1991, see Figure 3.9). The PI = 100 curve was selected because it exhibits the lesser modulus reduction and lower damping of all the family of curves modeled by Vucetic and Dobry (1991). Note that for the PI = 100 soil, the soil remains in the elastic range up to a strain level of 0.005 %. The associated damping ratio increase curve is illustrated in Figure 3.10. Again, the overprediction of the damping ratio from the model occurred but the value of the damping ratio falls into a reasonable range at strains smaller than 0.3 %. Meanwhile, the associated stress-strain curve is shown in Figure 3.11. The loading values used were the same as the ones used in Models 1 or 2. Table 3.4 shows the model and numerical parameters used in this FE model.

In static cases, the difference in behavior between the highly and mildly nonlinear soils can be seen in Figure 3.11. Both soils have the same initial stiffness. The highly nonlinear soil however has a lower strength and stiffness at higher strains than the mildly nonlinear soil. Note that the failure strength of the soil is 682 kN/m^2. This value is 6.2 times larger than the strength of the soil used in Model 4. This does not imply that a more plastic soil will be stronger than a non-plastic soil. The selection of model parameters, including soil strength (Tables 3.3 and 3.4), was made in order to fit the modulus reduction and damping curves for strain levels up to 1 %. Soil models 4 and 5 should be considered as models of two extremes of dynamic soil behavior, and not as representatives of the influence of plasticity on soil behavior.

Parameter	Value
v_s	300 m/s
ν	0.48
ρ	1762 kg/m^3
h	4.0
m	0.8
β	0.5
R	0.0043
H_o	1×10^{-4}

Table 3.4 Model and numerical parameters used in Model 5

3.4.2 FE Model for Single Micropile under Dynamic Loading

In order to properly model a single micropile under dynamic loading using FEM, a dynamic FE model as shown in Figure 3.6 should be implemented. The salient feature of this FE model is that the shear waves transmitted to the vertical lateral boundaries will not be reflected. For dynamic loading cases, 2-D FE models were used to reduce computational time. Anandarajah (2000) has shown that the results from his 2-D FE models of SSI problem agree well with centrifuge data.

Figure 3.12 illustrates the FE model for a single micropile under dynamic loading. It can be seen that a superstructure system with a single DOF was built on top of the micropile. The superstructure system consists of a single mass being linked to the micropile top with a solid element. Interface elements between the micropile and the clay were initially incorporated, unfortunately, divergence in the numerical solution was encountered. Therefore, perfect bonding between the micropile and the clay was used instead.

Three different soil models were used for the clay, i.e. linear elastic model, plasticity model with strong non-linearity, and plasticity model with weak non-linearity. The difference in dynamic behavior of highly and mildly nonlinear soils can be seen in Figures 3.9 and 3.10. Observe that the highly nonlinear soil has a larger modulus reduction and larger damping ratio increase than the mildly nonlinear soil. Linear elastic materials were used for the micropile and the superstructure system. A Ricker Wavelet was used as the input motion in place of a real earthquake motion in order to save computational time. Gazetas (2001) successfully used a similar input to study topographic amplification effects in the 1999 Athens Earthquake. The wavelet is defined by the following formula (Mavroeidis and Papageorgiou 2003):

$$a(t) = A\sum_{i=1}^{3}(1-2\pi^2 f_p^2 t^2)e^{-\left(\frac{\pi}{f_p}\right)^2 t^2} \tag{3.12}$$

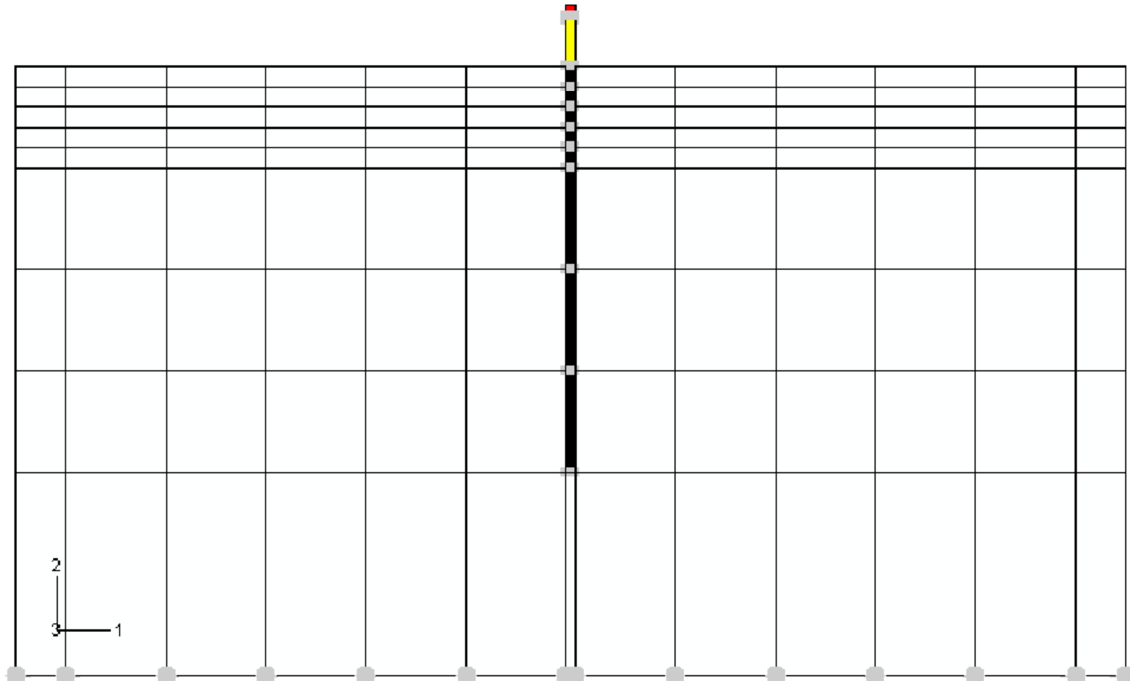

Figure 3.12 2-D FE model for single micropile analysis under dynamic loading

where $a(t)$ is the acceleration time history, t is the time, A is the maximum acceleration, and f_p is the prevailing frequency. Three different input motion intensities were used (A = 0.1 g, 0.3 g, and 0.5 g, respectively). Three prevailing frequencies were used to obtain a broadband motion ($1/f_{p1}$ = 0.1 s, $1/f_{p2}$ = 0.16 s, and $1/f_{p3}$ = 0.22 s). These frequencies were chosen to closely match the natural site period in order to study resonance effects due to site amplification. The input motion was applied as a displacement time history at the base of the clay. The displacement time histories obtained from double integration of the acceleration time history is shown in Figure 3.13. The spectral accelerations of the input motions are shown in Figure 3.14. Observe that the predominant period of the ground motions (e.g., the period corresponding to peak ground acceleration) does not exactly match any of the three prevailing periods (reciprocal of prevailing frequencies) used in the definition of the input motion. The duration of the wavelet pulse is 0.6 s, but analysis were executed for a total duration of 4.0s.

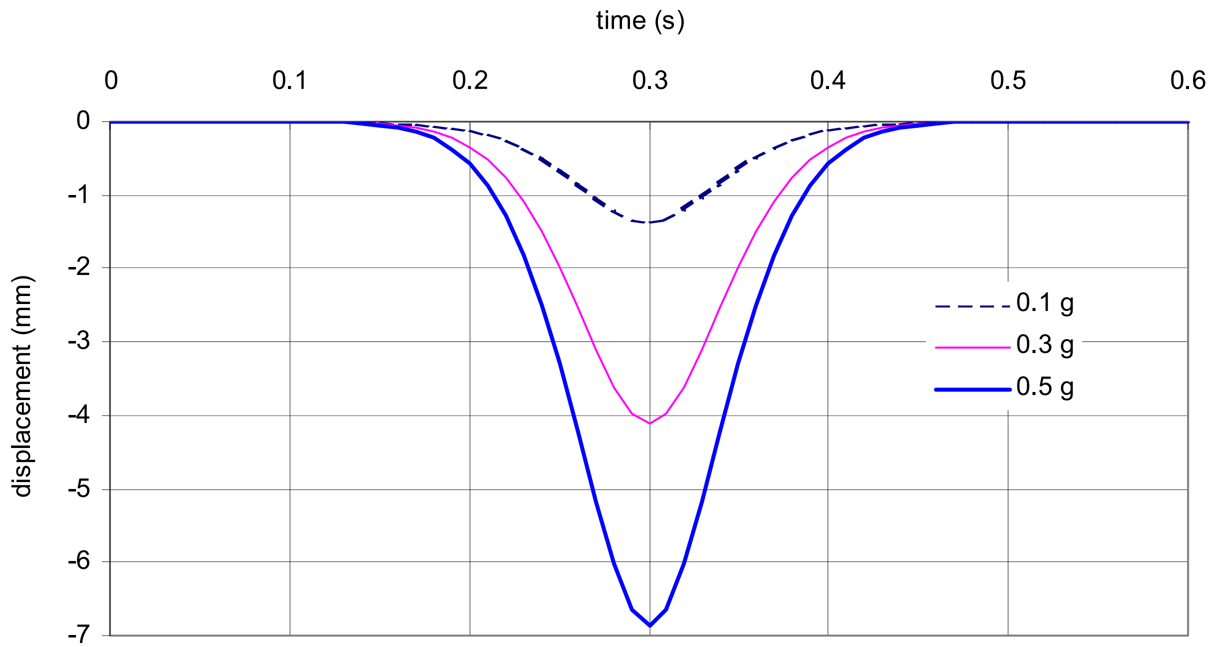

Figure 3.13 Displacement input motion of wavelet with various intensities

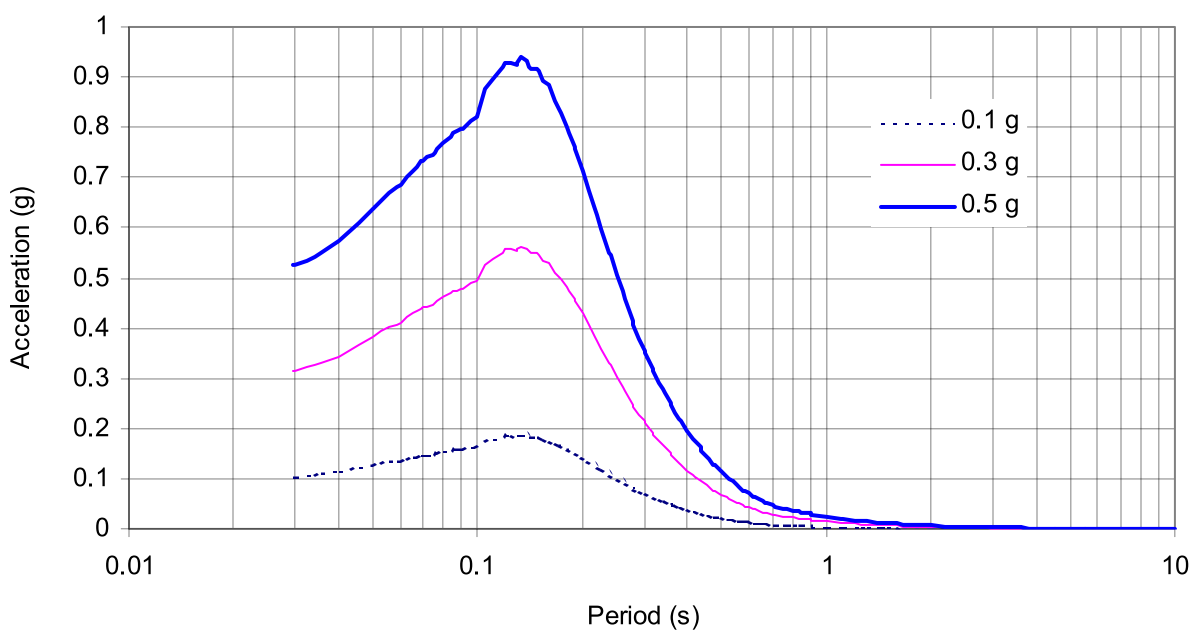

Figure 3.14 Response spectrum of wavelet input motion with various intensities

3.4.3 FE Models for Micropile Groups under Static Loading

Two FE models for micropile groups under static loading were developed. Both of them were constructed to perform a validation study against field test results reported by Geosystem, L.P. (2002). Therefore, the geometry and loading of the FE models were built as close as possible to the field load tests. One of them was a micropile group consisting of four vertical members whereas the other comprised four inclined micropiles raked at 25° to the vertical. Only half of the symmetrical geometry of the micropile group under load test was modeled in order to save computational time. Figures 3.15 and 3.16 illustrate the FE models of the vertical and the inclined micropiles, respectively.

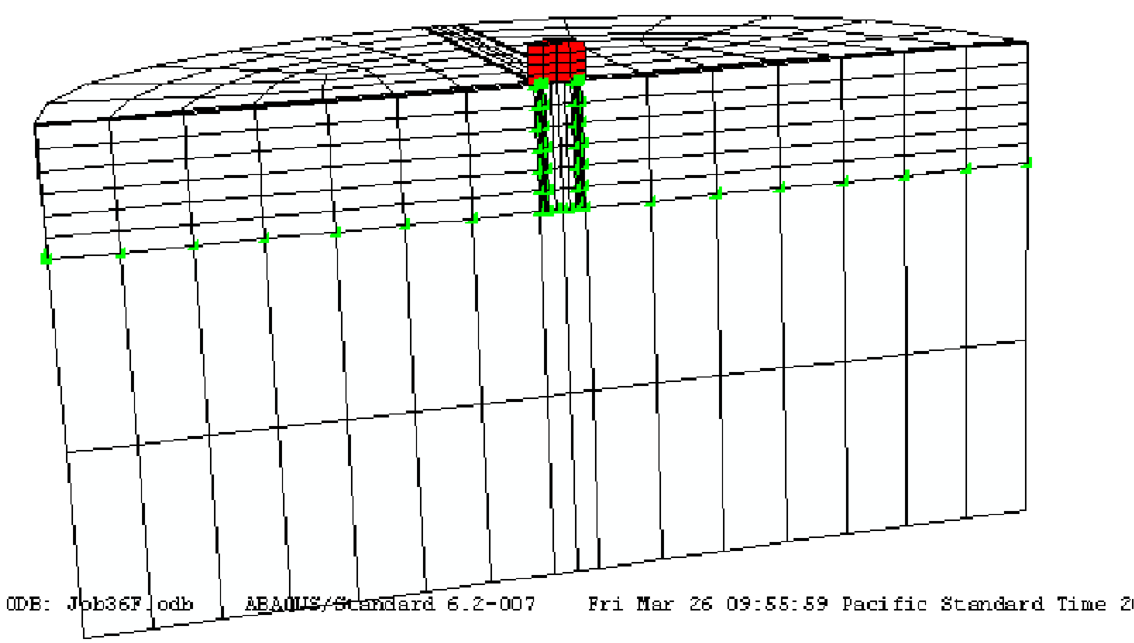

Figure 3.15 FE model for four vertical micropiles under static loading

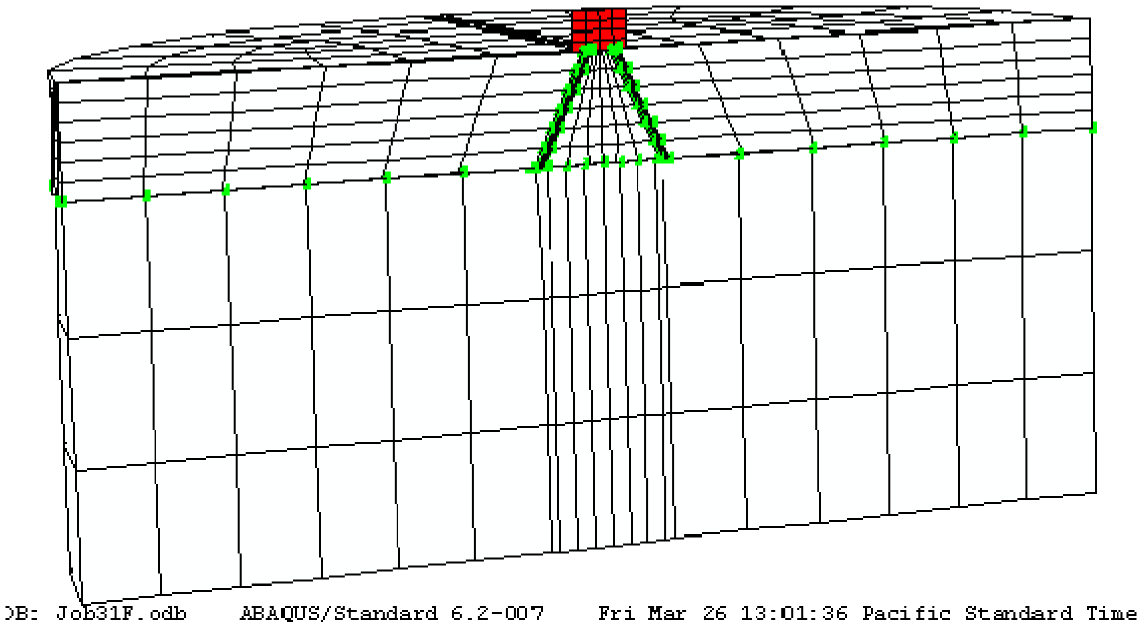

Figure 3.16 FE model for four inclined micropiles under static loading

The pile cap was 3 ft in diameter and 2 ft in height. The micropiles were roughly 6.5 ft in length below the bottom of the pile cap. A horizontal load was applied at approximately 6 in above the bottom of the pile cap. The stiffness information for the soils at the field was not available. Thus, the Young's modulus of the soil, *E*, was estimated from the input data, *k* for GROUP analyses done by Weinstein (2003), a member of a group in-charged of the field load tests. A *k* value of 100 lbf/in^3 was used for the entire soil layer in the GROUP analyses where $E_{py} = k\ x$; E_{py} is the secant modulus of the *p-y* curve (*p* = soil reaction per unit length, and *y* = lateral deflection of the pile at a point *x* along the pile length), *k* is a constant, and *x* is the depth of the pile below the pile head. Terzaghi (1943) approximated the relationship between E_{py} and *E* in sand as shown below:

$$E_{py} = \frac{E}{1.35} \tag{3.13}$$

A constant E_{py} was assumed for the entire soil layer and approximated as the value of E_{py} at the mid-depth of the micropile length. Thus, an approximated E of 5265 lbf/in^2 was used in the FE models.

Perfect bonding was used for the interaction between the micropiles and the soil. Interface elements with gapping and sliding were not used because divergence in the solution was encountered.

3.4.4 FE Models for Micropile Groups under Dynamic Loading

Two FE models were constructed for micropile groups under dynamic loading. The first one is a micropile group consisting of two vertical micropiles as shown in Figure 3.17. A pile cap was built on top of the two micropiles and a superstructure system was constructed on top of the cap. This superstructure system was similar to the one used in the FE model for single micropile under dynamic loading. Meanwhile, Figure 3.18 illustrates the second FE model consisting of two micropiles inclined at 20° to the vertical. The pile cap and the superstructure system were constructed in a similar manner.

For these two micropile groups, a similar input motion with the same intensities as the one used in the single micropile under dynamic loading was applied at the base of the clay. Apart from these, another input motion was imposed at the base of clay in the case of two vertical micropiles. This input motion was similar to the one in Section 3.4.2 except that the predominant natural period centered around 0.27 s. This was done to examine the effect of the frequency content of the input motions on the response of micropile groups.

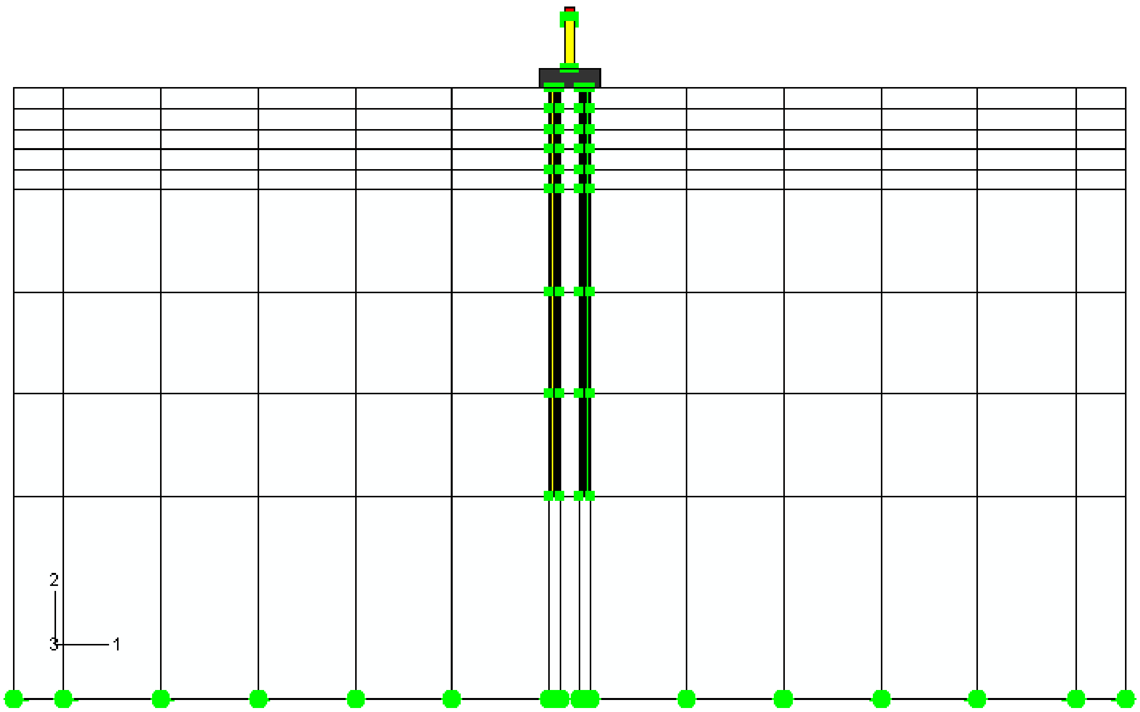

Figure 3.17 2-D FE model for two vertical micropiles under dynamic loading

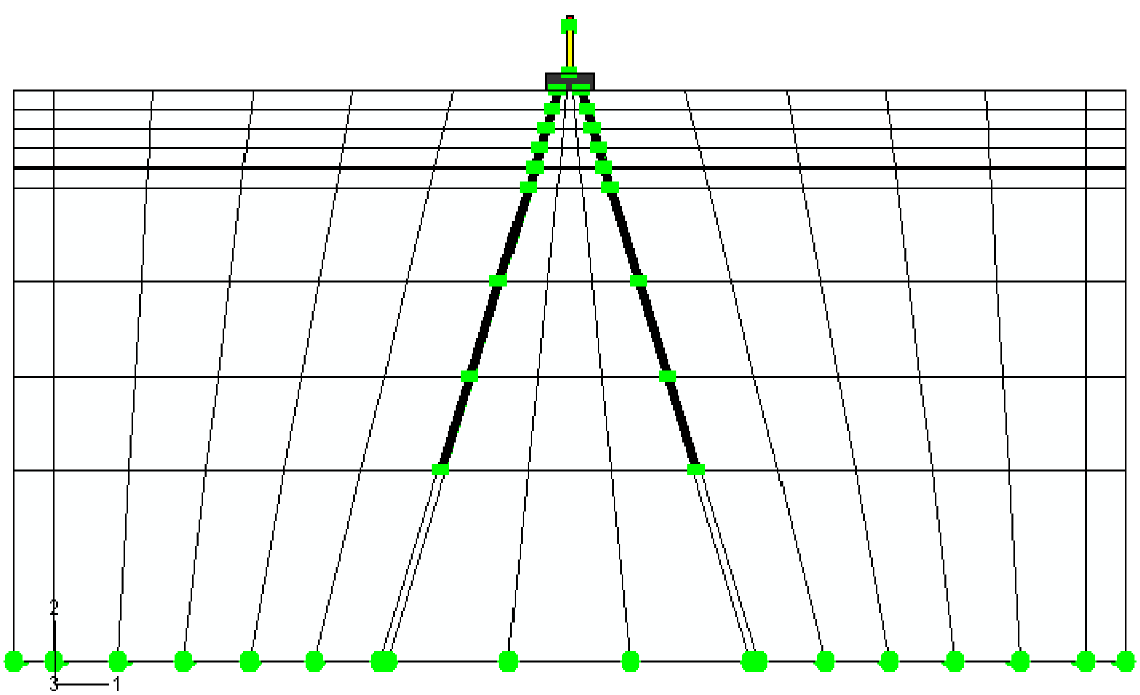

Figure 3.18 2-D FE model for two inclined micropiles under dynamic loading

3.5 VALIDATION OF FINITE ELEMENT MODEL

3.5.1 Validation of FE Models for Seismic Site Response

Figure 3.19 shows the horizontal total accelerations at the top of the soil layer from SHAKE and the FE soil column model (first model in Section 3.3.1) with linear elastic material and with no material damping. In SHAKE, modulus reduction curve as shown in Figure 3.3 was used for the soil layer using equivalent linear method. The discrepancy between these two results was significant and implies that Model 1 was not able to represent realistic soil response.

Meanwhile, Figure 3.20 shows the horizontal total accelerations at the top of the soil layer from SHAKE and the FE soil column model (second model in Section 3.3.1) with its material made out from plasticity model and with material damping. The results agreed with each other very well. This shows that the plasticity model developed by Borja and Amies (1994) works well in a dynamic analysis. It also demonstrates that the material damping (both hysteretic and viscous damping) does reduce the high frequency noise as compared to the results from Model 1 with no material damping. Note that in the first 7 s, the amplitude of the acceleration from SHAKE was significantly smaller than that from the FE model. This happened due to the fact that a constant damping corresponding to an effective strain (0.65 of maximum strain) was used for the entire history of shaking in SHAKE (equivalent linear method). Meanwhile, the damping changed with varying strains during the shaking history in the FE model (with plasticity model). It was believed that in the first 7 s, the strains were actually small as opposed to the constant effective strain used in SHAKE. Consequently, the damping corresponding to this constant effective strain used was higher than the one expected at low strain levels.

This results in an over-damped response in SHAKE and explains the aforementioned observation.

Figure 3.21 shows the horizontal total accelerations of the central node at the top of the free field soil model (Model 3 in Section 3.3.1) as compared to the ones from SHAKE. The results were promising and it indicates that the soil layer was long enough to simulate the free field condition.

Figure 3.22 shows the horizontal total accelerations of the central node at the top of the soil model coupling with two soil columns (Model 4 in Section 3.3.1) as compared to the ones from SHAKE. The results agree very well with each other, indicating that the soil columns prevented shear wave reflection at the two vertical boundaries.

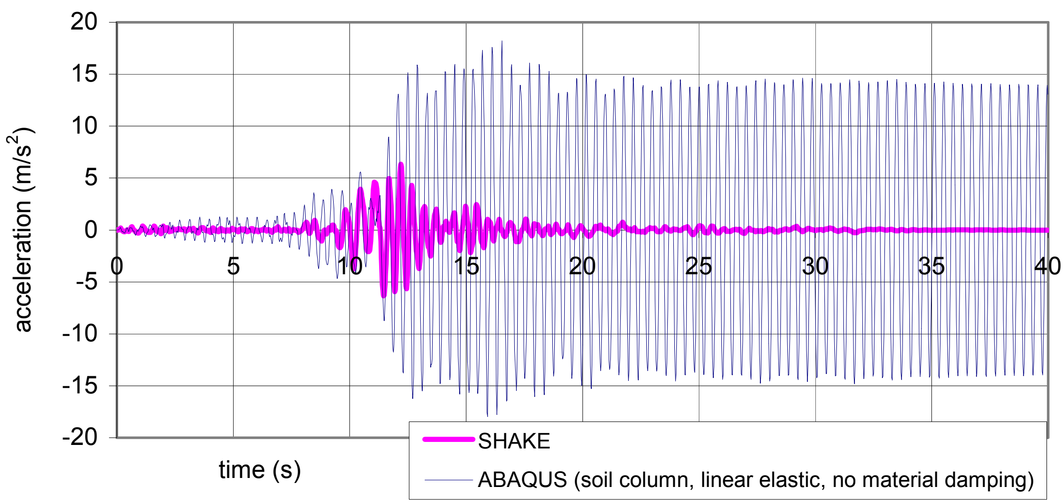

Figure 3.19 Total horizontal accelerations at the top of the FE soil column model with linear elastic material and no material damping, and from SHAKE

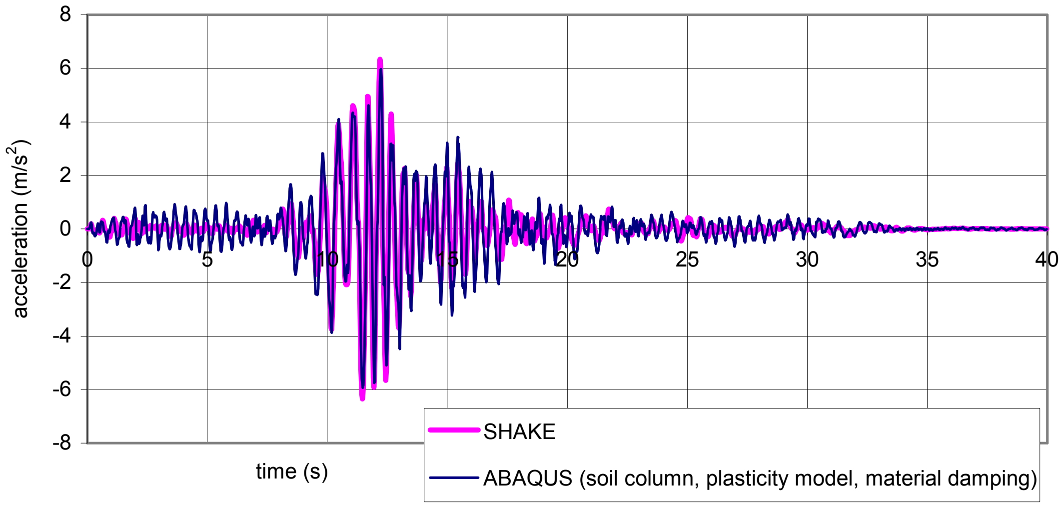

Figure 3.20 Total horizontal accelerations at the top of the FE soil column model with plasticity material and material damping, and from SHAKE

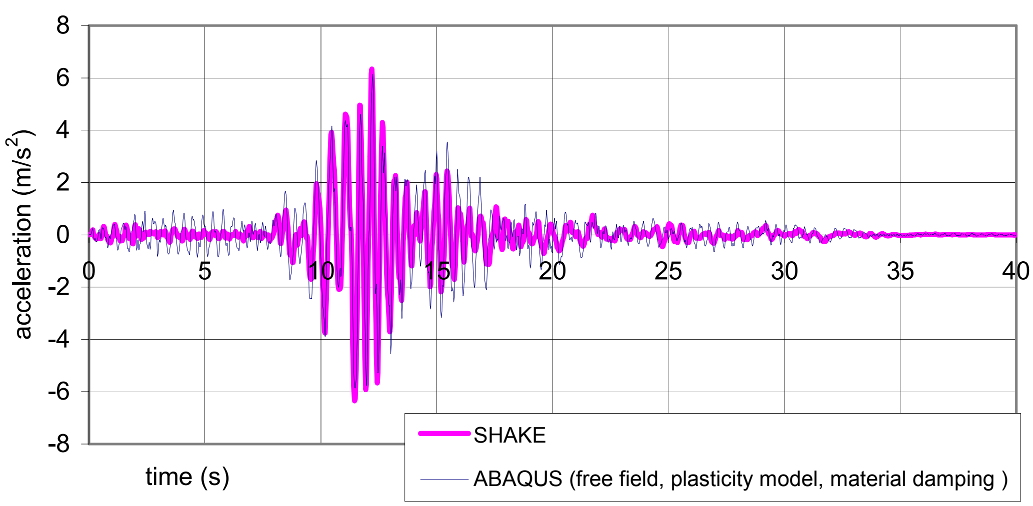

Figure 3.21 Total horizontal accelerations at the top of the FE free field model with plasticity material and material damping, and from SHAKE

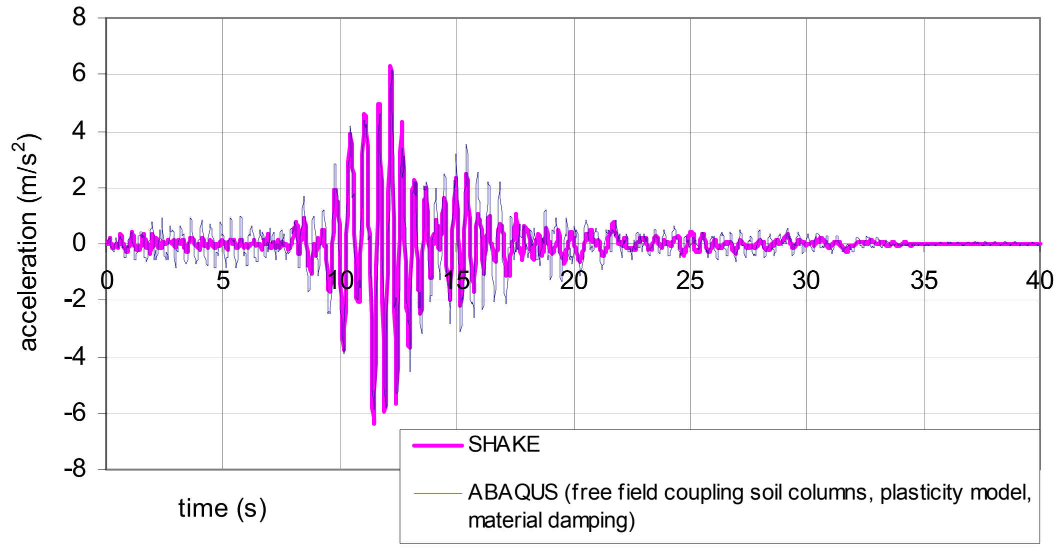

Figure 3.22 Total horizontal accelerations at the top of the FE soil model coupling with soil columns with plasticity material and material damping, and from SHAKE

Figure 3.23 shows the acceleration response spectra of the input motion, the results from SHAKE, the soil column (Model 2), and the free field model coupling soil columns (Model 4). The results from SHAKE and the two FE models were very close to each other. Amplification was observed at the top of the soil layer since the responses at the top surface were higher than the input motion at the base. It is interesting to note that there were three peaks in the acceleration response spectra from the FE models but only two peaks in SHAKE. This implies that the FE models were more effective in capturing higher order natural frequencies of the system as compared to SHAKE.

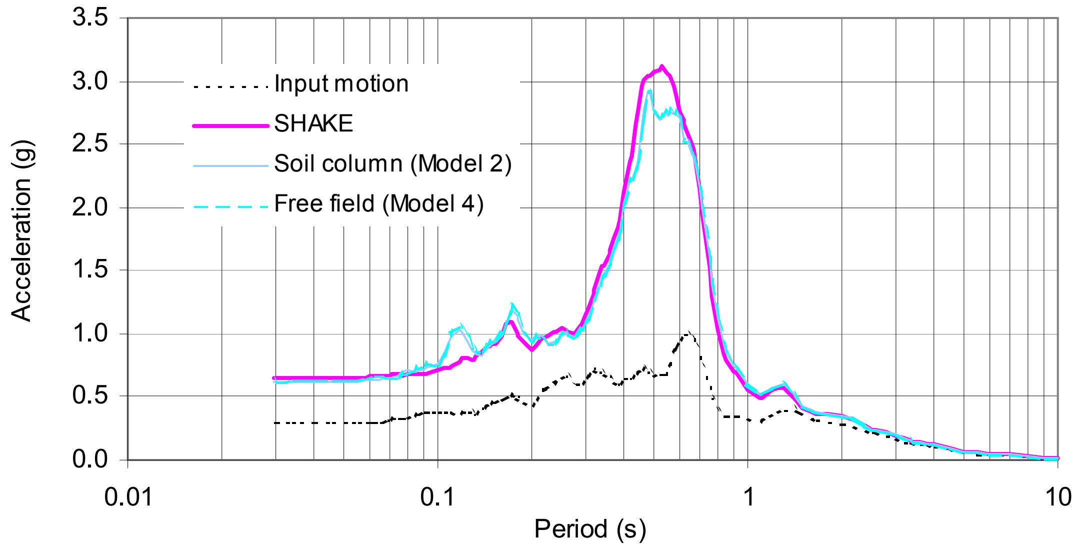

Figure 3.23 Response spectra of acceleration input motion at the base, the accelerations from SHAKE, soil column (Model 2), and free field model (Model 4)

Figure 3.24 illustrates the ratio of response spectra (RRS) of the accelerations from SHAKE, soil column (Model 2), and free field model (Model 4). In this graph, the RRS are defined as the ratio of the acceleration at the top surface to the one at the base (input motion) at its corresponding natural period. The soil has an initial natural period of 0.4 s (natural period = $4H/v_s$, where H = 10 m, and v_s = 100 m/s). The largest RRS from SHAKE, soil column (Model 2), and free field model (Model 4), took place at 0.48 s, 0.50 s, and 0.50 s, respectively. The shift of the spectral periods to higher values (as compared to 0.4 s) during shaking was due to the fact that the shear modulus or shear wave velocity during shaking was lower than the initial value.

In conclusion, these promising results imply that Model 4 was appropriate for conducting SSI analyses with micropiles installed in soil.

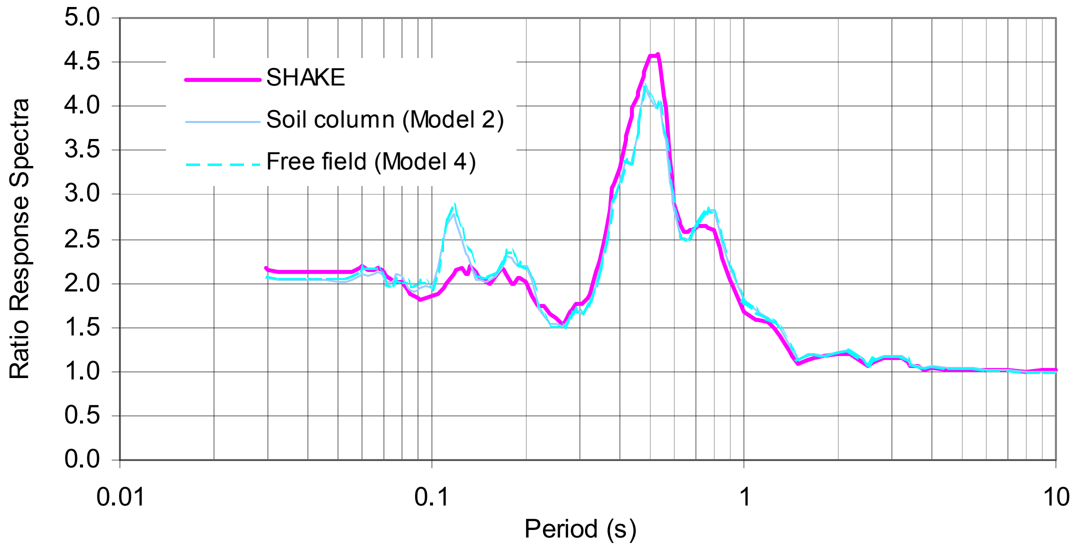

Figure 3.24 Ratio response spectra of acceleration input motion at the base, the accelerations from SHAKE, soil column (Model 2), and free field model (Model 4)

3.5.2 Validation of FE Model for Single Micropile using Linear Elastic Model

Figure 3.25 presents the 3-D FE mesh of a single micropile being displaced due to a static horizontal load of 20 kN at the micropile head with perfect bonding between the clay and the micropile. A linear elastic material was used for both clay and micropile in this FE model. The validation of this FE model was accomplished by comparing the deflection at the micropile head with the solutions given by Davies and Budhu (1986). Figure 3.26 shows the comparison of the deflections at the micropile head from the FE analyses and those from the elastic solutions proposed by Davies and Budhu (1986) with various Young's modulus values for clays. Based on the solution from the elastic continuum theory using the boundary element method proposed by Davies and Budhu (1986), the deflection at the pile head with fixed head condition is as follows:

$$y = 0.80K^{-2/11}\frac{H}{E_s d} \tag{3.14}$$

where y is the deflection at the micropile head; K is the ratio of the elastic modulus of micropile to the one of clay; H is the horizontal static load; E_s is the elastic modulus of clay; and d is the diameter. The results agree very well with each other except for very soft soils (E_s < 10 MN/m^2).

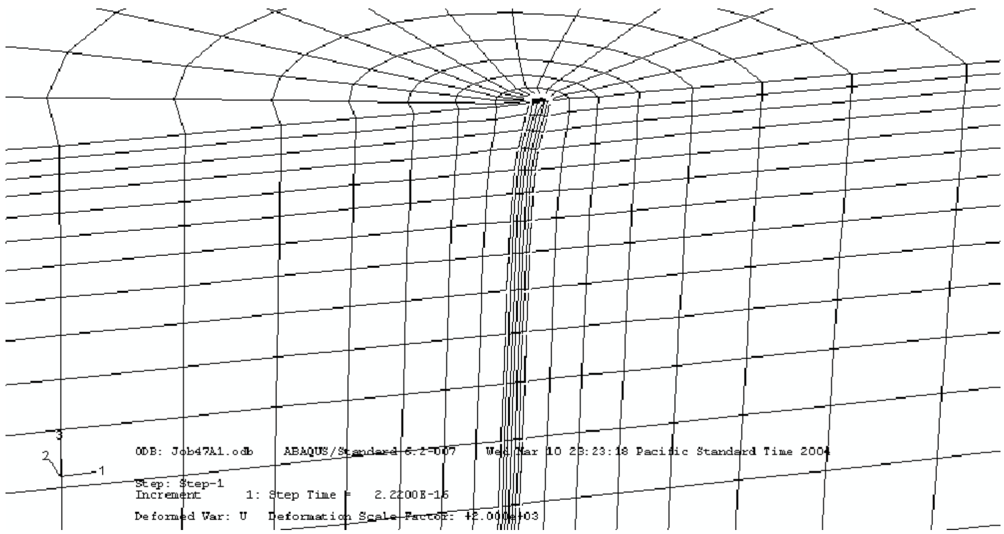

Figure 3.25 Deformed 3-D mesh of single micropile due to a horizontal static load at micropile head

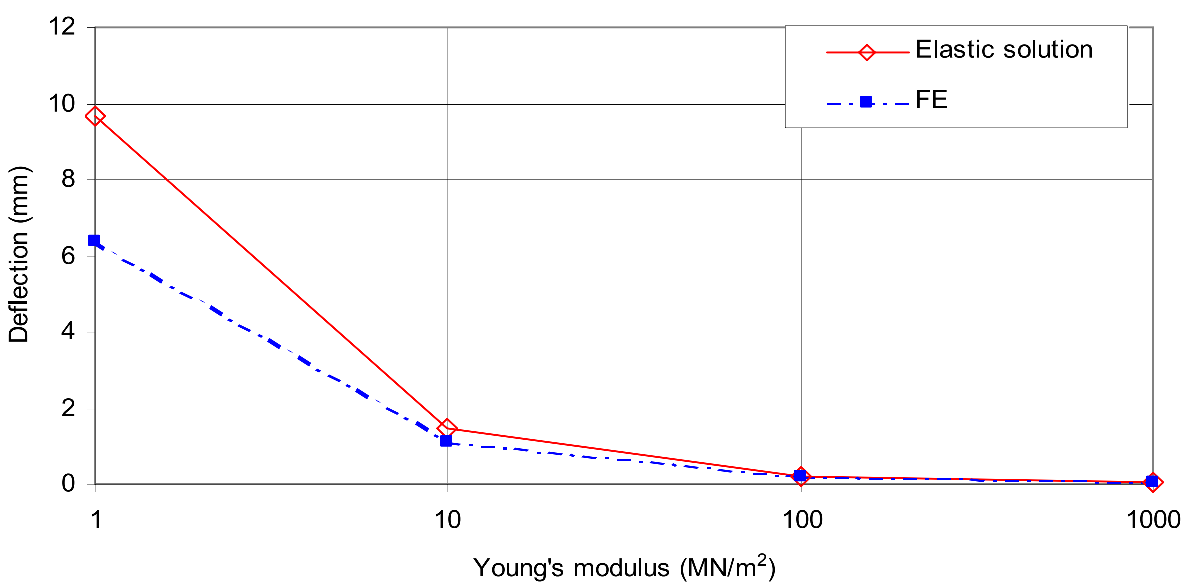

Figure 3.26 Comparison of micropile head deflections from FE analyses and solutions proposed by Davies and Budhu (1986) with various Young's modulus values for clays

3.5.3 Validation of FE Models for Micropile Group with Field Tests

The comparison between the deflections at the micropile head from the field tests and FE models (Geosystem 2002, also refer to Section 3.4.3) is summarized in Table 3.5.

Horizontal deflection at the micropile head (inches)		
Resource	Vertical micropiles	Inclined micropiles
Field tests	0.438	0.076
FE models	0.104	0.053

Table 3.5 Comparison of micropile head displacements from field tests and FE models

The results from Table 3.5 show that the deflections at the micropile head from the FE models were smaller than those from the field tests. This could be attributed to the absence of the gapping in the FE models. Apart from this, the Young's modulus of the soil used in the FE models was an approximated value. Further validation with full scale field tests is imperative.

CHAPTER 4
PARAMETRIC STUDY

4.1 INTRODUCTION

A parametric study was conducted in order to understand the seismic behavior of micropiles. The results of the parametric study will provide a better picture of the behavior of micropiles in engineering applications. The parametric study on a single micropile under static and dynamic loading, and micropile groups under dynamic loading is presented herein.

4.2 SINGLE MICROPILE : STATIC LOADING

The parametric study conducted for single micropile under static loading is presented in this section. The independent variables include the gapping between the micropile and soil, the non-linearity of the soil, the Young's modulus of the soil, and the load intensity. The static behavior was studied via the dependent variables of deflection and moment along the pile.

4.2.1 Gapping (Pile-Soil Separation)

Figure 4.1 shows the FE mesh of a single micropile being displaced by a static horizontal load at the micropile head with the incorporation of gapping and sliding elements between the micropile and the clay. The load was applied to the right of the symmetrical face, thus a gap was observed to appear at the backside of the micropile. The soil and micropile were assumed to behave elastically (Models 1 and 2 corresponding to Sections 3.4.1.1 and 3.4.1.2).

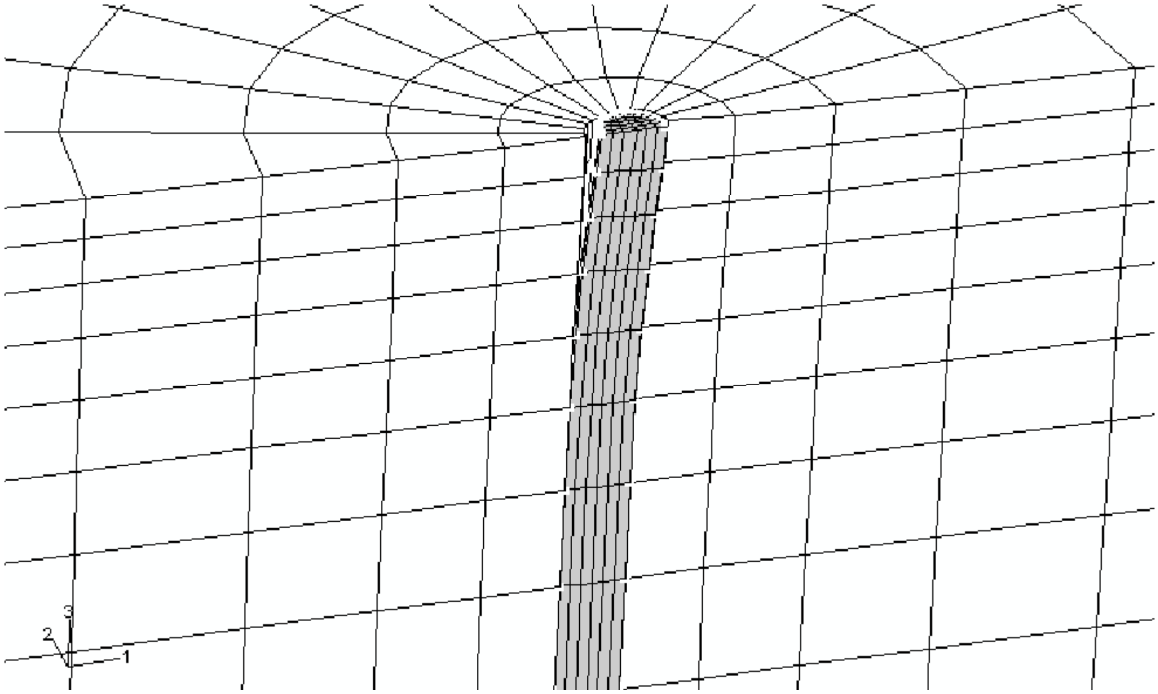

Figure 4.1 FE meshes of a single micropile being laterally loaded with gapping interface elements

Figure 4.2 shows the load-deflection curves of the micropile head for the cases where the pile and the clay were bonded perfectly or were allowed to separate when tensile normal stresses existed at their interface (with gapping elements). In these two cases, a linear elastic model was used for the clay. It can be seen that in the FE model with gapping elements, the deflection of the micropile head is larger than the one with perfect bonding. Moreover, the deflection due to gapping increases with increasing load as shown in Figure 4.3. Note that the relationship is linear between the load and the increased deflection due to gapping. This implies that the gapping elements do not introduce non-linearity in the pile-soil systems. The net effect of the gapping elements is to reduce tensile stresses at the backside of the pile. This results in a linear but less stiff load-deflection curve at the micropile head.

Even though the deflection due to gapping increased only slightly in magnitude, the percentage increase in deflection due to gapping with respect to the model with full bonding between soil and pile was significantly large. This phenomenon is illustrated in Figure 4.4. Note that the percentage increase ranges from 49.1 % to 55.5 %. However, it was observed that the percentage increase in deflection due to gapping decreases with increasing loading.

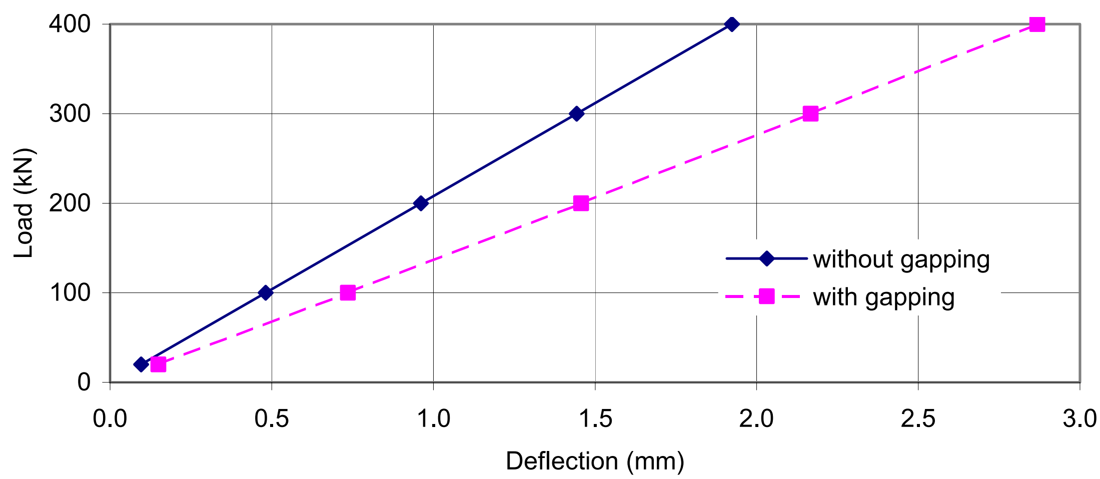

Figure 4.2 Comparison of micropile head deflections from FE models with and without gapping at various applied loading

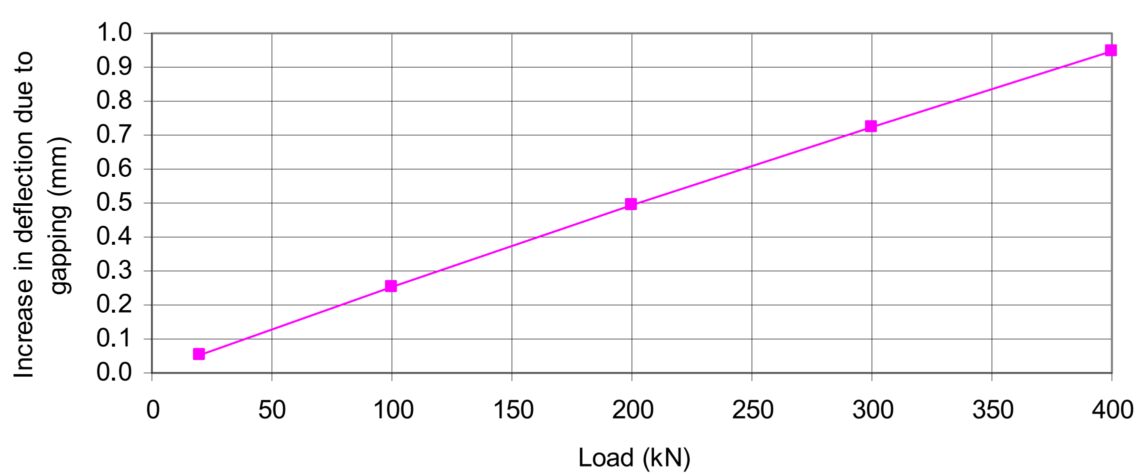

Figure 4.3 Relationship between the increase in micropile head deflection due to gapping and the applied load at the micropile head

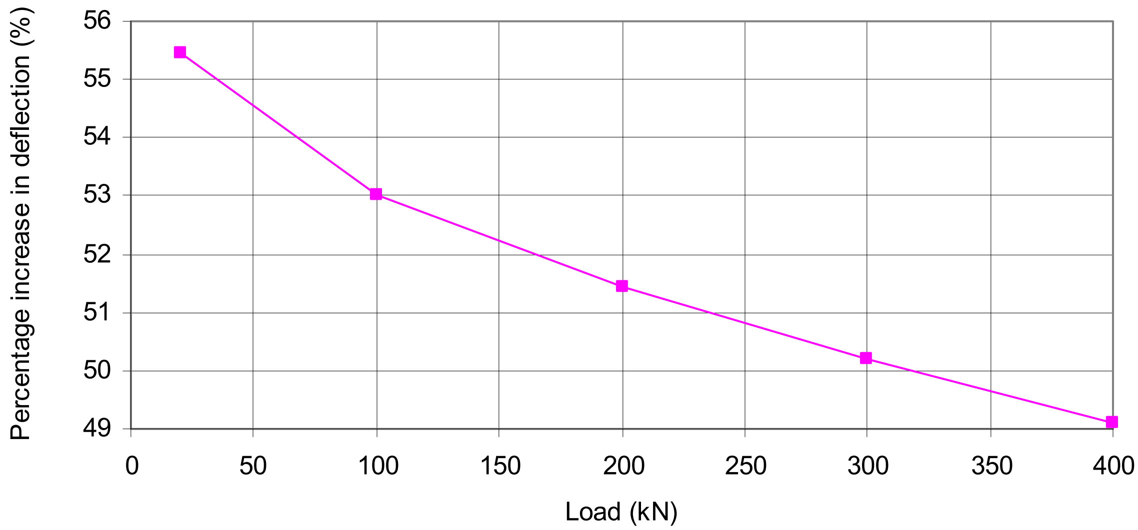

Figure 4.4 Relationship between the percentage increase in micropile head deflection due to gapping and the applied load at the micropile head

Figure 4.5 shows the variation of the deflection along the micropile length from the FE models with the interface between the micropile and the clay either bonded or with gapping elements. In Figure 4.5, x is the depth below the micropile head, and L is the length of the micropile. Figures 4.5 (a) and (b) show the variations at the smallest applied load used in this study (20 kN), and the largest one (400 kN), respectively, at the micropile head. It is noteworthy to observe that the gapping took effect from the micropile head to approximately 0.14 micropile length (5.6 diameter) at all the load intensities used. Therefore, this implies that it is very important to incorporate the gapping elements at least within a certain length (practically within 10 diameter) from the micropile head in order to correctly estimate the deflection along the micropile length.

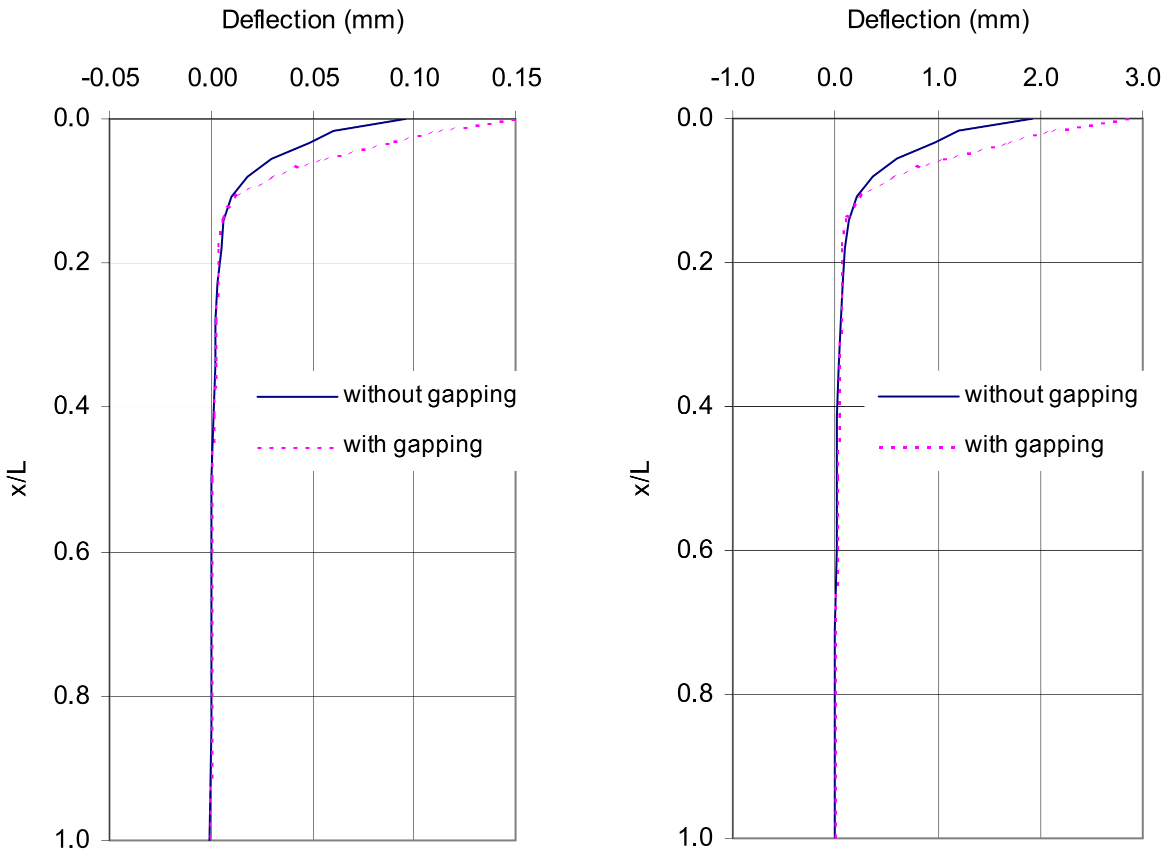

(a) 20 kN

(b) 400 kN

Figure 4.5 Variation of deflection with depth from FE models with and without gapping under a load of (a) 20 kN, and (b) 400 kN at the micropile head

Figure 4.6 presents the variation of the moment along the micropile length from the FE models with and without the gapping elements under the applied load of 400 kN. It clearly illustrates that the moment around the micropile head from the FE model with gapping was larger than the one without gapping. This implies that less load was transferred to the surrounding soil around that micropile head region due to gapping. Consequently, around that proximity, the axial stress was higher and subsequently the moment was larger than that in the case where more load was transferred to the neighboring soil with perfect bonding due to larger contact area.

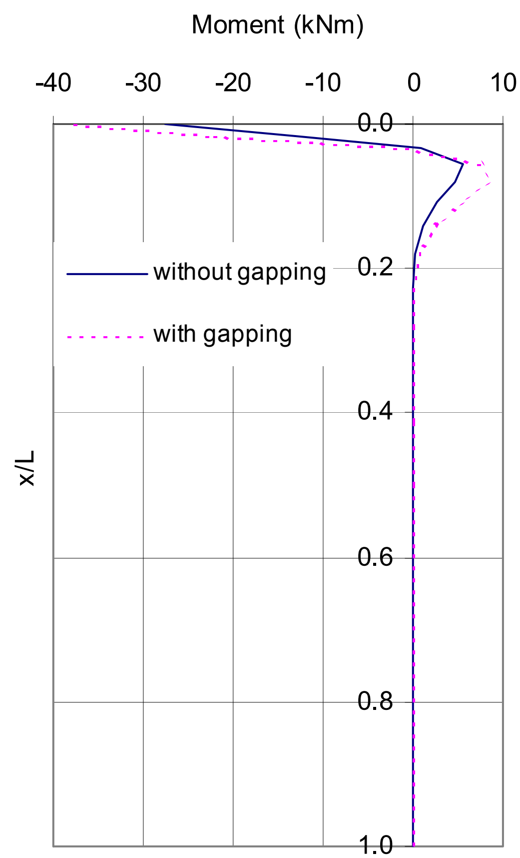

Figure 4.6 Variation of moment with depth from FE models with and without gapping under 400 kN at the micropile head

4.2.2 Non-linearity of Soil

Figure 4.7 shows the relationship between the deflection of the micropile head and the corresponding applied load for various load levels from the FE models with the soil made out of linear elastic, mildly nonlinear and highly nonlinear materials. The three soil models were fixed to have the same initial stiffness. The FE models in all these cases were incorporated with gapping elements. Generally, the deflections of the micropile head from the inelastic material were larger than those from the elastic material resulting from the non-linearity of the soil. Apart from this, it was noticed that the deflection from the highly nonlinear material was significantly larger than that of the mildly nonlinear material. This was due to the fact that the mildly nonlinear soil is more non-linear than the highly nonlinear soil. Referring to Figure 3.10, at a given shear stress, the shear strain in the soil with strong non-linearity is larger than that in the soil with weak non-linearity. In other words, when the soil is sheared, the soil with strong non-linearity will become softer and experience larger deflection than in the case with weak non-linearity even though they both have the same initial shear modulus before they are sheared.

The relationship between the percentage increase in deflection from the inelastic material with weak non-linearity with respect to the deflection from the elastic material, and the corresponding loading is plotted in Figure 4.8. The graph shows that the percentage increase ranges from 20 % (with 20 kN) to 82 % (with 400 kN). This depicts that the soil yielded dramatically at high loads.

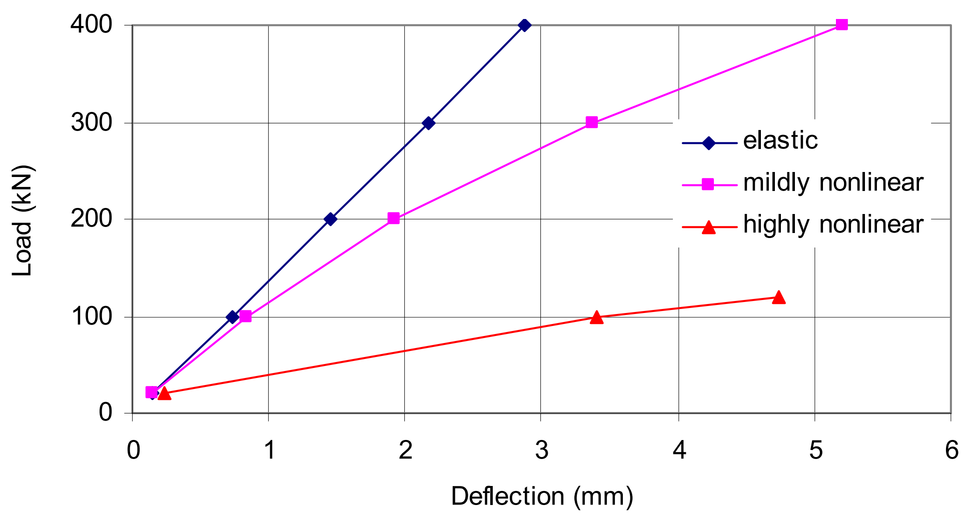

Figure 4.7 Load-deflection curves from elastic and inelastic soil materials at various loading

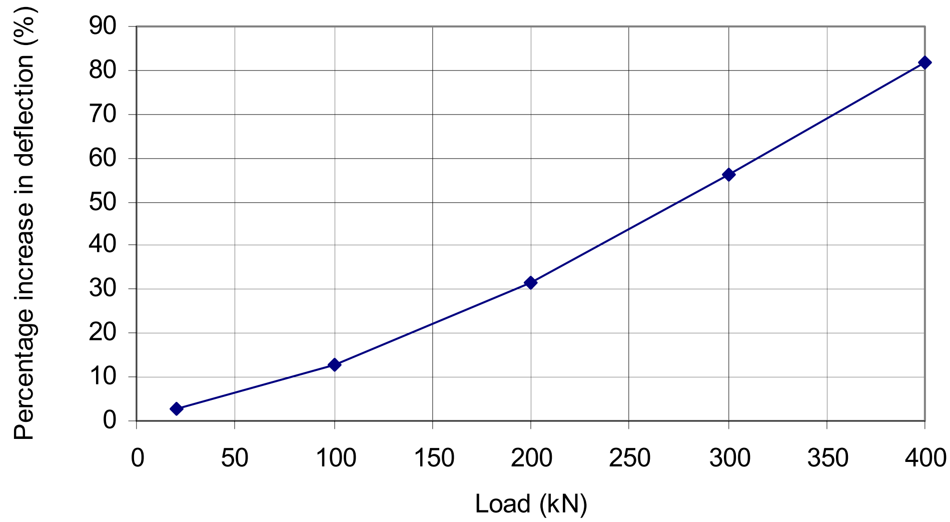

Figure 4.8 Percentage increase in deflection under various loading from elastic and mildly nonlinear soil materials

Figure 4.9 presents the variation of the deflections along the micropile length from elastic, mildly nonlinear and highly nonlinear materials under the applied load of 100 kN. The deflections from the inelastic material with weak non-linearity were slightly larger than those from elastic material. However, the deflections from the inelastic material with strong non-linearity were significantly larger than the ones with weak non-linearity. It was interesting to note that the deflection due to the weak non-linearity of the soil took place from the micropile head to approximately 0.1 length of micropile. Whereas in the case with strong non-linearity, the deflection due to yielding occurred from micropile head to roughly 0.2 length of micropile. This implies that the strong non-linearity of the soil leads to a larger stress transfer towards larger depths. This results in a larger volume of soils experiencing deflection.

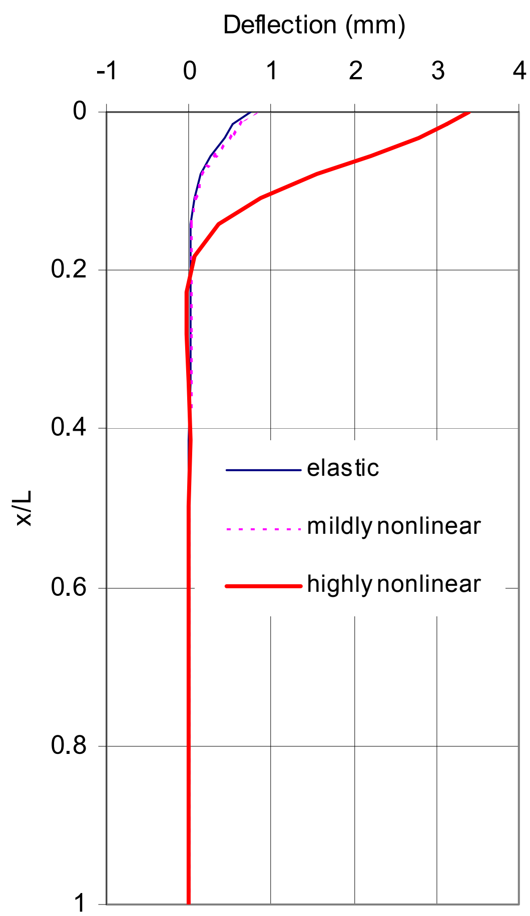

Figure 4.9 Variation of deflections with depth from elastic and inelastic soil materials with the load of 100 kN at the micropile head

Figure 4.10 shows the variation of the moments along the micropile length from elastic, mildly nonlinear and highly nonlinear materials under the applied load of 100 kN. The moments from the inelastic material with weak non-linearity was slightly higher than those from the elastic material but those with strong non-linearity were dramatically larger than those with weak non-linearity. This implicitly demonstrates that much lesser load was transferred to the surrounding soil with mildly non-linearity or higher relative rigidity, E_p/E_s (E_p = pile modulus, and E_s = soil modulus).

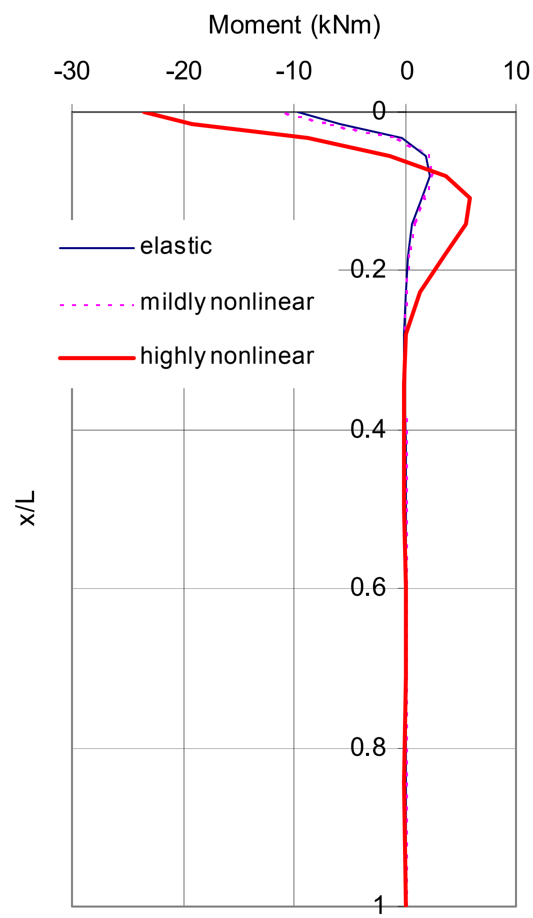

Figure 4.10 Variation of moments with depth from elastic and inelastic soil materials with the load of 100 kN at the micropile head

4.2.3 Young's Modulus of Soil

The variation of micropile deflections with varying Young's modulus of the soil, E, under a load of 200 kN at the micropile head is presented in Figure 4.11. All these runs were conducted with elastic materials for the clay with gapping elements incorporated. The graph generally shows that the deflection increased with decreasing E. Besides, the lower the E, the larger the stress transfer towards larger depth occurred. Consequently, the larger the depth of the soil from ground surface experiencing deflection. Besides, it was observed that at the lowest E, i.e. 1.0 x 10^6 N/m^2 (E/E_p = 4.35 x 10-5 where E_p is the

Young's modulus of micropile), the micropile did not behave as a long flexible pile since the deflection of the micropile tip was not zero. Extra caution should be taken care of when micropile (approximately with 0.2 m in diameter) is installed in a soil with E lower than 1.0×10^6 N/m^2.

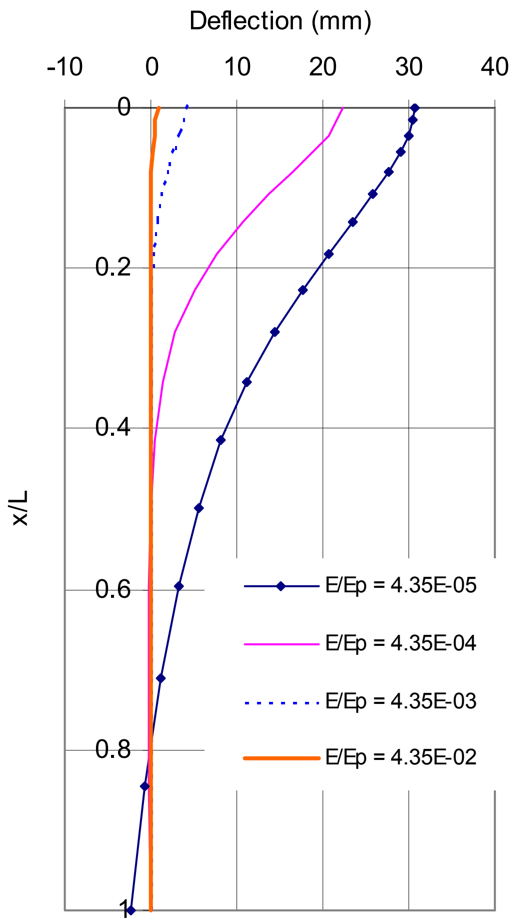

Figure 4.11 Variation of deflections with depth from soils with various Young's modulus with the load of 200 kN at the micropile head

Figure 4.12 shows the variation of the moments with different Young's modulus of the soil, E, under the load of 200 kN at the micropile head. It was interesting to note that the maximum moment at the micropile head was not directly related to the E of the soil. However, it was observed that the higher the E of the soil, the shorter the length of the micropile from the micropile head experienced moments greater than zero.

Both of these figures imply that if a soil is very stiff, the soil properties to a short depth from the ground surface are sufficient to predict the response of a micropile.

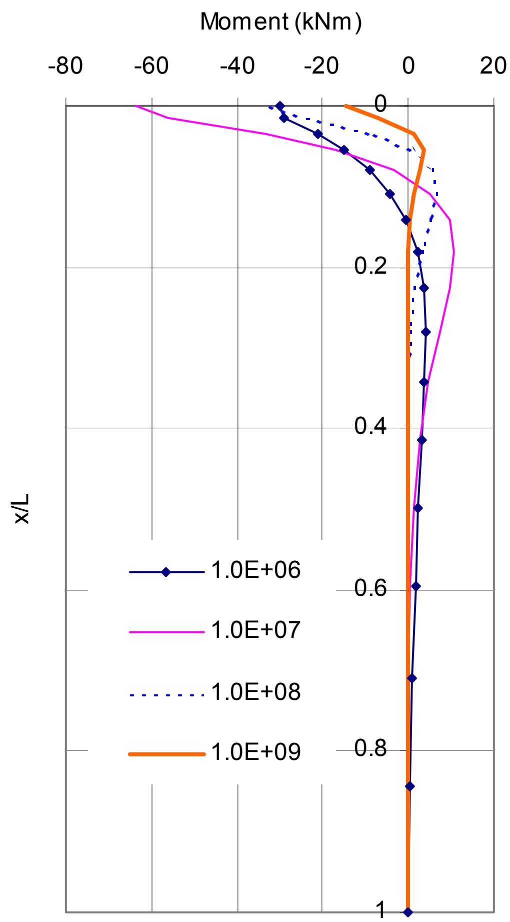

Figure 4.12 Variation of moments with depth from soils with various Young's modulus with the load of 200 kN at the micropile head

4.3 SINGLE MICROPILE : DYNAMIC LOADING

The parametric study conducted for single micropile under dynamic loading is presented in this section. The independent variables include the plasticity of the soil and intensity of input motion. The dynamic behavior was studied via the dependent variables of deflection and moment along the pile.

4.3.1 Non-linearity of Soil

Figure 4.13 presents the time history of the deflections at the micropile head from the FE models with the soils made out of linear elastic, mild nonlinear and highly nonlinear materials with the input motion of 0.3 g intensity at the base of clay layer (see Section 3.4.2). From the time of the peak accelerations, the response from the mildly and highly nonlinear soils lagged behind ones from the linear elastic material. At the same time, the responses from the inelastic material with strong non-linearity lagged behind those from the inelastic material with weak non-linearity. These two phenomenons result from the material damping and the degraded shear wave velocity of the inelastic soils. No damping was used in the linear elastic material and material damping was used in the inelastic materials. This explains why in the first phenomenon, there were delays in the responses from the inelastic materials as compared to those from the linear elastic material. As for the second phenomenon, the inelastic material with strong non-linearity has a higher hysteretic damping than in the inelastic material with weak non-linearity at a given strain. Consequently, the higher damping from the highly nonlinear material resulted in the delay of the responses as compared to those from the mildly nonlinear material (see Figure 3.10).

Besides that, it was observed that the deflection from the elastic material was a harmonic response due to resonance without material damping. However, the amplitude of the deflections from both inelastic materials decreased with time due to hysteretic damping. It was also believed that the material with strong non-linearity has significantly higher hysteretic damping (more non-linear damping curve) than in the material with weak non-linearity at a given strain (see Figure 3.9). Consequently, the deflections from the material with strong non-linearity were damped out sooner.

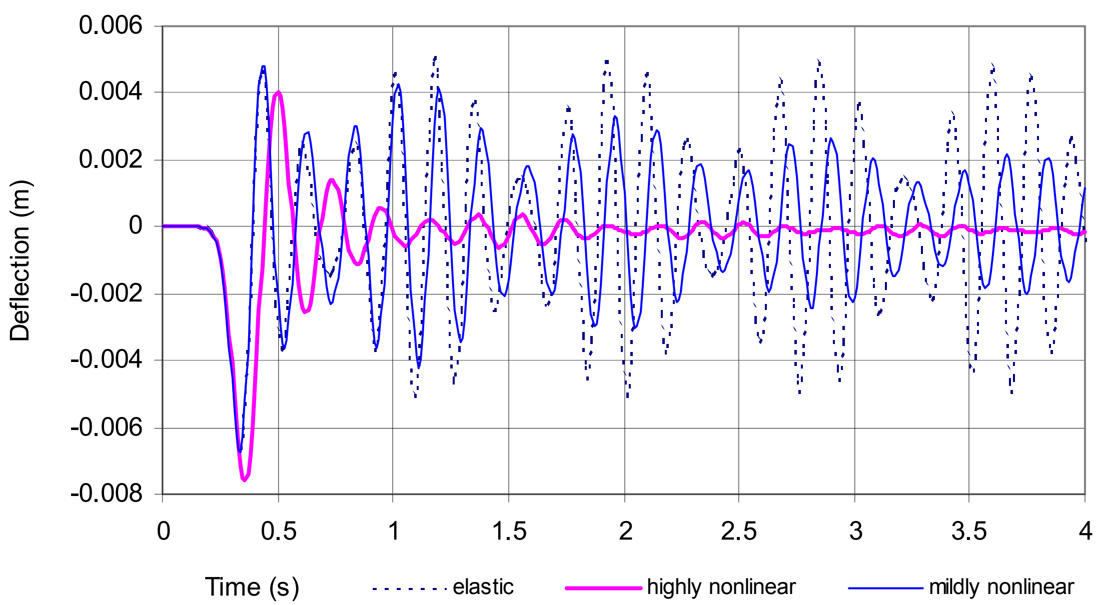

Figure 4.13 Time history of deflections at micropile head from various soil models

Alternatively, the micropile head responses are presented in terms of acceleration response spectra which is shown in Figure 4.14. The maximum spectral acceleration from elastic and inelastic (weak non-linearity) materials was 4.31 g and 3.39 g, respectively. These peaks happened at the same spectral period (i.e. 0.18 s) which indicated no significant reduction in shear modulus in the soil or the soil behaved nearly elastically for this input motion level. Thus, it was believed that the reduction in spectral acceleration was resulted mainly from the hysteretic damping of the inelastic material. Meanwhile, the maximum spectral acceleration from the inelastic material with strong non-linearity was only 1.07 g and the peak occurred at the natural period of 0.25 s. The shift of the peak to the right was attributed to the reduction of shear velocity due to a decrease in shear modulus. Meanwhile, the much lower peak from the material with strong non-linearity as compared to the one with weak non-linearity was resulted from the higher hysteretic damping in the highly nonlinear soil at a given strain (see Figure 3.10).

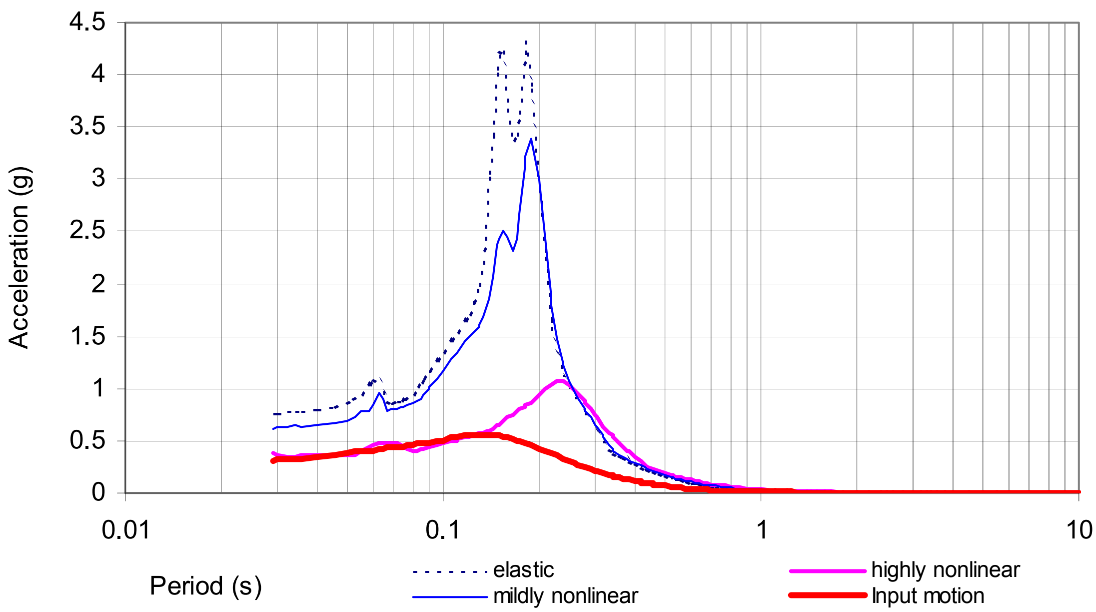

Figure 4.14 Acceleration response spectra from elastic and inelastic materials, and of input motion

Figure 4.15 presents the envelope of the bending moments along the micropile length for the 0.3 g input motion for both the elastic, mildly nonlinear and highly nonlinear materials. In all cases, the maximum bending moment happened at the micropile head due to the fixed head condition. The moment envelope from the inelastic material with weak non-linearity was smaller than the one from the elastic material. As mentioned in the above, this inelastic material behaved elastically with this input motion. Therefore, the smaller moment envelope was attributed to its hysteretic damping. Meanwhile, the much smaller moment envelope from the inelastic material with strong non-linearity as compared to the one with weak non-linearity resulted from the much higher hysteretic damping in the highly nonlinear soil.

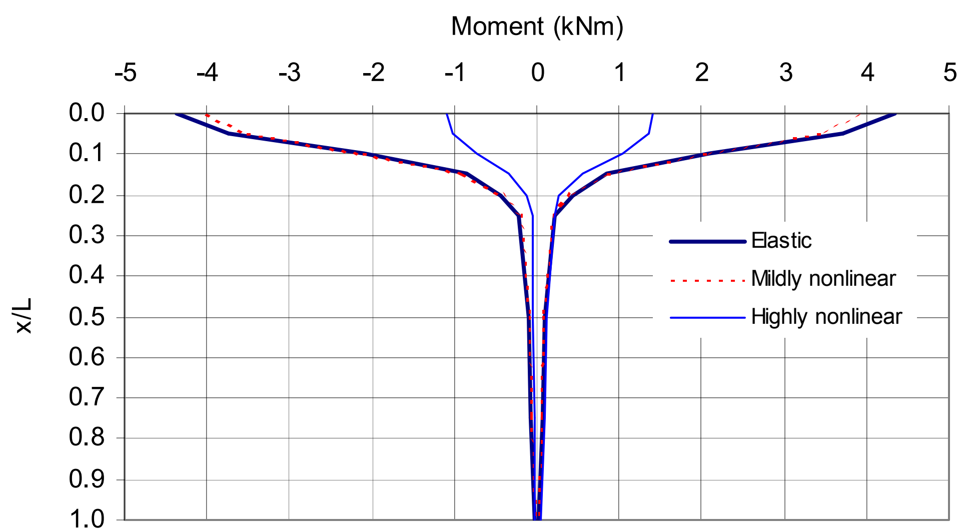

Figure 4.15 Bending moment envelopes from elastic and inelastic materials with 0.3 g input motion. Initial motion produces positive moment

The figure also reveals that the envelope is not symmetrical for the inelastic materials. In order to provide a better visual for checking the symmetry of the envelopes, Figure 4.16 plots the maximum positive moments in the horizontal axis and the maximum negative moments in the vertical axis. The reference line represents a line with the slope of 1:1. The figure clearly shows that the envelope from the elastic material was symmetrical and the one with mildly nonlinear soil was close to symmetrical due to the fact that it behaved essentially elastic for the input motion. The envelope from the inelastic material with strong non-linearity exhibits non-symmetry. This was due to the fact that after the micropile was displaced to a direction, it would be displaced to the opposite direction with a smaller magnitude due to material damping. It was also interesting to observe that the symmetry and the non-symmetry of the moment envelopes exhibit the linear elasticity and the non-linearity of the materials, respectively.

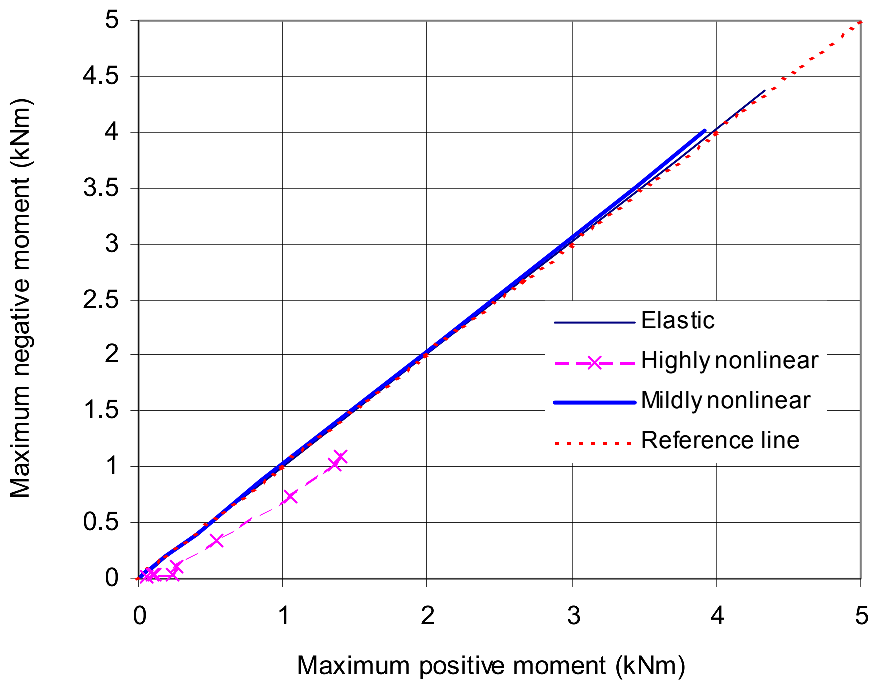

Figure 4.16 Comparison of maximum positive and negative moments from elastic and inelastic materials. Initial motion produces positive moment

4.3.2 Intensity of input motion

Figure 4.17 shows the acceleration response spectra of the micropile head from the soil with weak non-linearity at various intensities of input motion. Not surprisingly, the amplitude increased with increasing intensity of input motion. The maximum peak occurred at the same spectral period. This demonstrates that with these three input motions, the strains were small and the soil behaved linearly elastic.

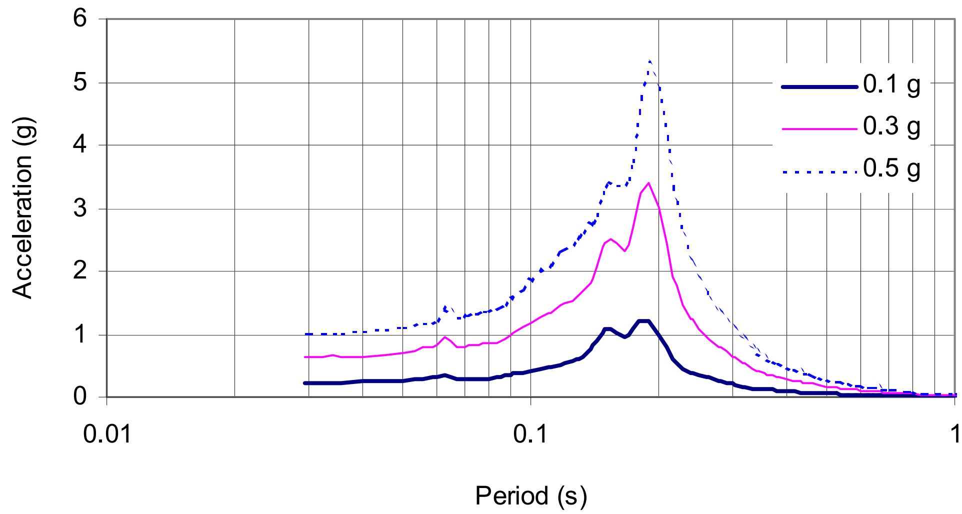

Figure 4.17 Acceleration response spectra from inelastic material with weak non-linearity with various input motions

Figure 4.18 illustrates the acceleration response spectra of the micropile head from the soil with strong non-linearity at different input motions. Similarly, the amplitude increased when the intensity of the input motion increased. However, the spectral period corresponding to the peak spectral acceleration shifted to the right with increasing intensity of the input motion. This indicates that with higher intensity, the soils experienced higher strains and consequently, more reduction in shear modulus of the soil occurred. The site period is given by $T_s = 4H/v_s$, where H is the height of the soil profile and v_s is the shear wave velocity. For lower values of v_s (e.g. at higher strains), the site period T_s increases.

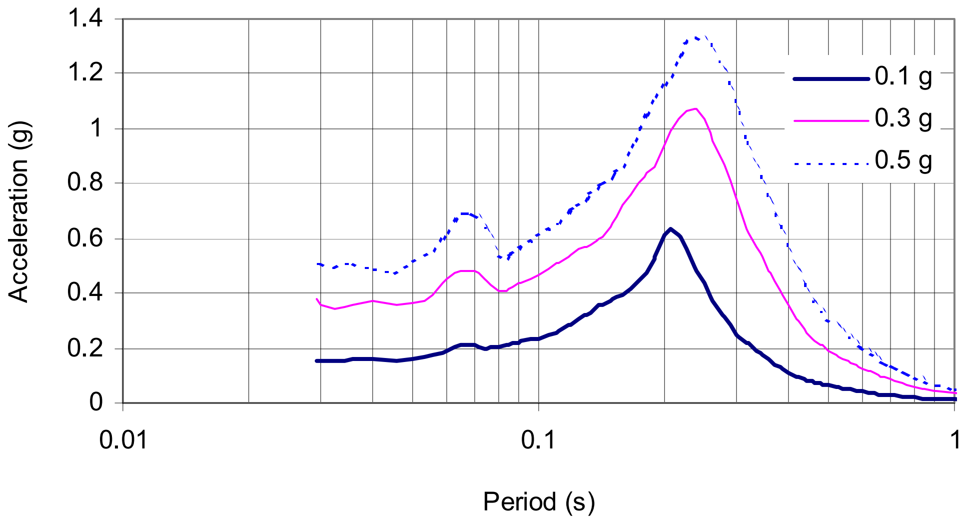

Figure 4.18 Acceleration response spectra from inelastic material with strong non-linearity with various input motions

The bending moment envelopes at three different input motion intensities from the models with mildly and strongly nonlinear materials are presented in Figures 4.19 and 4.20, respectively. In both figures, the bending moment envelope increases with increasing intensity. The symmetric shape of the envelope in Figure 4.19 implies that the soil with weak non-linearity behaved nearly elastically for all the input motion intensities. On the other hand, Figure 4.20 shows that with increasing input motion intensity, the soil with strong non-linearity exhibited higher level of non-symmetry of the envelope shape implying more non-linearity. This non-linear behavior is seen clearly in Figure 4.21.

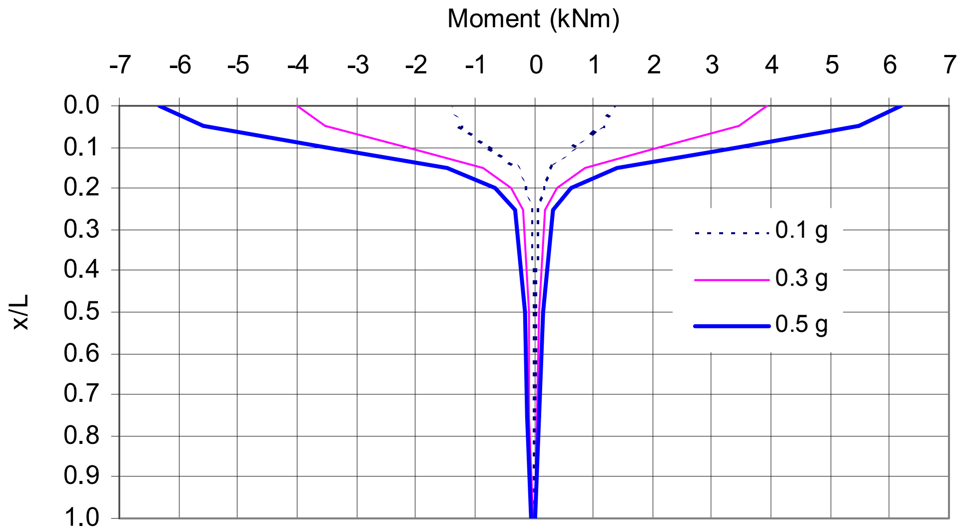

Figure 4.19 Bending moment envelope in inelastic soil with weak non-linearity at various input motion intensities

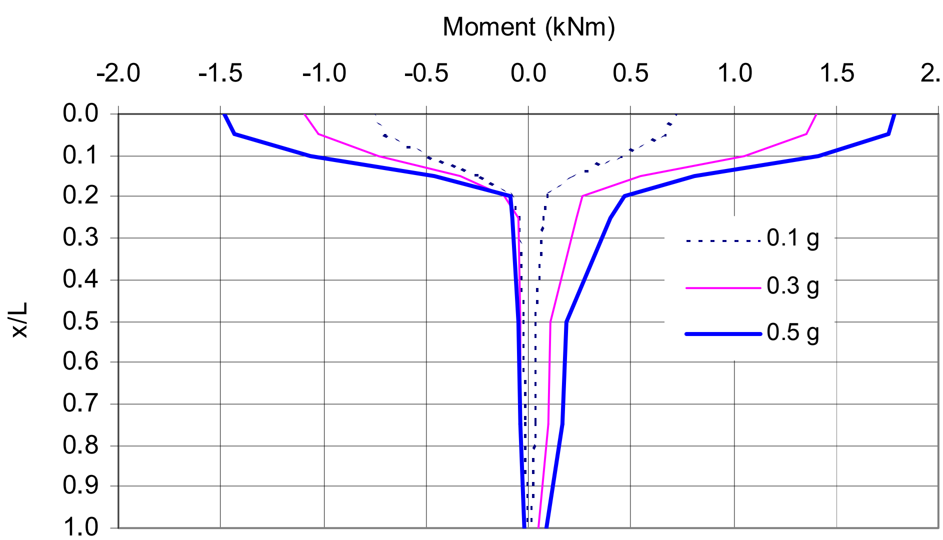

Figure 4.20 Bending moment envelope in inelastic soil with strong non-linearity at various input motion intensities. Initial motion produces positive moment

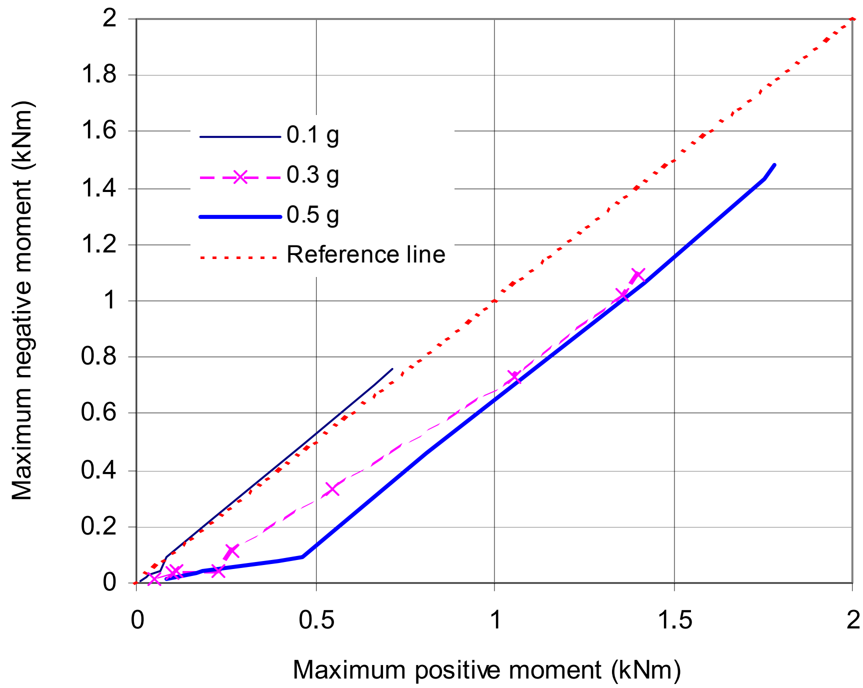

Figure 4.21 Comparison of maximum positive and negative moments from inelastic material with strong non-linearity at various intensities. Initial motion produces positive moment

4.4 MICROPILE GROUPS : DYNAMIC LOADING

The parametric study conducted for micropile groups under dynamic loading includes the study of the effect of variations in the intensity of input motion, inclination of micropiles, frequency content of input motion, and property of superstructure on deflection and moment. In this section, the study was conducted only on the inelastic material with strong non-linearity.

4.4.1 Input Motion Intensity

Figures 4.22 (a) and (b) present the time history of deflection at the micropile head of the vertical and inclined micropile groups at the input motion levels of 0.1 g and 0.5 g, respectively. Generally, the maximum deflection from both the vertical and inclined micropile groups was higher for higher input motion intensity. It was also observed that for both input motion levels, there was a residual displacement at the end of shaking. It appears that the residual displacement in the case with 0.5 g input motion, approximately 1.68 mm, was higher than that in the case with 0.1 g input motion, approximately 0.2 mm.

Figure 4.23 illustrates the acceleration response spectra of the micropile head in both vertical and inclined micropiles at 0.1 g and 0.5 g input motions. The spectral acceleration amplitudes for the case with 0.5 g input motion were larger than in the case with 0.1 g input motion. It was also interesting to note that the spectral period corresponding to the peak spectral acceleration was higher for the more intense input motion. This implies that the input motion with higher intensity caused the larger reduction in shear modulus (or shear wave velocity) due to higher strains.

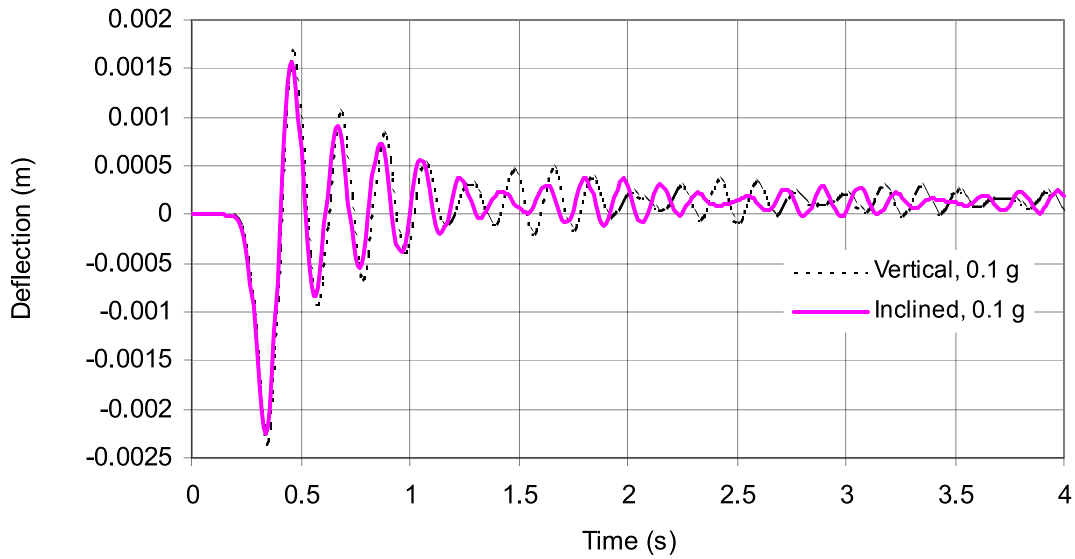

(a) 0.1 g

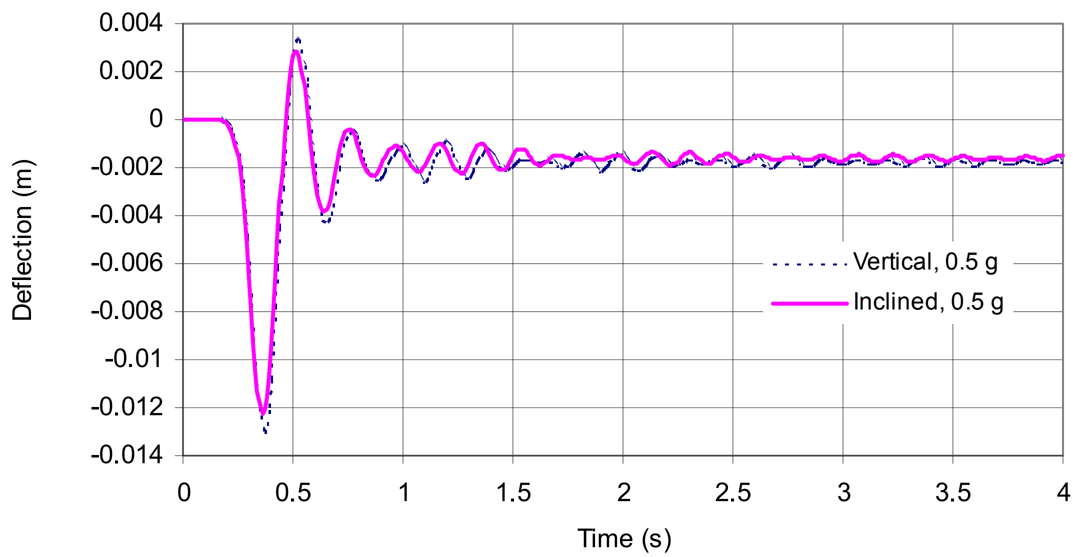

(b) 0.5 g

Figure 4.22 Time history of deflections at micropile heads in both vertical and inclined micropiles at (a) 0.1 g, and (b) 0.5 g input motions

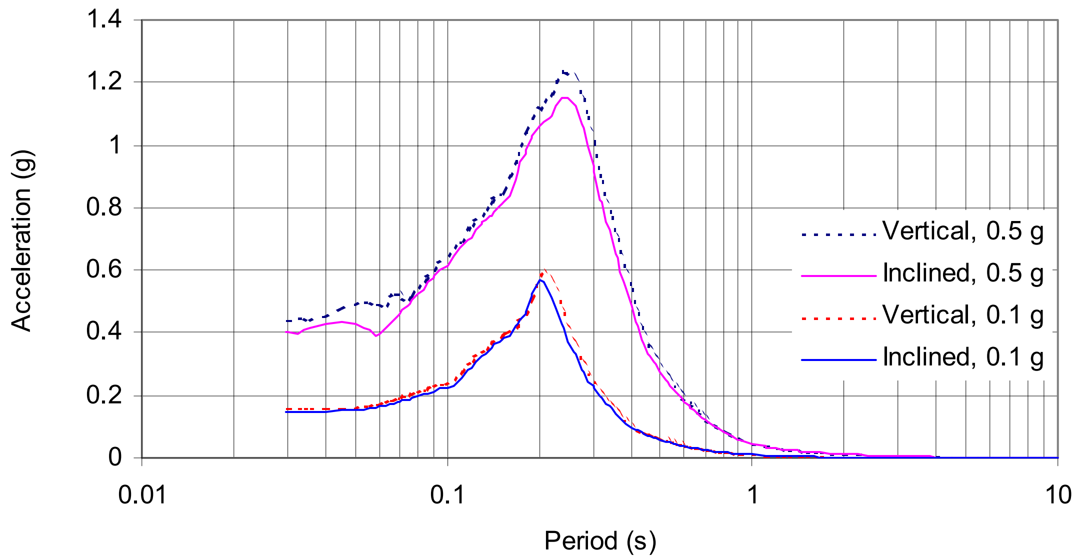

Figure 4.23 Acceleration response spectra of micropile head in vertical and inclined micropiles at 0.1 g and 0.5 g input motions

Figures 4.24 and 4.25 present the bending moment envelopes for vertical and inclined micropile groups, respectively, for varying input motion intensities. The bending moment envelope increases in both vertical and inclined micropiles with increasing intensity. Moreover, in both vertical and inclined micropiles, the lack of symmetry of the moment envelope increases with increasing input motion intensity. This demonstrates the larger degree of non-linearity of the soil with larger input motion intensity.

It was interesting to note that in the case of vertical micropile group, the moment envelope for the left and right vertical micropiles was similar at all input motion intensities. This indicates that there was an equal distribution of loading among the vertical micropile members under seismic loading. However, in the case of inclined micropiles, there was no equal distribution loading among the inclined micropiles. The left micropile appears to have carried higher loads. This indicates that the inclination of micropiles contributed to the unequal distribution of loads among the micropile group members.

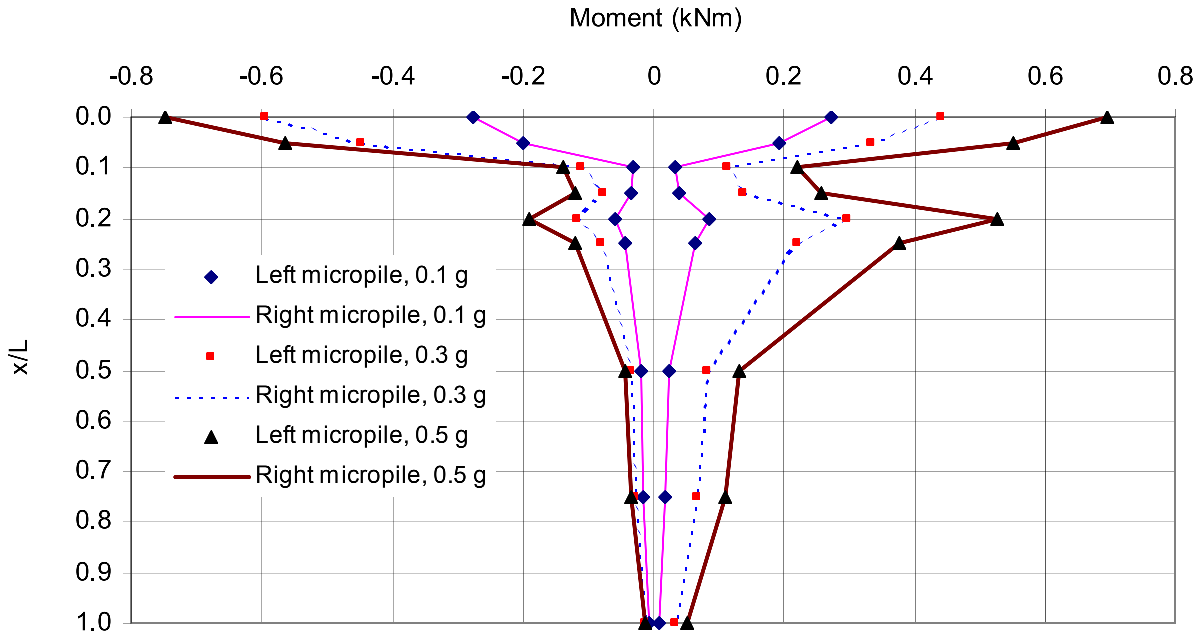

Figure 4.24 Bending moment envelope of left and right vertical micropiles at various intensities of input motion

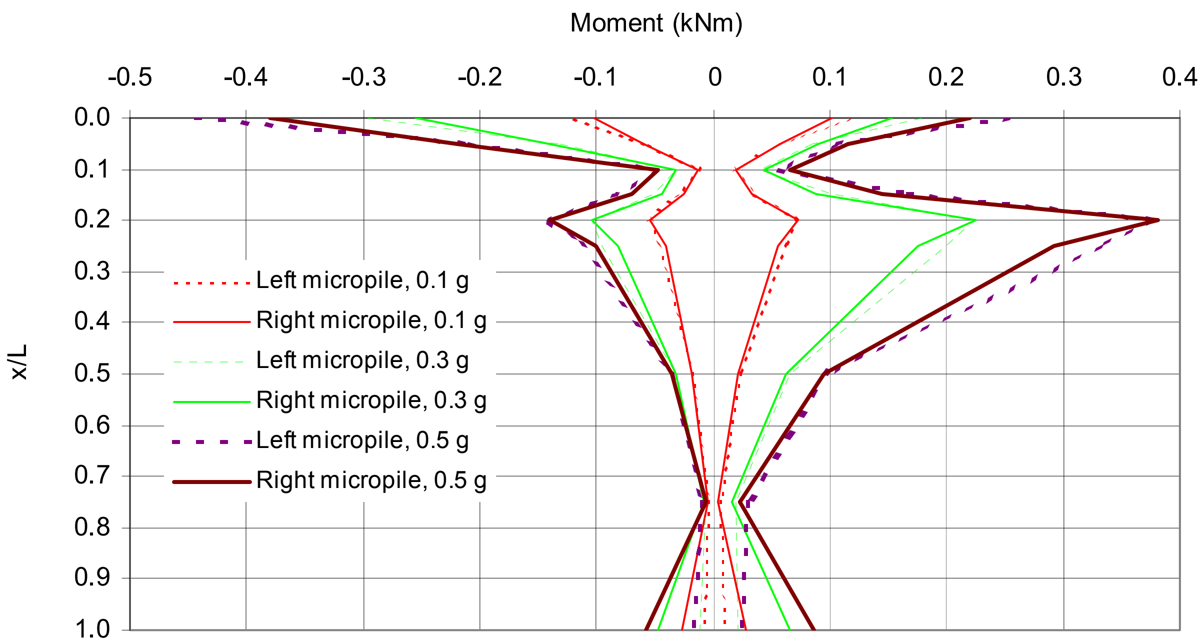

Figure 4.25 Bending moment envelope of left and right inclined micropiles at various intensities of input motion

4.4.2 Inclination

By referring to Figure 4.22, the maximum amplitude of deflection is lower in the inclined micropile group than in the vertical micropile group. This illustrates the higher stiffness of the inclined micropile group. Moreover, the deflection response from the vertical micropiles lagged behind the one from the inclined micropiles. This was attributed to the fact that the soil close to the vertical micropiles initially experienced higher strains since their displacements were higher than in the inclined micropiles. These higher strains resulted in higher hysteretic damping, thus causing the delay.

Figure 4.23 shows that the spectral accelerations from the vertical micropile group were larger than those from the inclined micropile group for both input motion levels (0.1 g and 0.5 g). This illustrates higher lateral stiffness of the inclined micropile group as compared to the vertical micropile group. It was noteworthy to observe that the spectral periods corresponding to the peak spectral acceleration from both vertical and inclined micropile groups were the same. This demonstrates that the inclination of the micropiles did not result in any change in the soil's strain level.

Figure 4.26 presents the bending moment envelope of two micropile members in the vertical and inclined micropile groups at the input motion intensity of 0.5 g. The bending moment envelopes from the inclined micropiles were smaller than those from the vertical micropile because the axial capacity of the inclined micropiles was mobilized.

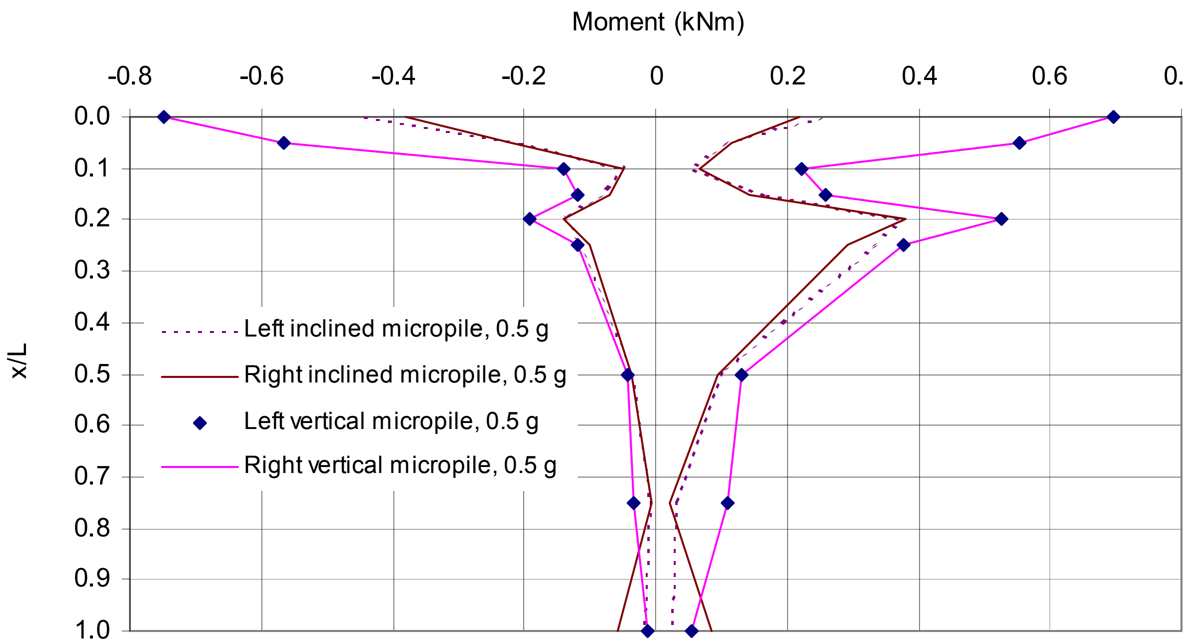

Figure 4.26 Bending moment envelope of vertical and inclined micropiles at 0.5 g input motion

4.4.3 Frequency Content of Input Motion

The acceleration response spectra of the micropile head in the vertical micropile group at the input motion of 0.5g with different frequency contents are presented in Figure 4.27. The legend f1 in the figure represents an input motion that has a predominant period of approximately 0.14 s. Meanwhile, the legend f2 means an input motion that has a predominant period of approximately 0.27 s. The peak spectral acceleration for f1 was smaller than the one for f2. This shows that the input motion with higher frequency (lower predominant period) tended to damp the response more than the one with lower frequency (higher predominant period). This resulted in the input motion with smaller predominant period caused smaller responses at the micropile head.

In Figure 4.27, the legend “f1, Tp = 0.14 s, no micropiles” represents the acceleration response spectrum of a FE analysis which is similar to the case associated with the legend “f1, Tp = 0.14 s” except that there were no vertical micropiles in the system. The results agree with each other very well, implying the high flexibility of micropiles, since the presence of micropiles did not change the accelerations at the ground surface. It is noteworthy to observe that there was a significant second peak in spectral acceleration associated with the second mode (approximately at spectral period = 0.065 s) in the case without micropiles. However, the second peak acceleration was attenuated by the presence of micropiles (see legend “f1, Tp = 0.14 s” in Figure 4.27). This demonstrates the benefit of micropiles in reducing the response at the micropile head during seismic conditions.

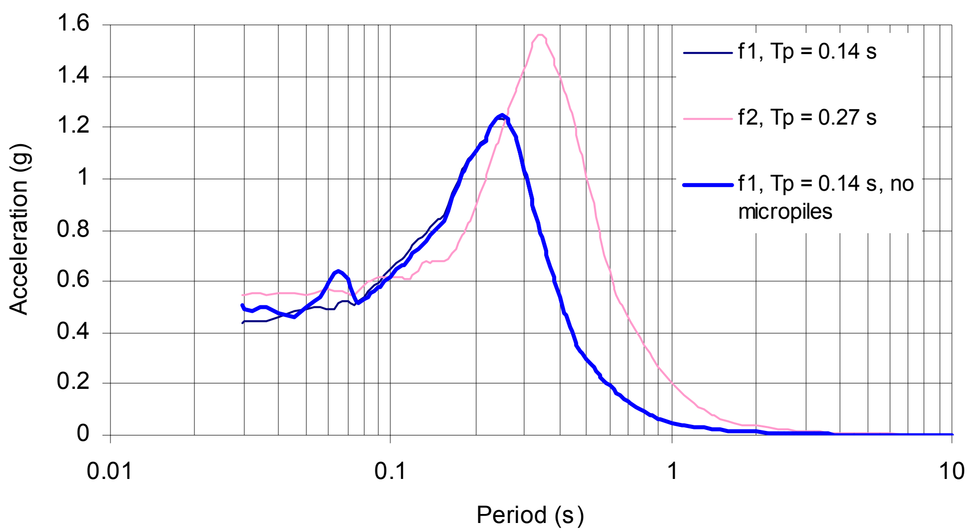

Figure 4.27 Acceleration response spectra of micropile head in vertical micropiles with different frequency contents at input motion of 0.5g

Figure 4.28 illustrates the bending moment envelopes of vertical micropiles at various frequency contents of input motion. The input motion with larger predominant period (f2) generally had a larger maximum moment than the one in the case with smaller predominant period (f1). This was attributed to the larger kinematic loading from the input motion with a larger natural period. However, it was observed that the input motion with larger predominant period decreased the moment envelope at the micropile head as compared to the case with lower predominant period.

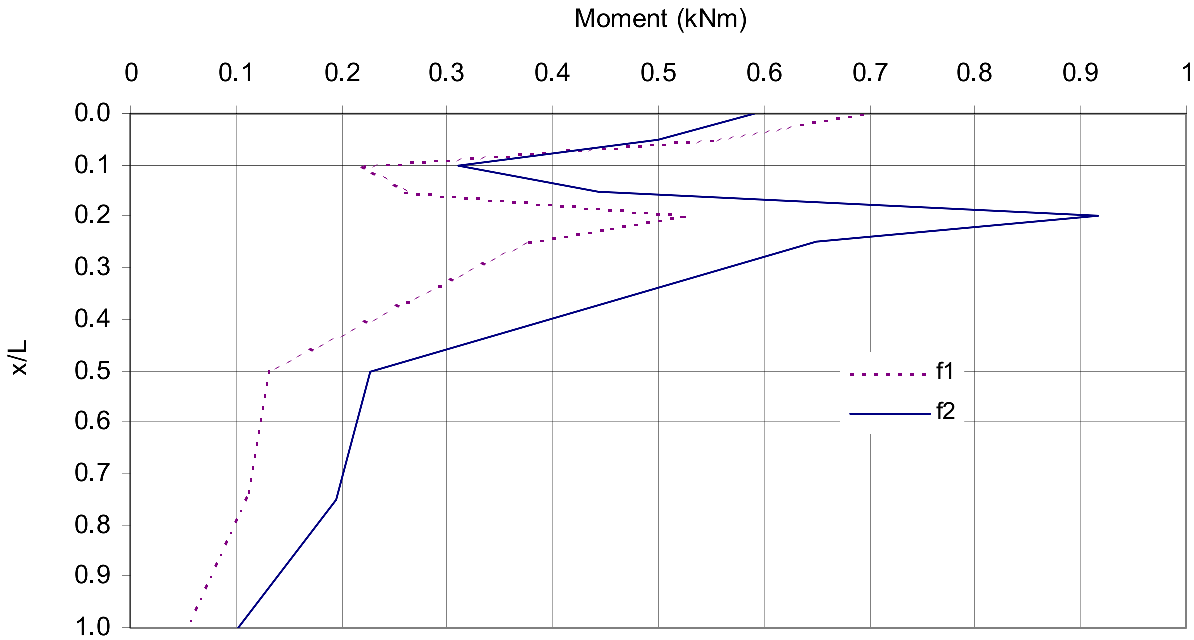

Figure 4.28 Bending moment envelopes of vertical micropile groups at different frequency contents of input motion

4.4.4 Natural Period of Superstructure

For this parametric study, the superstructure supported by the micropile groups was idealized or simplified into a mass with single degree-of-freedom (SDOF). This will serve only as an approximation to the response of a structure. Note that the FE analysis does not represent the actual responses of a superstructure, especially a tall building. This clarification is important because the seismic response of a superstructure depends on many factors, such as the number of DOF, the materials used for the building, the quality of the construction (especially the detailing for ductility), the stiffness, the matching of the frequency contents of the superstructure with the ones of input motion (McDaniel, 2004), and other factors.

Figure 4.29 plots the acceleration response spectra of the superstructure with various superstructure natural periods for the case of a vertical micropile group for the input motion intensity of 0.5 g. The natural periods of the SDOF were 0.1s, 0.16 s, and 0.225 s. These natural periods were increased by increasing the density of the mass of the superstructure. It was observed that the magnitude of the acceleration increased with the increasing superstructure natural period.

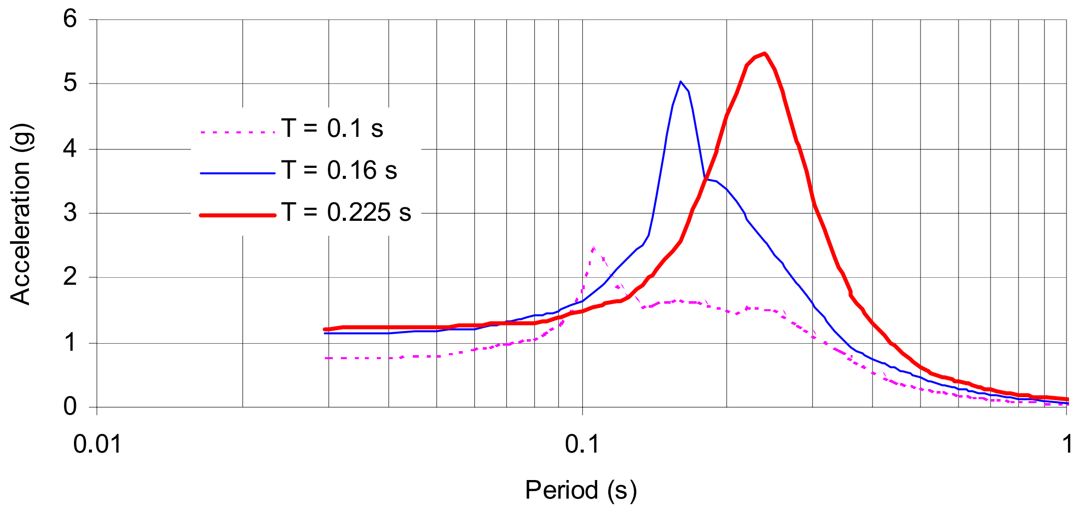

Figure 4.29 Acceleration response spectra of the superstructure with its various natural periods

Figure 4.30 shows the acceleration response spectra at the micropile head with various natural periods of superstructure. The peak accelerations in case with 0.1 s and 0.16 s of the natural period of superstructure were higher than the one in the case with 0.25 s. The predominant period of the input motion was approximately 0.14 s. Probably the peak magnitude in the case of 0.1 s and 0.16 s was due to the close matching of the predominant period of input motion (i.e. 0.14 s) with the natural periods of superstructure (0.1 s and 0.16 s).

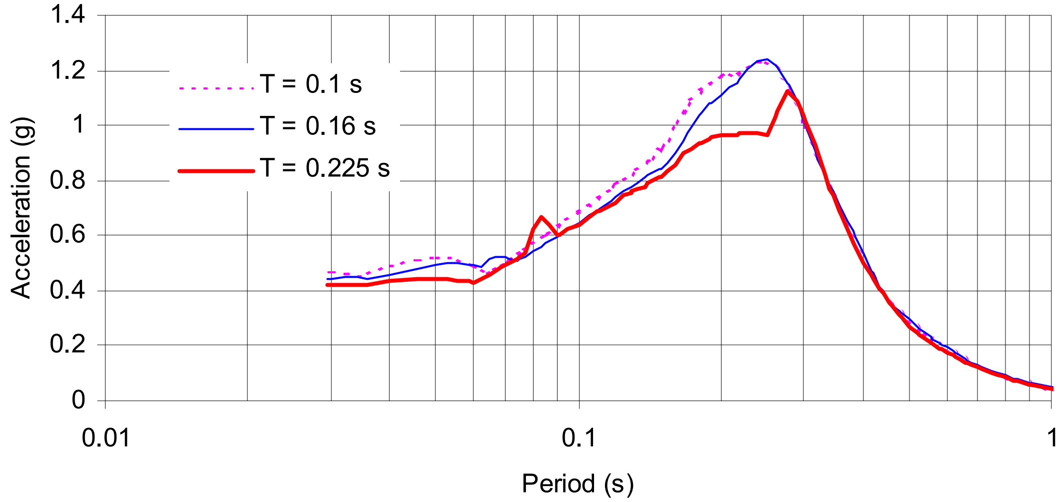

Figure 4.30 Acceleration response spectra at the micropile head with various natural periods of superstructure

Figure 4.31 illustrates the bending moment envelope of vertical micropiles at the input motion of 0.5 g with increasing natural periods of superstructure (due to increasing density of the mass of the superstructure). The moment envelope at the micropile head increased with increasing natural period of superstructure. This was attributed to the inertial force from the superstructure. It was interesting to observe that the increasing inertial force from the increasing natural period of superstructure did not contribute to the increase in moment at the point of 0.2 length of micropile.

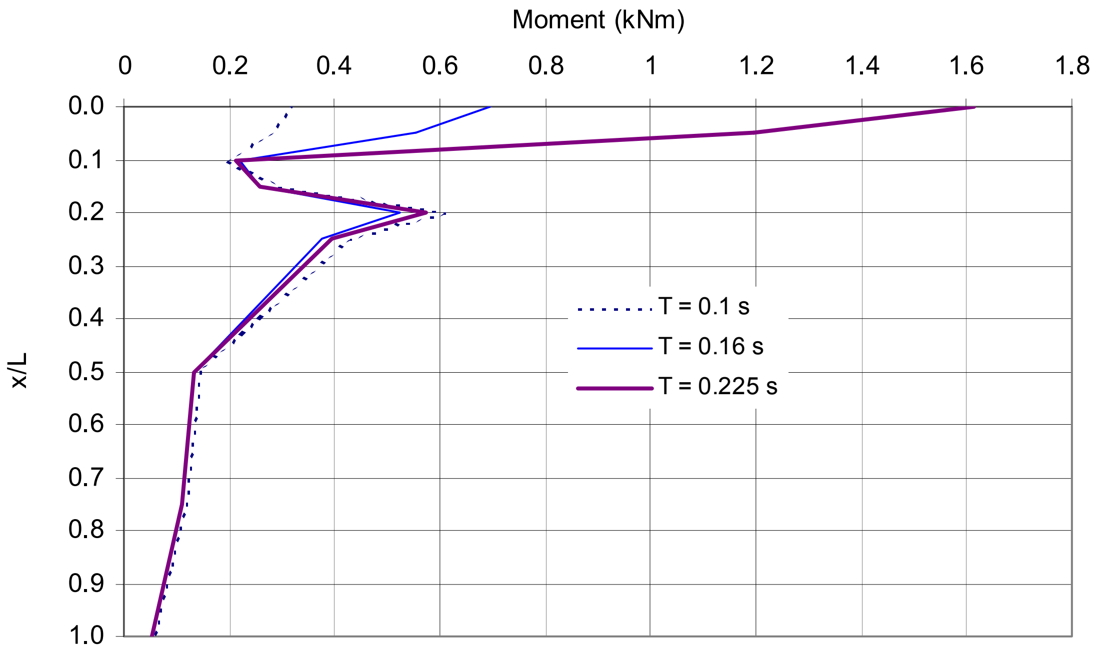

Figure 4.31 Bending moment envelope of vertical micropiles at various natural periods of superstructure

CHAPTER 5
p-y CURVES

5.1 INTRODUCTION

The load transfer mechanism at the interface between the pile and the soil for a laterally loaded pile usually is represented by *p-y* curves. These *p-y* curves have been incorporated into computer programs, such as COM624, Florida Pier, and LPILE. They are used mainly to estimate the deflection and moment along the piles at a given load. Therefore, *p-y* curves serve as a useful tool in the design of a laterally loaded pile. In this study, *p* is defined as the lateral soil resistance per unit length of the pile, and *y* is the lateral deflection. In this chapter, the back-calculation, validation, and behavior of *p-y* curves are presented.

5.2 BACKCALCULATION OF *p-y* CURVES

There are several ways to back-calculate *p-y* curves from FE analyses or full-scale load tests. One of the most commonly used methods is by making use of the bending moments along the pile. An analytical expression is fitted to the discrete moment data along the pile. Subsequently, the expression is differentiated twice to derive the soil resistance, *p*. Another method to obtain *p* is by summing the normal and shear stresses applied to the pile by the soil immediately surrounding it (Bransby, 1999). In this study, the former method was used.

Bending moment data were derived from the axial stresses in the micropile elements using Equation 5.1 as shown in the followings. These axial stresses were located at the two opposite nodes on the outermost diameter of the micropile at various depths.

$$M = \frac{(\sigma_L - \sigma_R)}{d} I \tag{5.1}$$

where M is the bending moment, σ_L and σ_R are the axial stresses at the left and right outermost micropile diameter, respectively, d is the micropile diameter, and I is the moment inertia of the micropile.

Soil reaction, p was derived from the differential equation for a beam on a Winkler type of subgrade:

$$p = -\frac{d^2 M}{dx^2} \tag{5.2}$$

where x is the depth from ground surface. In this study, a 6th degree polynomial was used to fit the moment data using least squares method to provide some degree of smoothing. The resulting polynomial should predict a shear force at the micropile head equal to the applied load, i.e.

$$V = \frac{dM}{dx}(x = 0) \tag{5.3}$$

In order to satisfy this additional constraint, a method suggested by Weaver (2004) was implemented. The method was to create an artificial moment data point above the micropile head and vary its value until the calculated shear force (Equation 5.3) equaled the applied horizontal force at the micropile head. The deflections y were obtained directly from the output of the FE analysis.

5.3 VALIDATION OF *p-y* CURVES

The *p-y* curves back-calculated from the FE models of a single micropile (in Section 3.4.1) under static loading except from Model 3 are validated herein. An additional FE model was built with lower Young's modulus (i.e. 5.22×10^{7} N/m^{2} opposed to 4.69×10^{8} N/m^{2}) for the clay. This FE model was constructed with linear elastic soil material and incorporated with interface elements. The same values of loading, i.e. 10 kN, 50 kN, 100 kN, 150 kN, and 200 kN were applied at the micropile head

The validation was performed by using the *p-y* curves obtained from the FE analyses at various depths in a finite difference (FD) code, LPILE where the pile is treated as a beam-column and the soil is represented by non-linear Winkler-type springs.

5.3.1 Model 1 (Linear Elastic and Perfect Bonding)

Figure 5.1 shows the back-calculated *p-y* curves from Model 1 (Section 3.4.1.1) at the depths of 0.00, 0.12, 0.27, 0.44, and 0.64 m from the micropile head. All these *p-y* curves were used in the FD analysis except the one at the ground surface. This was done because the *p-y* curves at the ground surface obtained from the other models (Section 5.3.1 through Section 5.3.5) were unreasonable. Thus, in order to maintain consistency, the *p-y* curve at the depth of 0.00 m was not used in the FD analysis. Instead, the *p-y* curve obtained at the depth of 0.12 m was used for the depth of 0.00 m assuming that the springs at these two locations had the same properties.

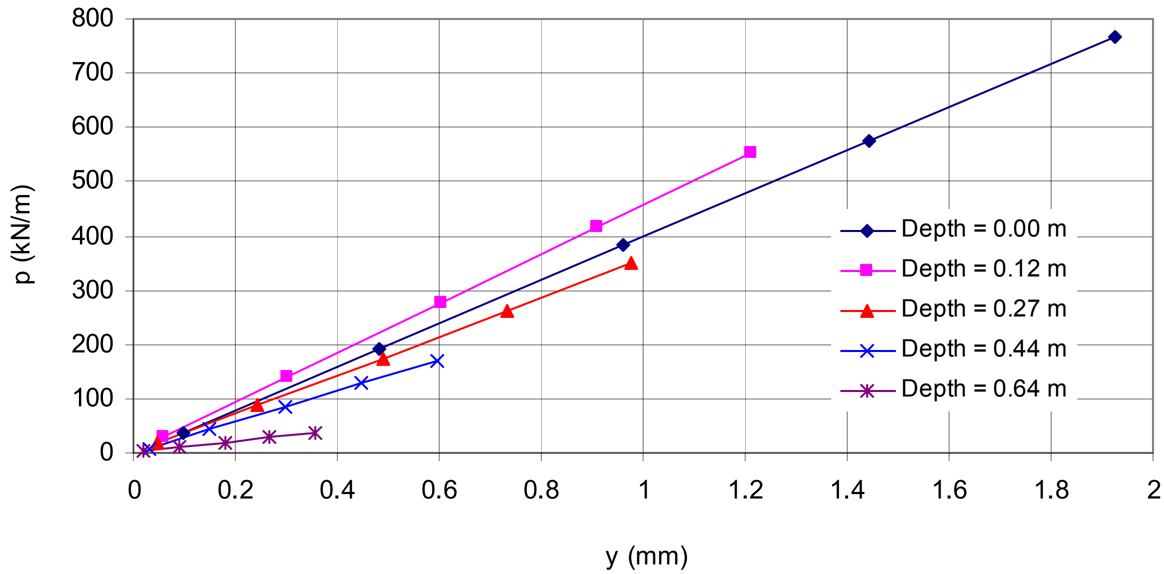

Figure 5.1 Load-transfer curves at various depths from Model 1 (Section 3.4.1.1)

Figure 5.1 reveals that the *p-y* stiffness (modulus of subgrade reaction, in the unit of force per area) reduced with depth assuming that the *p-y* curve at the 0.00 m depth was faulty. The similar observation was reported by Bransby (1999). This shows that the *p-y* curve stiffness was not unique along the micropile length even though linear elastic material was used for the clay.

Figure 5.2 presents the deflections and the bending moments along the micropile length under the load of 400 kN at the micropile head from the finite element (ABAQUS) and finite difference (LPILE) analyses. Except for the deflections at the depths of 0.05 to 0.40 micropile length, the results of deflections and moments from both analyses agreed very well to each other. This validates that the *p-y* curves obtained from the FE model are reasonable.

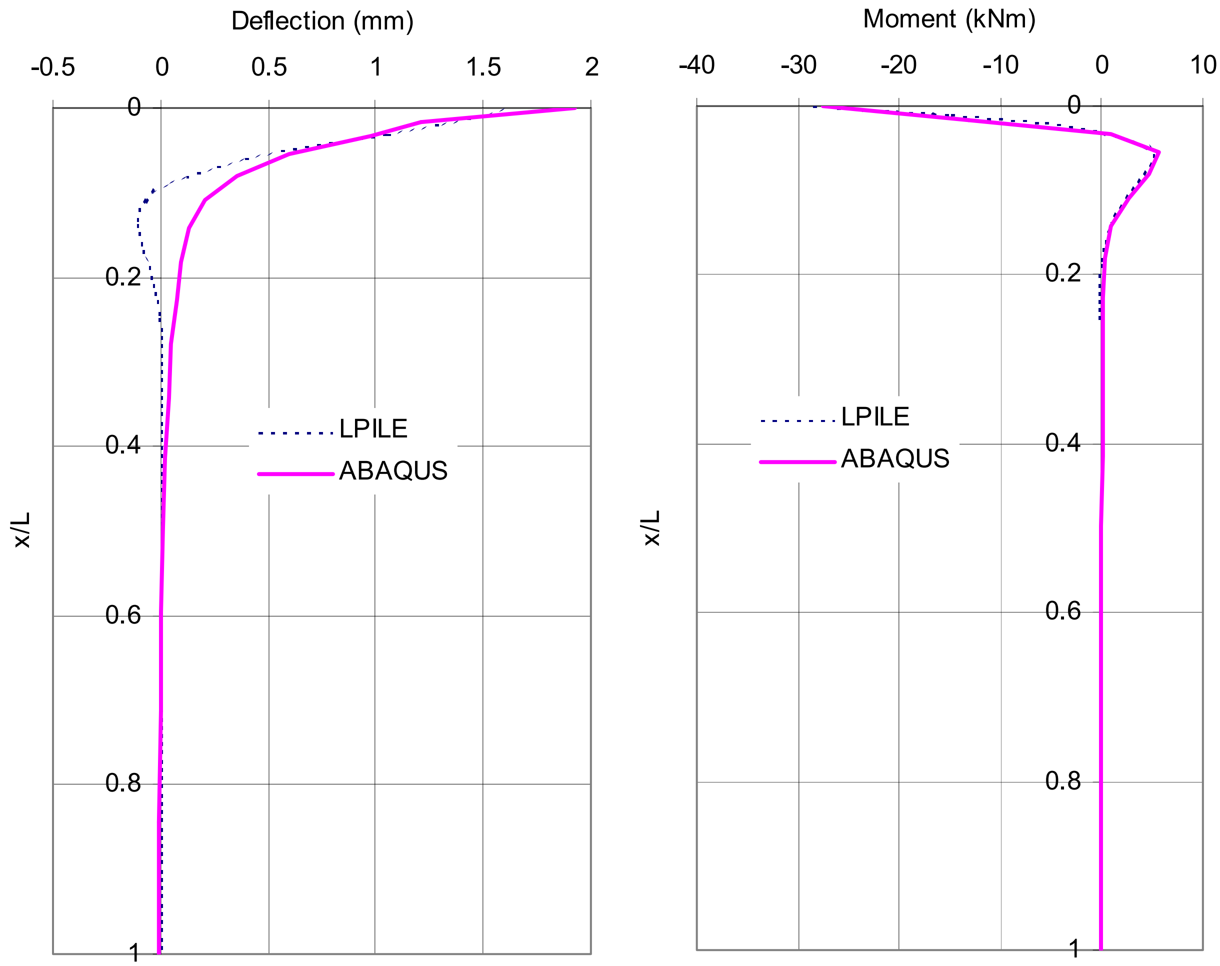

Figure 5.2 Deflection and bending moment profiles under the load of 400 kN at the micropile head from LPILE and ABAQUS

5.3.2 Model 2 (Linear Elastic and Interface Elements)

The derived *p-y* curves at various depths from Model 2 (Section 3.4.1.2) are presented in Figure 5.3. Again, the *p-y* curve at the depth of 0.00 m was not used in the FD analysis. Similar to Model 1, the graph shows that the *p-y* stiffness at various depths were not the same in a linear elastic soil. However, the *p-y* stiffness generally increased with depth (except the one at the 0.64 m depth). This is opposite to the trend found in the linear elastic soil (Model 1).

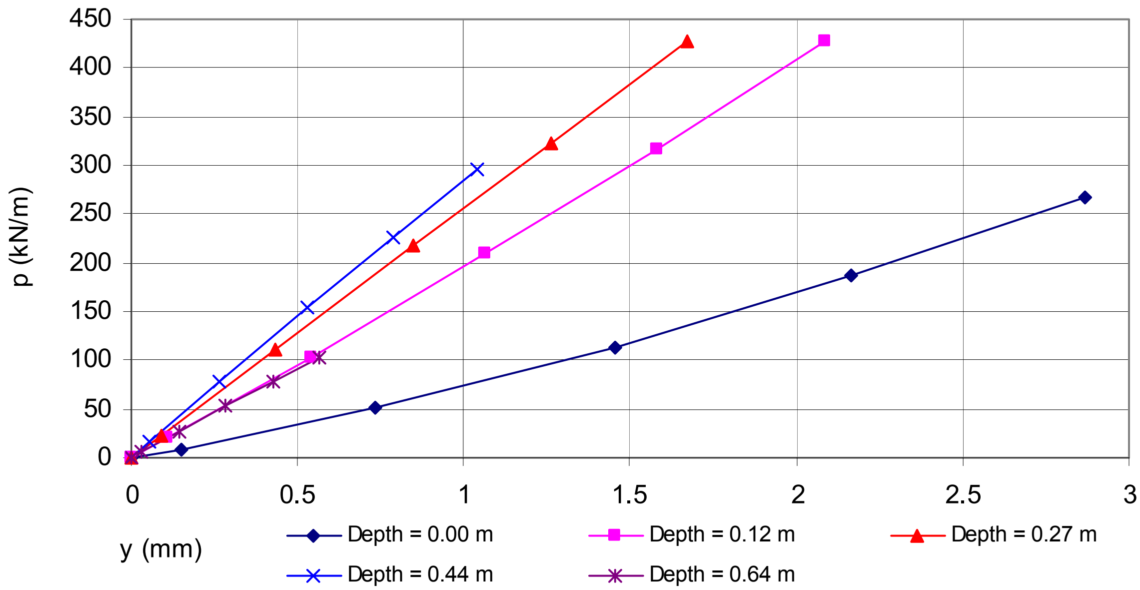

Figure 5.3 Load-transfer curves at various depths from Model 2 (Section 3.4.1.2)

The deflections and the bending moments along the micropile length under the load of 400 kN at the micropile head from FE and FD analyses are plotted in Figure 5.4. Again, the results from both analyses agree well with each other, thus validating the *p-y* curves obtained from the FE analyses.

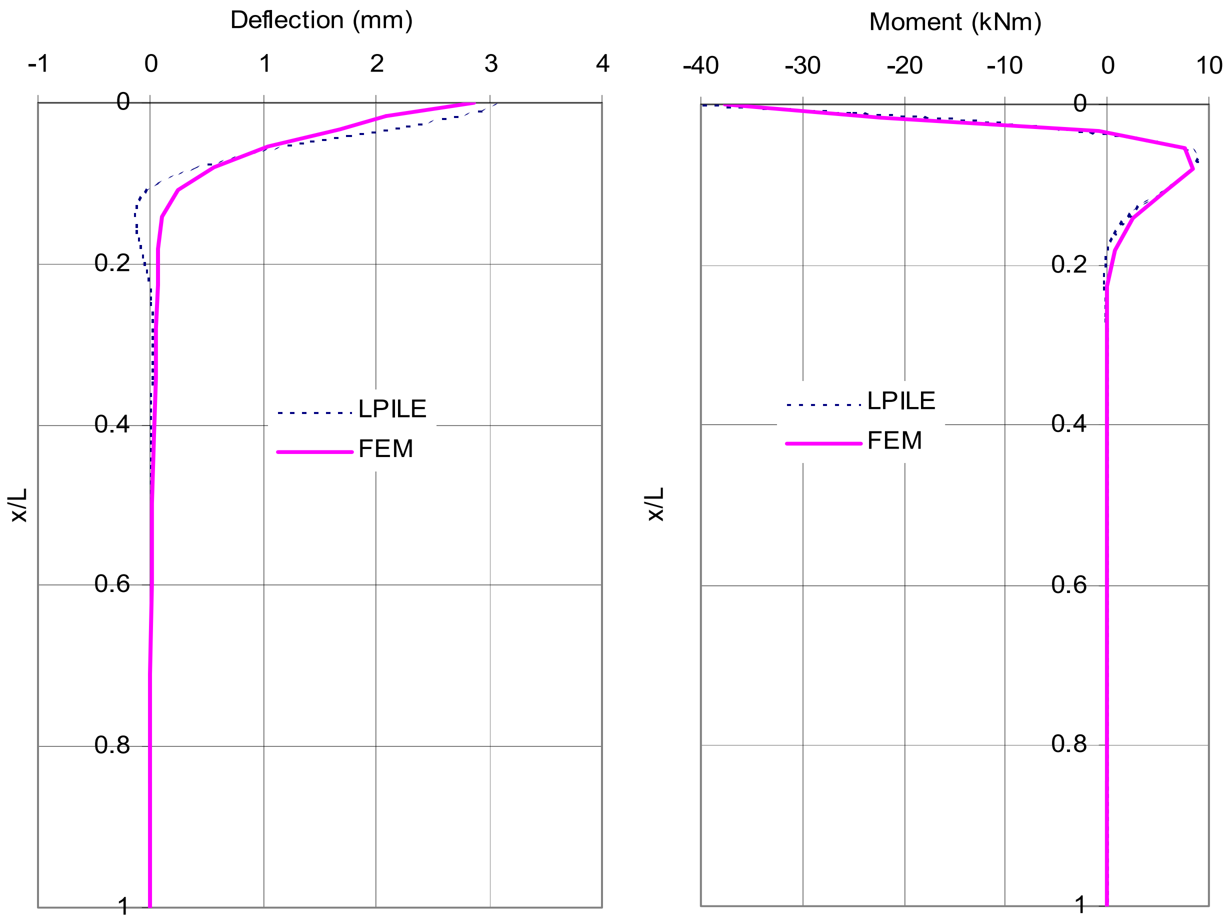

Figure 5.4 Deflection and bending moment profiles under the load of 400 kN at the micropile head from LPILE and ABAQUS

5.3.3 Model 4 (Plasticity Model (PI = 0) and Interface Elements)

The *p-y* curves obtained at several depths from the fourth model (Section 3.4.1.4) are presented in Figure 5.5. The values of the back-calculated *p* at the depths of 0.00 m and 0.12 m were negative. These values were considered erroneous since there were very unlikely to have a tensile reaction (negative *p*) in a soil at the front of the micropile when the soil was displaced (positive *y*). Therefore, the *p-y* curve obtained at the depth of 0.27 m was used at the depth of 0.00 m as well.

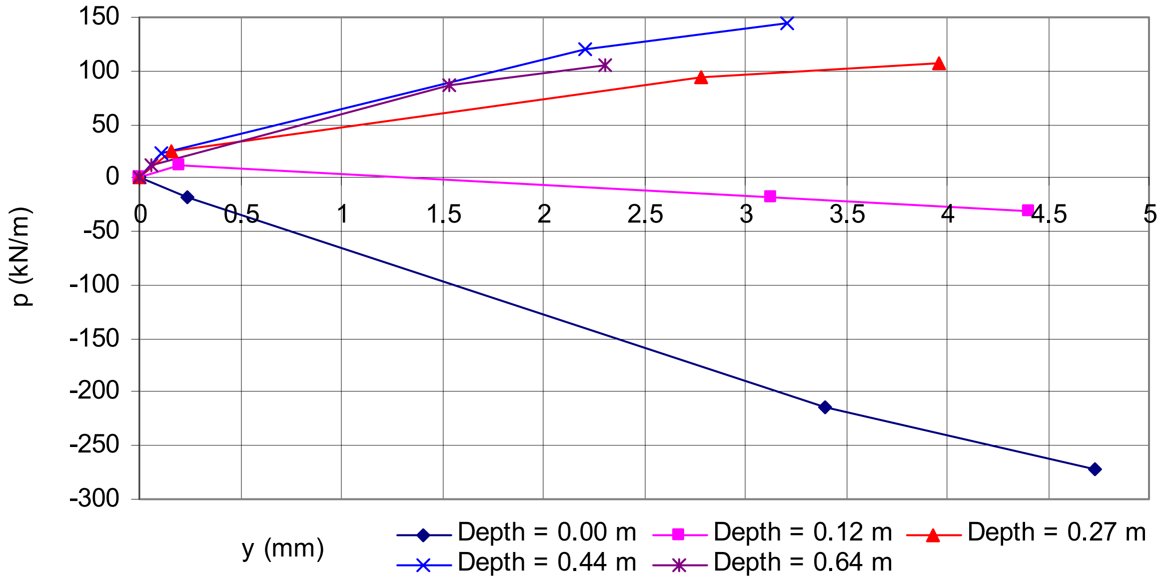

Figure 5.5 Load-transfer curves at various depths from Model 4 (Section 3.4.1.4)

The deflection and the bending moment profiles along the micropile length under the load of 400 kN at the micropile head from FE and FD analyses are illustrated in Figure 5.6. The results from both analyses did not agree well with each other. Hence, this shows that the *p-y* curves back-calculated from the inelastic soil model with PI = 0 were not acceptable for use as inputs in a FD code. This also warns us about the reliability of using the *p-y* curves back-calculated from FE analyses when the soil has potential to reduce its shear modulus significantly at moderate and high strains. The discrepancies between the FD and FE codes may be are due to the limitations of the Winkler model in representing the continuum model when the soil is highly nonlinear.

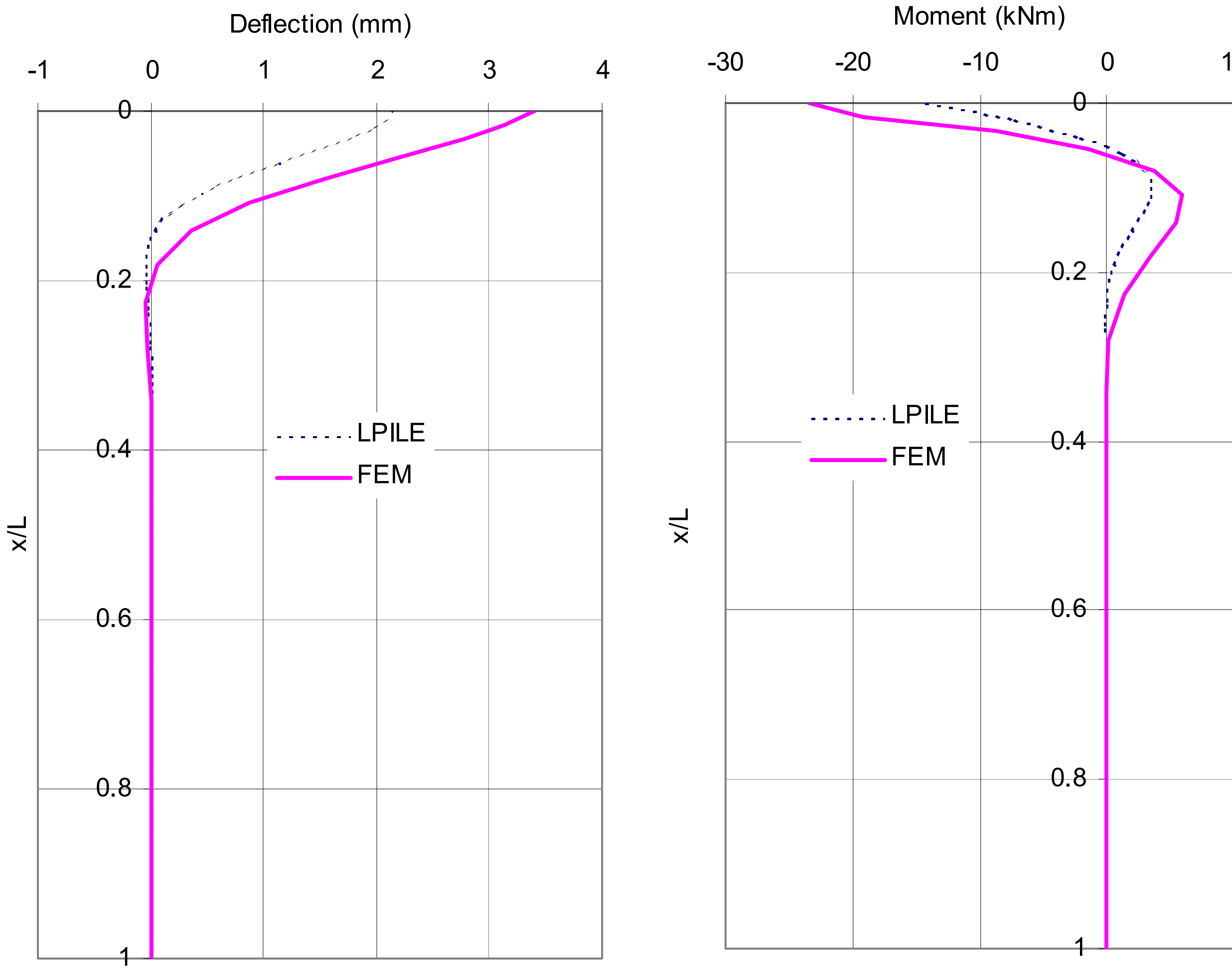

Figure 5.6 Deflection and bending moment profiles under the load of 400 kN at the micropile head from LPILE and ABAQUS

5.3.4 Model 5 (Plasticity Model (PI = 100) and Interface Elements)

Figure 5.7 illustrates the *p-y* curves derived at various depths from the fifth model (Section 3.4.1.5). Again, the *p-y* curve back-calculated at the ground surface was considered faulty since the fact of getting a negative soil reaction when the soil immediately adjacent to the front of the micropile was displaced is not acceptable. Similarly, the *p-y* curve obtained at the depth of 0.12 m was used at the depth of 0.00 m. Generally, the graph shows that the *p-y* stiffness increased with depth except the one at the depth of 0.64 m. This is opposite to the trend found in the linear elastic soil without gapping (Model 1) but similar to the one in the linear elastic soil with gapping (Model 2). The *p-y* curves near the ground surface were more non-linear (*p-y* stiffness increased with depth). This is likely due to the higher strain levels near the surface. The softer soils near the surface resulting from soil non-linearity imply that stresses are transmitted to lower portion of the micropile.

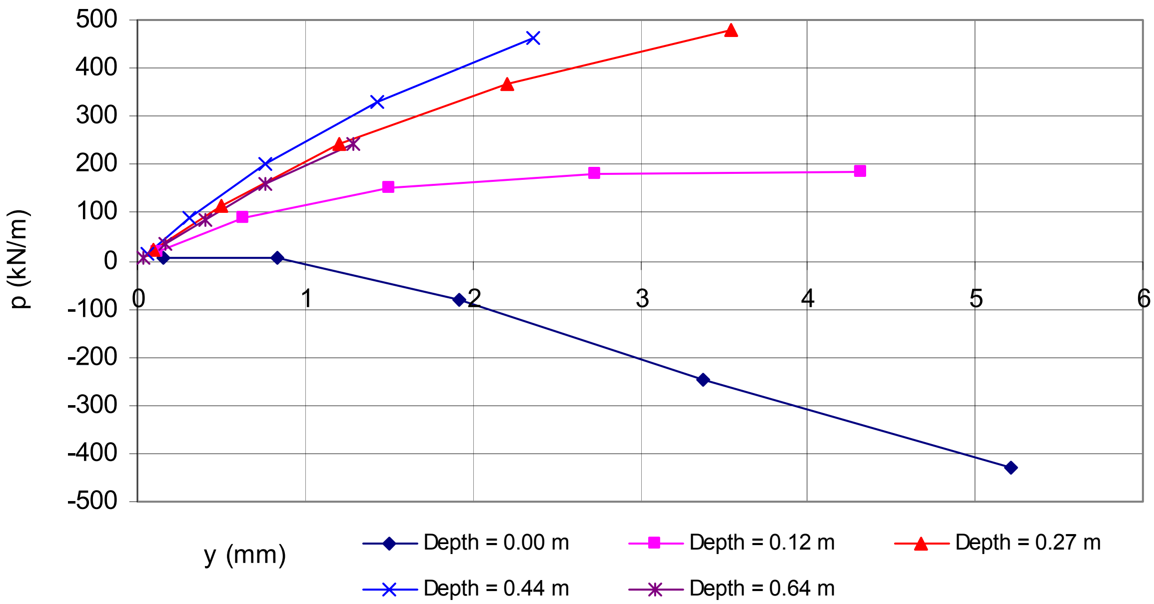

Figure 5.7 Load-transfer curves at various depths from Model 5 (Section 3.4.1.5)

Figure 5.8 illustrates the deflection and bending moment profiles along the micropile length with the load of 400 kN at the micropile head from the FD and FE analyses. The results from LPILE and ABAQUS agreed well to each other and this validates the reliability of the derived *p-y* curves.

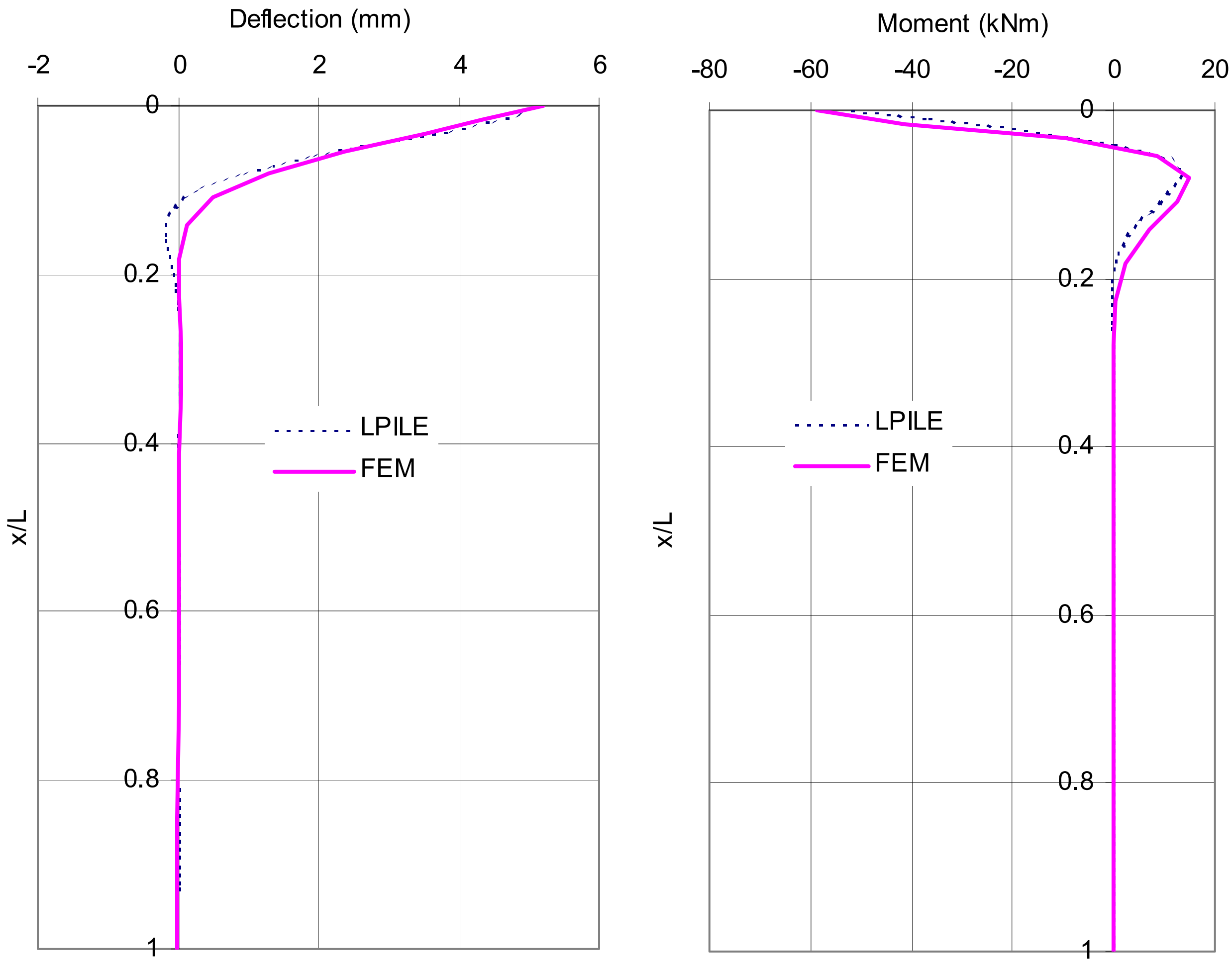

Figure 5.8 Deflection and bending moment profiles under the load of 400 kN at the micropile head from LPILE and ABAQUS

5.3.5 Lower Young's Modulus, Linear Elastic, and Interface Elements

This FE model had the properties of linear elastic soil, incorporated with interface elements, and a lower Young's modulus (i.e. 5.22×10^7 N/m^2) was used for the soil. This additional FE model was made so as to investigate the effect of the Young's modulus of the soil on the behavior of *p-y* curves. Figure 5.9 shows the load-transfer curves at different depths of the micropile from this FE model. Similarly, the *p-y* curve at the ground was found faulty and the *p-y* curve at this location was implemented with the one at the depth of 0.12 m. Basically, with increasing depth, the *p-y* stiffness increased except the one at the depth of 0.64 m.

Figure 5.10 illustrates the deflection and bending moment profiles along the micropile length under the application of 400 kN force at the micropile head from LPILE and ABAQUS. The results from the finite element analysis agreed well with the ones from the FD analysis except the deflections at certain depths below the ground surface. This verifies the validity of the back-calculated *p*-y curves.

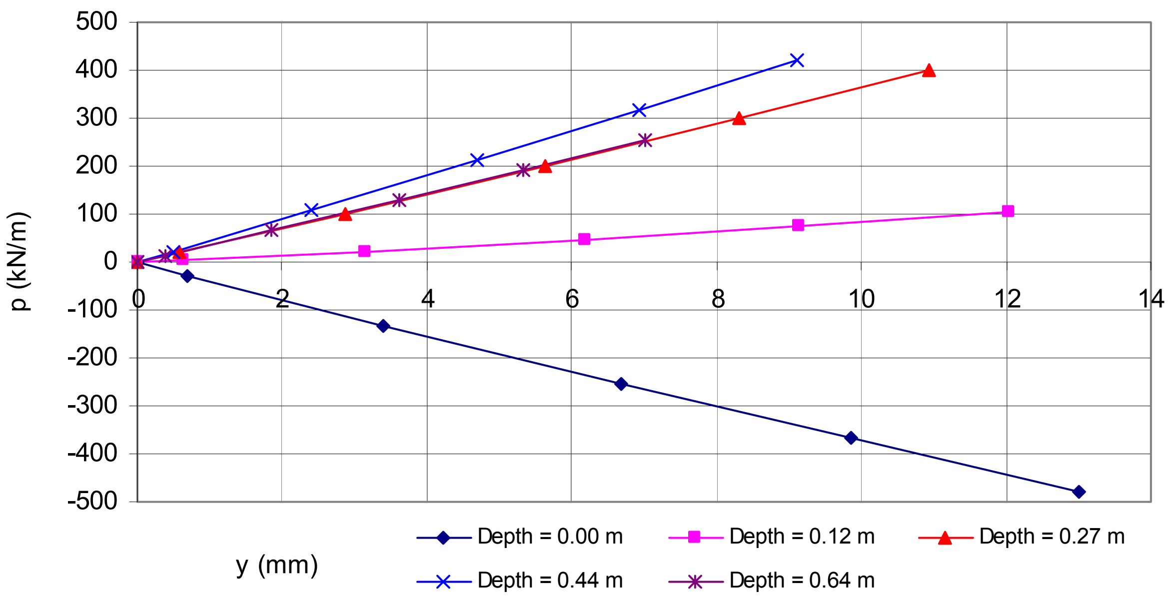

Figure 5.9 Load-transfer curves at various depths from FE model with lower Young's modulus for clay

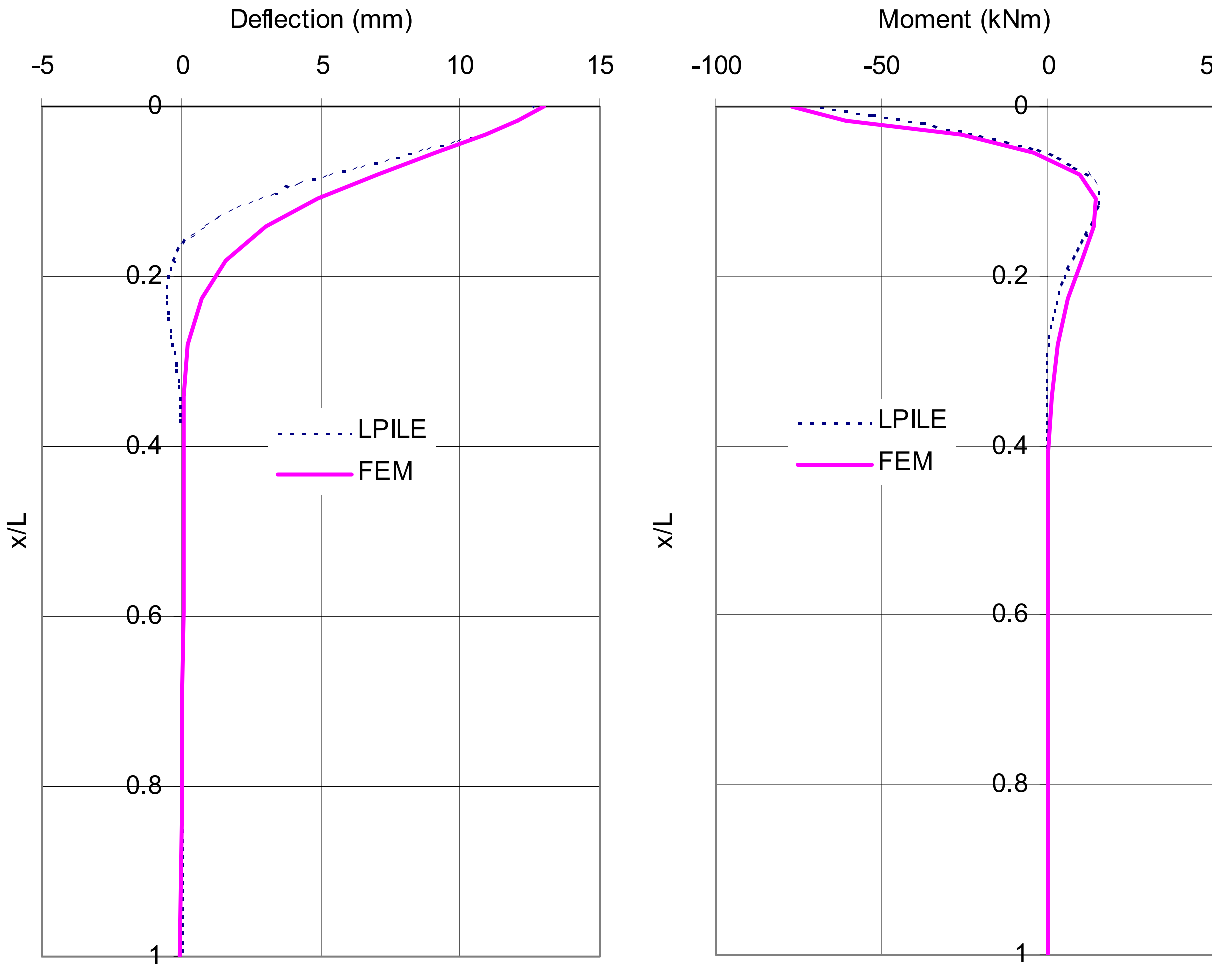

Figure 5.10 Deflection and bending moment profiles under the load of 400 kN at the micropile head from LPILE and ABAQUS

5.4 BEHAVIOR OF *p-y* CURVES

The behavior of the validated *p-y* curves back-calculated above is described herein. The behavior was investigated by studying the effects of several factors on the stiffness of *p-y* curves, such as gapping, non-linearity of the soil, and Young's modulus of the soil. The behavior was studied at the depths of 0.12, 0.27, 0.44, and 0.64 m from the micropile head.

5.4.1 Gapping

Figure 5.11 shows the *p-y* curves obtained at different depths from the linear elastic models with and without gapping. The *p-y* stiffness from the model with gapping was lower than the one without gapping at the depth of 0.12 and 0.27 m. Basically, there was a deflection difference at a given *p*. The difference reduced with depth until the deflection from the model with gapping was larger than the one without gapping at a given *p* at the depth of 0.64 m. The change of *p-y* stiffness with depth from the models with and without gapping was contradictory. Therefore, the contribution of the gapping to the behavior of *p-y* curves was inconclusive.

5.4.2 Non-linearity of Soil

Figure 5.12 presents the *p-y* curves derived at various depths from the FE models with the clay made out from linear elastic and inelastic (PI = 100) materials. Interface elements were incorporated in both models. Generally, the linearity of *p-y* curves demonstrates the linear elasticity of the soil material, and the non-linearity of *p-y* curves depicts the non-linearity of the soil as well. The *p-y* curve from the inelastic material at the ground surface shows high non-linearity due to high strain. It was interesting to note that the *p-y* curves from the inelastic material behaved closer to the ones from elastic material with increasing depth. This was said so because the gap between them became smaller with depth. This phenomenon is attributed to the decreasing strains with increasing depth. In other words, the inelastic soil behaved essentially more elastically with depth at smaller strains.

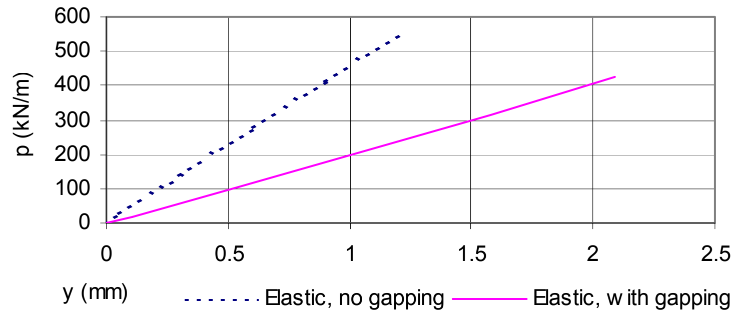

(a) 0.12 m

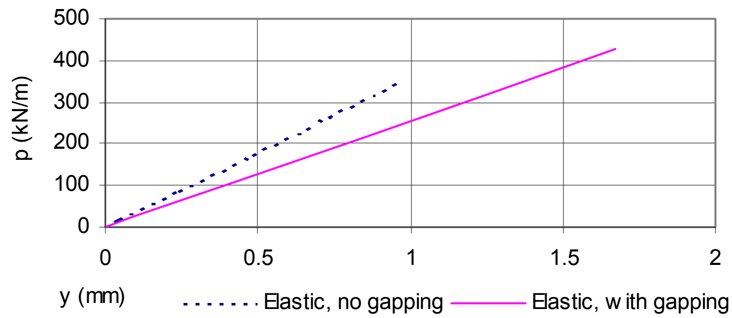

(b) 0.27 m

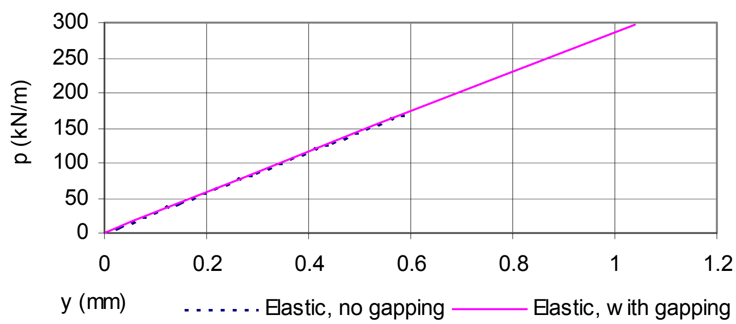

(c) 0.44 m

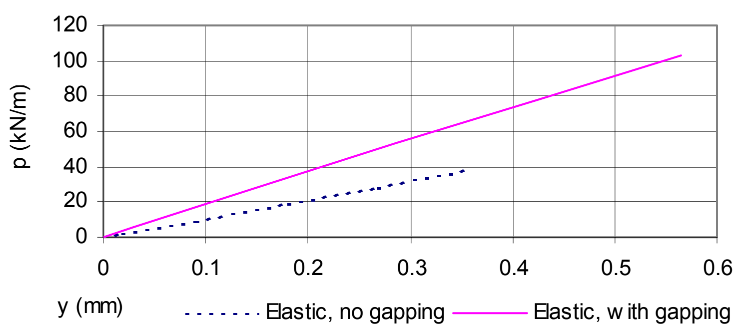

(d) 0.64 m

Figure 5.11 Effect of gapping on *p-y* curves at various depths

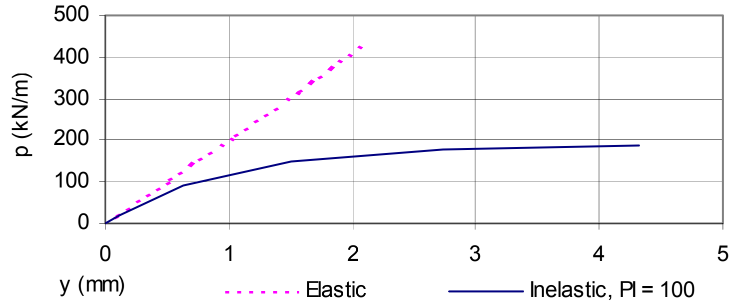

(a) 0.12 m

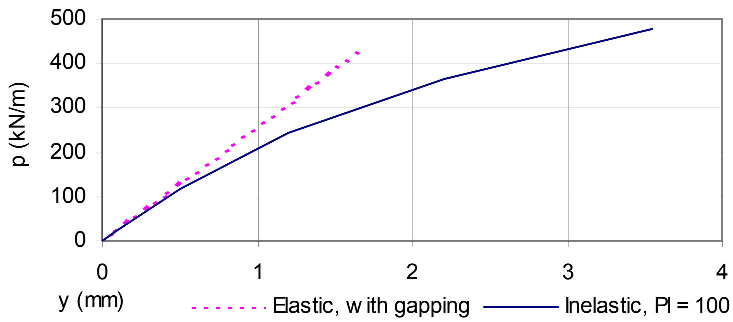

(b) 0.27 m

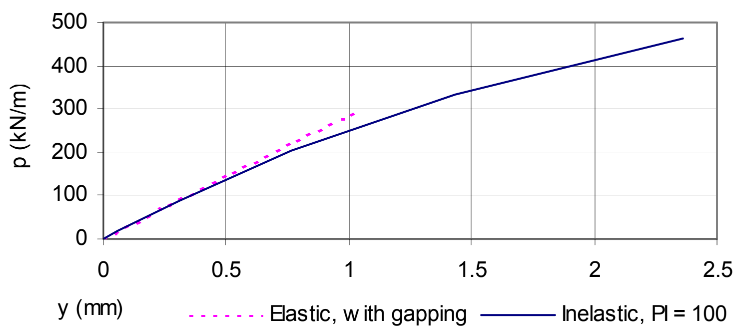

(c) 0.44 m

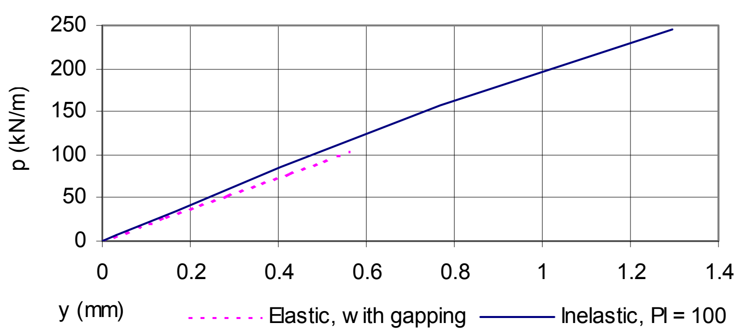

(d) 0.64 m

Figure 5.12 Effect of soil inelasticity on *p-y* curves at various depths

5.4.3 Young's Modulus of Soil

Figure 5.13 shows the *p-y* curves back-calculated at various depths from the linear elastic models with two different Young's modulus for clay. The values of the Young's modulus were 4.68 x 10^8 N/m^2 (corresponding to shear wave velocity of 300 m/s) and 5.22 x 10^7 N/m^2 (corresponding to shear wave velocity of 100 m/s). Table 5.1 presents the slope of the *p-y* curves at various depths from these analyses. At all these depths, the slope of the *p-y* curves was larger in the clay with higher Young's modulus than in the case with lower Young's modulus. Besides, the slopes from both materials increased with depth except the ones at the depth of 0.64 m.

Table 5.2 tabulates the increase percentage in *y* at a given *p* of 100 kN/m due to the reduction of Young's modulus in soil. The table shows that the increase percentage decreased with depth. This implies that at very large depth, there is a possibility that the *p-y* curves at that depth might be unique even though the materials are made out from different Young's modulus.

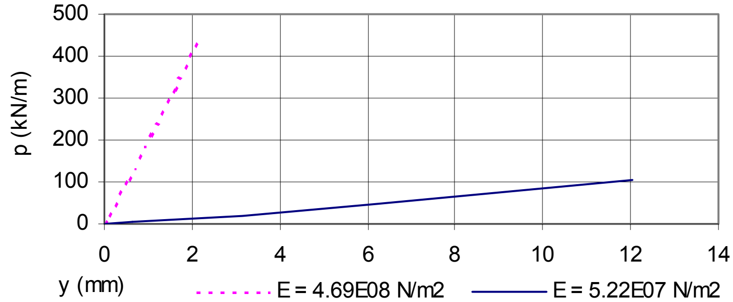

(a) 0.12 m

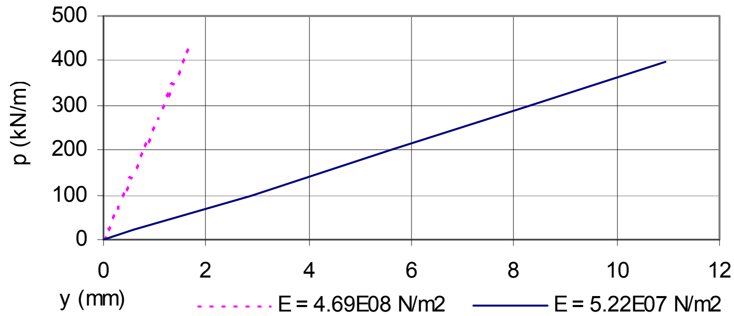

(b) 0.27 m

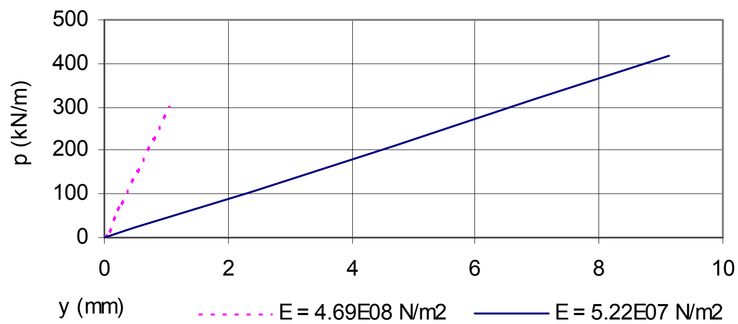

(c) 0.44 m

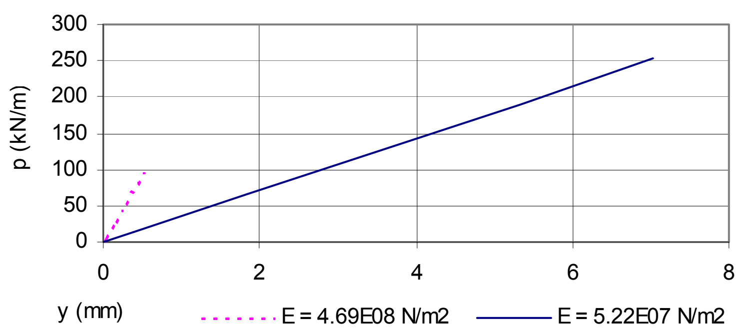

(d) 0.64 m

Figure 5.13 Effect of soil's Young's modulus on *p-y* curves at various depths

Depth (m)	Slope of *p-y* curves	
	E = 4.68 x 10^8 N/m^2	E = 5.22 x 10^7 N/m^2
0.12	201.73	8.217
0.27	256.04	36.07
0.44	286.45	45.711
0.64	184.31	35.893

Table 5.1 Slope of *p-y* curves at various depths from clay with different E

Depth (m)	Increase percentage in y
0.12	2355
0.27	610
0.44	527
0.64	413

Table 5.2 Increase percentage in y at a given p of 100 kN/m at various depths from clays with decreasing E

CHAPTER 6

CONCLUSIONS AND RECOMMENDATIONS

6.1 SUMMARY

The FE model was used to study the behavior of micropiles subjected to seismic loading. Various configurations of single and groups of micropiles were studied under both static lateral loads and dynamic input motions. A bounding surface plasticity model was implemented in the FE code ABAQUS to represent the dynamic behavior of soils. The ability of the FE implementation to represent dynamic soil behavior was verified by using the FE model to solve a site response problem. The FE solution was successfully compared to the solution of the well-validated equivalent linear code SHAKE. This study focused on the analysis of specific micropile configurations. Namely, single micropiles and groups of two micropiles with various inclinations were studied. In all cases, a fixed head condition was imposed on the micropiles, representing a rigid connection between the micropile and the pile cap. For seismic loading cases, the superstructure was represented by means of a simple model of a rigid mass on an elastic column with a behavior close to that of a SDOF system. The mass of the superstructure was kept relatively small, implying that the loading on the micropile under dynamic loadings resulted mainly from kinematic effects. Two dynamic response variables were studied in detail, micropile head movement (displacements and accelerations) and moment demand on the micropiles. The FE analyses were also used to establish *p-y* curves for the soil-pile system to be used in finite difference analysis.

The FE method proved to be a useful tool to study the effects of various variables on the response of micropiles to dynamic loadings. In addition, the results presented herein indicate that *p-y* curves calculated from the FE analyses can be used in commonly used finite difference codes for the design of micropiles. This chapter revisits the most important conclusions of this study and presents recommendations for further study.

6.2 CONCLUSIONS

The main conclusions from this study can be grouped into four categories:

(a) Behavior of a single micropile under static loading,

(b) behavior of a single micropile under seismic loading,

(c) behavior of micropile groups under seismic loading, and

(d) behavior of *p-y* curves for a single micropile.

Conclusions from this study are presented in detail in the remainder of this section. For each of the cases listed above, the influence of various parameters on the response of the micropile systems is described. These parameters include the soil stiffness, the soil's nonlinear behavior, the use of gapping elements between the soil and the micropiles, static load intensity, and input motion characteristics.

6.2.1 Static Behavior of Single Micropile

- Gapping results in an increase in deflection. For a linear elastic soil, the increase in deflection due to gapping is linearly related to the applied horizontal load. This implies that the gapping elements (described in Section 3.4) do not introduce non-linearity in the pile-soil systems. The increase in deflection when gapping elements are used compared to deflections in a system with perfect bonding between soil and pile is significant. Most of the deformation occurs near the top of the micropile. Hence, it is important to incorporate interface elements between the micropile and the soil at least within six diameter lengths from the micropile head. Gapping also causes higher moments near the micropile head because a lesser amount of load will be transferred to the neighboring soils. This, in turn, is due to the lower contact area between the pile and the soil.

- An increase in soil's non-linearity causes an increase in deflection. In this context, an increase in non-linearity implies a more significant degradation in stiffness and strength with increasing strain levels. As expected, the deflection of micropiles in non-linear soils increases nonlinearly with increasing load. The micropile in a soil with higher non-linearity will have higher deflections due to the fact that the soil with higher non-linearity will have a smaller stiffness at large strains even though both soils have the same initial stiffness. A larger volume of the soil around the micropile head will yield in the case of more non-linear behavior. The moments from the inelastic materials, especially the one with more non-linearity, are higher than those with elastic material because of the lesser degree of load transfer from the pile to the soil in the more non-linear material.
- The deflection increases with decreasing Young's modulus of the soil, E. Based on one of the numerical studies, the soil with E lower than 1.0×10^6 N/m^2, the deflection at the tip of the micropile was not zero. This implies that the micropile behaves as a stiff pile and not as a long flexible pile, as it is

commonly assumed for the design of micropiles. There is no unique relationship between the change in soil stiffness, *E*, and the maximum moment at the micropile head. However, the higher the stiffness of the soil, the lower the length of the micropile (measured from the micropile head) that mobilizes moment resistance.

6.2.2 Dynamic Behavior of a Single Micropile

- The non-linear behavior of the soil has a significant influence on the response of the micropile to seismic excitation. Two extremes of nonlinear behavior were studied: a soil with a large elastic range and a soil with strong non-linear behavior (e.g., large damping values and strong modulus degradation at low strains). Two material models were used to represent these two extremes, one model that matches the modulus degradation and damping characteristics of a soil with weak non-linearity, and another model matching the characteristics of a soil with strong non-linearity. The former represents a material with a large elastic range, the latter a material with strong non-linearity. The material with strong non-linearity will have higher damping than the one with weak non-linearity and thus causing delay in the responses decreasing the amplitude of the response, and also damping free vibrations of the micropile sooner. The maximum bending moment at the micropile head from the material with weak non-linearity (e.g. a material with a large elastic range) is slightly smaller than the one from the elastic material. The maximum bending moment at the micropile head from the material with strong non-linearity is significantly smaller than the one from the material with weak non-linearity.

The smaller moment is due to the larger hysteretic damping in the soil for the highly non-linear material. For the pulse-motion used as an input motion, the soil non-linearity resulted in non-symmetric bending moment envelopes for the pile. The asymmetry of the bending moment envelope was not observed in linear soils.

- With higher intensity of input motion, the strains in the soil are higher and thus results in lower shear modulus in the soil and consequently in higher predominant periods (e.g., the period corresponding to peak spectral acceleration) for spectral acceleration at the pile head.. The bending moment envelope increases with increasing input motion intensity. The soil with strong non-linearity demonstrates higher level of non-symmetry of the moment envelope with increasing input motion intensity, resulting from the higher non-linearity.

6.2.3 Dynamic Behavior of Micropile Groups

- Higher input motion intensity results in higher responses at the micropile head. At the end of shaking, there is a residual deflection at the micropile head and the residual deflection is higher with higher intensity. Note that this result is particular to the type of input motion used and does not necessarily apply to other input motions. An input motion with higher intensity causes larger reduction in shear modulus due to higher strain levels in the soil, resulting in a significant degradation of soil stiffness with the initial pulse motion. The bending moment envelope increases with increasing input motion intensity in both vertical and inclined micropile groups. Moreover, a higher degree of non-symmetry of the moment envelope with increasing input motion intensity, implying higher level of non-linearity of the soil in both micropile groups. Once again, note that the non-symmetry of the moment envelope is also a result of the pulse-type input motion used in this study.

- At all input motion intensities, the moment envelopes of the left and right vertical micropiles were the same, implying equal distribution of loads among the vertical micropile members. However, the moment envelopes for the left and right inclined micropiles were different, implying unequal distribution of loads among the inclined micropile members. Therefore, inclination of micropiles results in unequal distribution among the micropile groups under dynamic loading. This is due to the fact that the axial resistance of the inclined micropiles also contributes to the load carrying capacity of the micropile group.
- The inclination of micropiles provides larger lateral stiffness and results in smaller displacements and accelerations at the micropile head as compared to the case of vertical micropiles. The inclination of the micropiles does not affect the strain levels in the soil, implying that no additional stresses are being transmitted to the soil. The inclination of micropiles also decreases the bending moment at the micropile head. This, again, is due to the fact that the axial capacity of inclined micropiles is also mobilized (in addition to the bending capacity).
- The response at the micropile head is a function of the frequency content of the input motion. The input motion with higher frequency content results in a

smaller response at the micropile head. This is likely due to the fact that the higher frequency motion tends to introduce more damping than the input motion with lower frequency (longer period) content. With the exception of moments near the micropile head, an input motion with a larger predominant period results in larger maximum bending moments along the length of the micropile. This is attributed to the larger kinematic loading from the input motion with a larger natural period.

- The magnitude of the response of the superstructure increases with increasing natural period of the superstructure under a seismic loading. The close matching of the natural periods of superstructure with the predominant period of the input motion results in larger response at the micropile head. The natural period of the superstructure was increased by increasing the superstructure's mass. Consequently, the superstructures with longer natural periods (i.e., larger masses) increases the bending moment at the micropile head as a result of the larger inertial forces from the superstructure. It is likely that for structures that initially have a long predominant period (e.g. longer than the predominant period of the input motion and the natural period of the soil column), an increase of the natural period of the structure could result in a decrease in structural demands and inertial forces.

6.2.4 *p-y* Curves of a Single Micropile

- Generally, the *p-y* stiffness increases with depth in all cases except for the model with a linear elastic soil without gapping, in which case the *p-y* stiffness decreases with depth.

- The contribution of gapping to *p-y* curves is inconclusive. While in some cases gapping results in stiffer *p-y* curves, in other cases it results in softer *p-y* curves. However, in the linear elastic soil, gapping was found to make the *p-y* stiffness increase with depth.
- The linearity and non-linearity of the soil is also reflected in the resulting *p-y* curves.
- The *p-y* curves of the inelastic material at shallow depths shows high non-linearity, especially at the ground surface. The *p-y* curves of the inelastic material behave more elastically at large depth due to smaller strain levels at depth. This illustrates the need to adequately incorporate non-linear soil behavior in the analysis of micropiles.
- As expected, the *p-y* stiffness at a given depth is larger in the clay with higher Young's modulus compared with the one with lower Young's modulus. For the linear soil, the *p-y* stiffness increases with depth. However, the increase in *p-y* stiffness with depth is not as pronounced for the stiffer soils as compared to the softer soils. This implies that the *p-y* curves at very large depths might be unique regardless of the Young's modulus of the soil.

6.3 RECOMMENDATIONS FOR FUTURE RESEARCH

The following are recommendations for further research in the subject of seismic response of micropiles. Most of the recommendations were not implemented in this study as a result of time constraints . The recommendations are also the results of encountering unresolved convergence problems when trying to implement certain boundary conditions and/or interface elements in the FE models.

- A real earthquake input motion should be used in addition to the wavelet input motions used in this study.
- A three-dimensional FE models for dynamic site response and SSI analyses should be implemented if time is permitted.
- Various degrees of inclination of micropiles should be attempted in order to investigate how the inclination affects the response.
- Many attempts were done to incorporate the interface elements in the dynamic analysis. However, divergence in solution was encountered. Hopefully, this task could be performed with other commands in the program, ABAQUS or with other software.
- Probably a more realistic superstructure, like a building with several stories, should be connected to the pile cap to investigate the effect of the number of DOF to the response of the micropiles.
- Probably, full- or model- scale tests with sufficient material property information should be used for the validation of the FE models, especially for the dynamic cases.
- Other factors might have effects on the behavior of *p-y* curves should be investigated, such as the type of loading (cyclic and seismic loading), different soil type, and also the coefficient of friction.
- Buckling of micropiles has been an increasing focus and concern of engineers and researchers. Therefore, it is worth to investigate the problem using FEM by creating a void or soils with very poor strength properties such as peat, very loose sand, and soft clay around the micropile.

REFERENCES

AASHTO (1992). "Standard specification for highway bridges, revised." American Association of State Highway and Transportation Officials, Washington, D.C.

American Petroleum Institute (1988). "Recommended practice for planning, designing, and constructing fixed offshore platforms." American Petroleum Institute, Washington, D.C., API Recommended Practice 2A (RP2A), 18th edition.

Anandarajah, A. (2000). "Fully-coupled analysis of a single pile founded in liquefiable sands." Proceedings of Sessions of Geo-Denver 2000 – Computer Simulation of Earthquake Effects, Geotechnical Special Publication No. 110, ASCE, pp. 117-131.

BCNYC (1991). Building Code of New York City.

BOCA (1990). National Building Code, section 1221, Caisson Piles, and section 1217, Cast in Place Concrete Piles.

Berrill, J.B., Christensen, S.A., Keenan, R.J., and Okada, W. (1997). "Lateral-spreading loads on piled bridge foundation." Seismic Behavior of Ground and Geotechnical Structures, P.Seco e Pinto, Ed., Balkema, pp. 173-183.

Blaney, G., Kausel, E., and Roesset, J. (1976). "Dynamic Stiffness of Piles." Proc. 2nd Intl. Conf. on Numerical Methods in Geomechanics, Blacksburg, Vol. 2, pp. 1001-1012.

Bogard, D.A., and Matlock, H. (1983). "Procedures of analysis for laterally loaded pile groups in soft clay." Proceedings of Specialty Conference of Geotechnical Engineering in Offshore Practice, ASCE, pp. 499-535.

Borja, R.I., and Amies, A.P. (1994). "Mutiaxial Cyclic Plasticity Model for Clays," Journal of Geotechnical Engineering., ASCE, 120(6), pp. 1051-1070.

Borja, R.I., Chao, H.Y., Montans, F.J., and Lin, C.H. (1999). "Nonlinear ground response at Lotung LSST site." Journal of Geotechnical and Geoenvironmental Engineering, ASCE, 125, pp. 187-197.

Bransby, M.F. (1999). "Selection of p-y curves for the design of single laterally loaded piles." International Journal for Numerical and Analytical Methods in Geomechanics, 23(15), pp. 1909-1926.

British Standards Institution (1989). Ground Anchorages. BSI, Milton Keynes, BS 8081.

Brown, D.A., Shie, C.F., and Kumar, M. (1989). "P-y curves for laterally loaded piles derived from three-dimensional finite element model." Numerical Models in Geomechanics, NUMOG III, pp. 683-690.

Brown, D.A., and Shie, C.F. (1990). "Three dimensional finite element model of laterally loaded piles." Computers and Geotechnics, v 10, n 1, 1990, pp. 59-79.

Bruce, D.A., and Juran, I. (1997). "Drilled and grouted micropiles: State-of-practice review. Volume II: Design" U.S. Department of Transportation, Federal Highway Administration, Publication No. FHWA-RD-96-017.

Brown, D.A., Reese, L.C., and O'Neill, M.W. (1987). "Cyclic lateral loading of a large-scale pile group." Journal of Geotechnical Engineering, Vol. 113, No. 11, pp. 1326-1343.

Bustamante, M., and Doix, B. (1985). "Une méthode pour le calcul des tirants et des micropieux injectés." Bulletin de Liaison des Laboratoires des Ponts et Chaussées, LCPC, Paris, pp. 75-92.

Butterfield, R., and Banerjee, P.K. (1971). "The elastic analysis of compressible piles and pile groups." Geotechnique, 21, No. 1, pp. 43-60.

Caltrans – California Department of Transportation (1994). Highway Design Metric. Office of Geotechnical Engineering, Foundation Testing and Instrumentation Branch.

CCTG (1993). Technical Rules for the Design and Calculation of the Foundations of the Civil Engineering Works, Fascicule 62, Titre V. CCTG.

Chow, Y.K. (1986). "Analysis of vertically loaded pile groups." International Journal of Numerical and Analytical Methods in Geomechanics, 10, pp. 59-72.

Dafalias, Y.K., and Popov, E.P. (1977). "Cyclic loading for materials with a vanishing elastic region." Nuclear Engrg. and Des., 41, North-Holland, Amsterdam, The Netherlands, pp. 293-302.

Davies, T.G., and Budhu, M. (1986). "Non-linear analysis of laterally loaded piles in heavily overconsolidated clays." Geotechnique, 36, No. 4, pp. 527-538.

Eurocode EC8 (1994). Structures in Seismic Regions, Part 5: Foundations, Retaining Structures, and Geotechnical Aspects.

Finn, L.W.D. (1988). "Dynamic analysis in geotechnical engineering." Proc. Earthquake Engineering and Soil Dynamics II - Recent Advances in Ground-Motion Evaluation, Geotechnical Special Publication No. 20, ASCE, pp. 523-591.

Finn, L.W.D., Wu, G., and Thavaraj, T. (1997). "Soil-pile-structure interactions." Geotechnical Special Publication, n 70, pp. 1-22.

Fleming, W.G.K., Weltman, A.J., Randolph, M.F., and Elson, W.K. (1985). Piling Engineering, Wiley.

Gazetas, G. (2001). "The 1999 Parnitha (Athens) Earthquake: soil effects on distribution of damage." XV ICSMGE TC4 Satellite Conference on "Lessons Learned from Recent Strong Earthquakes", Istanbul, Turkey.

Gazetas, G., and Mylonakis, G. (1998). "Seismic soil-structure interaction: New evidence and emerging issues." ASCE Special Edition No. 75 Geotechnical Earthquake Engineering and Soil Dynamic.

Geosystem, L.P. (2002). "Description of full scale tests conducted and data obtained in the three phases of tests conducted for the U.S. Military in Baltimore, M.D." Federal Highway Administration, Order DTFH61-02-P-00162, Requisition/Reference No. 41-08-2011.

Gohl, W. (1991). "Response of pile foundations to simulated earthquake loading: experimental and analytical results." Ph.D. Dissertation, University of British Columbia.

Mavroeidis, G. P. and A. S. Papageorgiou (2003). "A mathematical representation of near-fault ground motions." Bulletin of the Seismological Society of America 93(3): pp. 1099-1131.

Mitchell, D., Tinawi, R., and Sexsmith, R.G. (1991). "Performance of bridges in the 1989 Loma Prieta earthquake, Lessons for Canadian designers." Canadian Journal of Civil Engineering, Vol. 18, Issue n4, 1991, pp. 711-734.

Idriss, I.M., and Seed, H.B. (1968). "Seismic response of horizontal soil layers." J. Soil Mech. Found. Div., ASCE, 94 (SM4), pp. 1003-1029.

Idriss, I., and Sun, J. (1992): "User's Manual for SHAKE 91." Center for Geotechnical Modeling, Dep. of Civil & Env. Engng, University of California, Davis.

Iwan, W.D. (1967). "On a class of models for the yielding behavior of continuous and composite systems." Transactions of the American Society of Mechanical Engineers, September, pp. 612-617.

Joyner, W.B., and Chen, A.T.F. (1975). "Calculation of non-linear ground response in earthquakes." Bull. Seism. Soc. Am., 65(5), pp. 1315-1336.

Juran, I., Benslimane, A., and Hanna, S. (2001). "Engineering analysis of the dynamic behavior of micropile systems." Transportation Research Record, 1772, Paper No.

01-2936, pp. 91-106.

Kausel, E. (1974). “Forced vibrations of circular foundations on layered media,” Research Report R74-11, Civil Engrg. Dept., MIT.

Kausel, E., Roesset, J.M., and Waas, G. (1975). “Dynamic analysis of footings on layered media,” Proc. ASCE, Engrg. Mech. Division, No. EM5.

Kishishita, T., Saito, E., and Miura, F. (2000). “ Dynamic-response characteristics of structures with micropile foundation system.” 12th World Conference on Earthquake Engineering, Auckland, New Zealand, pp. 1-8.

Kondner, R.L. (1963). “ Hyperbolic stress-strain response: Cohesive soils.” Journal of the Soil Mechanics and Foundation Division, ASCE, 89(1), pp. 115-143.

Kuhlemeyer, R. (1979). “Static and Dynamic Laterally Loaded Floating Piles.” Journal of Geotechnical Engineering, ASCE, 105(2), pp. 289-304.

Lee, C.Y. (1993). “Pile group settlement analysis by hybrid layer approach.” Journal of Geotechnical Engineering, ASCE, 119, No. 9, pp. 1449-1461.

Lee, M.K.W., and Finn, W.D.L. (1978). “DESRA-2: Dynamic effective stress response analysis of soil deposits with energy transmitting boundary including assessment of liquefaction potential.” Soil Mechanics Series, No. 38, Department of Civil Engineering, University of British Columbia, Vancouver, B.C.

Lee, M.K.W., and Finn, W.D.L. (1991). “DESRA-2C: Dynamic effective stress response analysis of soil deposits with energy transmitting boundary including assessment of liquefaction potential.” University of British Columbia, Faculty of Applied Science.

Li, X.S., Shen, C.K., and Wang, Z.L. (1998). “Fully-coupled inelastic ground response analysis for 1986 Lotung Earthquake Events.” Journal of Geotechnical Engineering, ASCE, 124(7).

Littlejohn, G.S., and Bruce, D.A. (1977). Rock Anchors – State of the Art. Foundation Publication Ltd, Brentwood.

Lizzi, F. (1978). “Reticulated root piles to correct landslides.” ASCE Convention, Chicago, Reprint 3370.

Lizzi, F. (1982). “The pali radice (root piles).” Symposium on Soil and Rock Improvement Techniques including Geotextiles, Reinforced Earth and Modern Piling Methods, Bangkok, Paper D-3.

Lok, M.H. (1999). “Numerical modeling of seismic soil-pile-superstructure-interaction in soft clay.” Ph.D. Dissertation, University of California, Berkeley.

Lysmer, J., and Kuhlemeyer, R.L. (1969). “Finite dynamic model for infinite media.” Journal of the Engineering Mechanics Division, ASCE, Vol. 95, No. EM 4, pp. 859-877.

Maleki, K. (1995). “Contribution a l’Etude des Micropieux Isoles et en Groupe.” Ph.D Dissertation, Ecole Nationale des Ponts et Chaussées, Paris.

Maleki, F. and Frank, R. (1994). “Groupes de Pieux Charges Axialement.” Project National FOREVER, Programme 1993, CERMES, 1994.

Martin, P.P., and Seed, H.B. (1982). “One-dimensional dynamic ground response analyses.” J. Geotech. Engng. Div., ASCE, 108(7), pp. 935-953.

Matlock H. (1970). “Correlation for design of laterally loaded piles in soft clay.” Proceedings of 2nd Offshore Technology Conference, Houston, I, pp. 577-594.

Mc. Daniel, C. (2004). Personal communication.

Meyerhof G.G. (1976). “Bearing capacity and settlement of pile foundations.” Journal of Geotechnical Engineering, ASCE, 102, No. GT3, pp. 195-228.

Mindlin, R.D. (1936). Foundation and Earth Structures. Naval Facilities Engineering Command, Alexandria, VA.

O’Neill, M.N., Ghazzaly, O.I., and Ha, H.B. (1977). “Analysis of three-dimensional pile groups with nonlinear soil response and pile-soil-pile interaction.” Proceedings of the 9th Annual OTC, pp. 245-256.

Ostadan, F. (1983). “Dynamic Analysis of Soil-Pile-Structure Systems.” Ph.D. Dissertation, University of California, Berkeley.

Ousta, R., and Shahrour, I. (2001). “ Three-dimensional analysis of the seismic behavior of micropiles used in the reinforcement of saturated soil.” International Journal for Numerical and Analytical Methods in Geomechanics, Vol. 25, pp. 183-196.

Plumelle, C. (1984). “Improvement of the bearing capacity of soil by inserts of group and reticulated micro piles.” International Symposium on In-situ Reinforcement of Soils and Rocks, Paris, ENPC Presses, pp. 83-89.

Poulos, H.G., and Davies, E.H. (1980). Pile Foundation Analysis and Design, Wiley, New York.

Pyke, R.M. (1992). “TESS: A computer program for nonlinear ground response analyses.” TAGA Engin. Systems and Software, Lafayette, CA.

Ramberg, W., and Osgood, W.T. (1943). “Description of Stress-Strain Curves by Three Parameters.” Technical Note 902, National Advisory Committee for Aeronautics.

Randolph, M.F., and Wroth, C.P. (1979). “An analysis of the vertical deformation of pile groups.” Geotechnical Engineering, ASCE, 104, No. GT12, pp. 1466-1488.

Reese, L.C., Wang, S.T., Awoshika, K., and Lam, P.H.F. (1994). “Analysis of a group of piles subjected to axial and lateral loading.” Documentation of Computer Program GROUP, Ensoft, Inc., Austin, Texas.

Rodriguez-Marek, A. (2000). “Near-fault seismic site response.” Ph.D. Dissertation, University of California, Berkeley.

Sadek, M., and Shahrour, I. (2003). “Influence of piles inclination on the seismic behavior of groups of flexible piles.” 82nd Annual Meeting of the Transportation Research Board, pp. 1-14.

Schnabel, P.B., Lysmer, J., and Seed, H.B. (1972). “SHAKE - A computer program for earthquake response analysis of horizontally layered soils.” Report No. EERC-72/12, University of California, Berkeley.

Scott, R.F. (1985). “Plasticity and constitutive relations in soil mechanics.” J. of Geotechnical Enging, ASCE, 111(5), pp. 563-605.

Seed, H.B., Dickenson, S.E., and Mok, C.M. (1993). “Recent Lessons Regarding Seismic Response Analysis of Soft and Deep Clay Sites.” Seminar Proc., Seismic design and retrofit of bridges, U.C. Berkeley, EERC, Caltrans, June, 1992.

Shahrour, I., Sadek, M., and Ousta, R. (2001). “Seismic behavior of micropiles used as foundation support elements.” Transportation Research Record 1772, pp. 84-90.

Simo, J.C., and Hughes, P.J.R. (1998). Computational Inelasticity. Interdisciplinary Applied Mathematics. IAM (Springer).

Skempton, A.W. (1935). “Discussion: Piles and pile foundations, settlement of pile foundations.” Proceedings of the 3rd International Conference on Soil Mechanics and Foundation Engineering, 3, 172 p.

Streeter, V.L., Wylie, E.B., and Richart, F.E. (1974). “Soil motion computations by characteristics method.” J. Geotech. Engng. Div., ASCE, 100(3), pp. 247-263.

Structural Engineers Association of California (1991). “Reflections on October 17, 1989 Loma Prieta Earthquake.” Ad Hoc Earthquake Reconnaissance Committee, Sacramento.

Taylor, P.W. and Larkin, T.J. (1978) “Seismic Response of Nonlinear Soil Media,” J. Geotech. Engng. Div., ASCE, 104 (GT3), pp. 369-383.

Teerawut Juirnarongrit (2002). “Effect of diameter on the behavior of laterally loaded piles in weakly cemented sand.” Ph.D. Dissertation, University of California, San Diego.

Terzaghi, K., and Peck, R.B. (1948). Soil Mechanics in Engineering Practice, 1st edition, Wiley, New York.

Terzaghi, K. (1943). Theoretical Soil Mechanics, Wiley, New York.

Trochanis, A., Bielek, J. and Christiano, P. (1988). “A three-dimensional nonlinear study of piles leading to the development of a simplified model.” Carnegie Institute of Technology, Report No. R-88-176.

UBC (1994). Uniform Building Code. International Conference of Building Officials, Whittier, California.

Vesic, A.S. (1969). “Experiment with instrumented pile groups in sand.” ASTM Special Technical Publication, No. 444, pp. 172-222.

Vucetic, M., and Dobry, R. (1991). “Effect of soil plasticity on cyclic response.” Journal of Geotechnical Engineering, ASCE, 117, No. 1, pp. 89-107.

Weinstein, G. (2003). Personal communication.

Wu, G. (1994). “Dynamic soil-structure interaction: Pile foundations and retaining structures.” Ph.D. Dissertation, University of British Columbia.

Wu, G. and Finn, D.L.W. (1997). “Dynamic nonlinear analysis of pile foundations using finite element method in the time domain.” Canadian Geotechnical Journal, v 34, n 1, pp. 44-52.

Yamane, T., Nakata, Y., and Otani, Y. (2000). “Efficiency of micropile for seismic retrofit of foundation system.” 12th World Conference on Earthquake Engineering, Auckland, New Zealand, pp. 1-8.

Yamashita, K., Tomono, M., and Kakurai, M. (1987). “A method for estimating immediate settlement of piles and pile groups.” Soils and Foundations, 27, No. 1, pp. 61-76.

Yang, J.X., McManus, K.J, and Berrill, J.B. (2000). “Kinematic soil-micropile interaction.” 12th World Conference on Earthquake Engineering, Auckland, New Zealand, pp. 1-8.

Zienkiewicz, C., Chang, C.T., and Bettess, P. (1980). “Drained, undrained, consolidating and dynamic behavior assumptions in soils.” Geotechnique, 30, pp. 385-395.